



THE HONG KONG  
POLYTECHNIC UNIVERSITY

香港理工大學

Pao Yue-kong Library

包玉剛圖書館

---

## Copyright Undertaking

This thesis is protected by copyright, with all rights reserved.

**By reading and using the thesis, the reader understands and agrees to the following terms:**

1. The reader will abide by the rules and legal ordinances governing copyright regarding the use of the thesis.
2. The reader will use the thesis for the purpose of research or private study only and not for distribution or further reproduction or any other purpose.
3. The reader agrees to indemnify and hold the University harmless from and against any loss, damage, cost, liability or expenses arising from copyright infringement or unauthorized usage.

### IMPORTANT

If you have reasons to believe that any materials in this thesis are deemed not suitable to be distributed in this form, or a copyright owner having difficulty with the material being included in our database, please contact [lbsys@polyu.edu.hk](mailto:lbsys@polyu.edu.hk) providing details. The Library will look into your claim and consider taking remedial action upon receipt of the written requests.

**A STUDY OF BROADBAND AND PERIODICALLY  
TIME-VARYING VIBRATION CONTROL OF  
BUILDING SERVICES EQUIPMENT**

**WANG JUNFANG**

**Ph. D**

**The Hong Kong Polytechnic University**

**2014**

**The Hong Kong Polytechnic University**  
**Department of Building Services Engineering**

**A Study of Broadband and Periodically Time-Varying  
Vibration Control of Building Services Equipment**

**Wang Junfang**

**A thesis submitted in partial fulfillment of the requirements for the  
Degree of Doctor of Philosophy**

**August 2013**

# Certificate of Originality

I hereby declare that this thesis is my own work and that, to the best of my knowledge and belief, it reproduces no material previously published or written, nor material that has been accepted for the award of any other degree or diploma, except where due acknowledgement has been made in the text. I also declare that the intellectual content of this thesis is the product of my own work, even though I may have received assistance from others on style, presentation and language expression.

\_\_\_\_\_ (Signed)

**Wang Junfang** \_\_\_\_\_ (Name of student)

Department of Building Services Engineering

The Hong Kong Polytechnic University

Hong Kong, China

August, 2013

# Dedication

**To my parents**

Wang Guang and Tian Sanronghua

**and brother**

Wang Yichuan

who always provide me with unconditional love and support

# Abstract

Vibration and noise control of equipment have been a long-standing research topic because of its effect on people's health and comfort. The common characteristics of building services equipment pose great challenges to current methods of structure-borne sound control. Some of building services equipment experience frequent transient excitations which may disable the spring isolators traditionally designed for steady-state vibration isolation. Besides, broadband vibration isolation is desirable when the vibratory system has high modal density and the frequency of interest fluctuates in a wide band. In addition, the oversimplification of time-varying systems as time-invariant systems may lead to the failure of an active vibration control system. These problems is not only limited to the area of building service engineering, but can be commonly seen in the field of machine-induced vibration and acoustics. To solve these problems, this research aims to present a power transmissibility approach for the assessment of transient vibration isolation by spring isolators, develop adaptive-passive methods for broadband vibration control using periodic structures, and propose an active control system for the suppression of periodically time-varying vibration.

Firstly, a transient power transmissibility approach is proposed to assess the

performance of isolators in the situation of a transient vibration excitation. The numerical study demonstrates the necessity of using transient power transmissibility in the selection of isolators for a system that experiences a transient vibration.

Secondly, this part focuses on the broadband vibration attenuation by adaptive-passive methods of periodic structures with smart materials. The application of a dual-beam periodic structure with SMA branches to broadband vibration control is explored, and two methods are developed to determine the optimal Young's modulus of the SMA branches. As this semi-two-dimensional periodic structure is a realistic simulation of a real-life problem, this study provides an insight into the general problem of broadband vibration control using smart periodic structures.

Thirdly, an active control system is proposed to attenuate periodically time-varying vibration. It is characterized by an adaptive process for system identification and a nonadaptive process for controller design to avoid the coupling effect between the two adaptive processes in many AVC systems. The convergence and the stability of proposed system are proved by rigorous derivation and numerical simulation.

# Publications Arising from the Thesis

## **Published and accepted journal papers**

J. Wang, C. M. Mak, Y. Yun, A methodology for direct identification of characteristic wave-types in a finite periodic dual-layer structure with transverse connection. *Journal of Vibration and Control* (2011). DOI: 10.1177/1077546311419699.

J. Wang and C. M. Mak, An indicator for the assessment of isolation performance of transient vibration, *Journal of Vibration and Control* (2012). DOI: 10.1177/1077546312458135.

## **Conference papers**

J. Wang and C. M. Mak, A power transmissibility approach for evaluating the performance of transient vibration isolation, *In the 19th International Congress on Sound and Vibration*, Vilnius, Lithuania, 2012, pp.214 - 220.

## **Papers under review**

J. Wang and C. M. Mak, An active vibration control system for periodically time-varying systems, Submitted to *Applied Acoustics* (2013).

J. Wang and C. M. Mak, Adaptive-passive vibration isolation between non-rigid machines and non-rigid foundations using a dual-beam periodic structure with SMA transverse connection, Submitted to *Journal of Sound and Vibration* (2013).



# Acknowledgements

I am honored to take this opportunity to express my gratitude to all people supporting and encouraging me during the period of the three-year Ph. D research.

First of all, I sincerely offer my appreciation and respect to my supervisor, Prof. Mak Cheuk-ming, who has supported me with his valuable guidance and warm encouragement throughout my three-year study.

I would also like to express the gratitude to Prof. Zhang Zhiyi, who was the supervisor of my Mphil program during the period between 2006 and 2009 in Shanghai Jiao Tong University, and has provided constructive advices to my Ph.D research work.

Finally, I would like to sincerely thank all the members in our research group, especially Dr. Yun Yi. All of them are my friends and provided me with their kindness and affection. Besides, I cannot end without thanking my intimate friends, especially Shi Xiaofeng and Wang Xiaonan, who are always supportive throughout my study and personal life. Last but not least, all tutors and members in the BoYi Dance Club have my gratitude for their warm-hearted dedication and cooperation.

# Nomenclature

$d(n)$	Primary disturbance applied on a system
$D_{kN}$	Mean-square deviation (MSD) in the $k^{th}$ period of a periodically time-varying system
$e(n)$	Present identification error with additive noise
$e_f(n)$	Tuned present identification error
$\tilde{e}(n)$	Predicted identification error
$\tilde{e}_f(n)$	Tuned predicted identification error
$E$	Young's modulus
$f(\cdot)$	Self-tuning function of the active control system
$\mathbf{F}_L$	Column vector of general forces including forces and moments of the foundation
$\mathbf{F}_{MU}$	Column vector of general forces including forces and moments of the mount at the interface of the mount and the foundation
$\mathbf{F}_{ML}$	Column vector of general forces including forces and moments of the mount at the interface of the mount and the foundation
$\mathbf{F}_U$	Column vector of general forces including forces and moments of the machine
$\mathbf{F}_{Ue}$	Column vector of the external excitations

$\mathbf{F}_{Uc}$	Column vector of internal forces of the machine
$\mathbf{G}_L$	Matrix of mobilities of the foundation
$H_c$	Controller
$H_r$	Reference path
$H_s$	Secondary path
$H_{po}$	Primary path
$H_p$	Equivalent primary path of $H_{po}$ .
$\mathbf{H}_U$	Matrix of mobilities of the machine
$P_s$	Power transmitted to the floor with a spring isolator
$P_{ns}$	Power transmitted to the floor without a spring isolator
$\mathbf{P}_{wv}$	Matrix governing wave propagation
$r(n)$	Reference signal
$\mathbf{S}_{FV}$	Matrix of the relation between wave motion and vibration
$\mathbf{T}$	Transfer matrix of one periodic cell from the machine to the foundation
$\mathbf{T}_{m+1,m}^{fin}$	Relation between $\mathbf{Y}_{m+1,j}$ and $\mathbf{Y}_{mj}$
$\mathbf{Tr}_{m+1,m}^{fin}$	Transfer matrix from the $m^{th}$ junction to the next junction of a finite periodic structure
$\mathbf{Tr}^{fin}$	Common matrix of $\mathbf{Tr}_{m+1,m}^{fin}$
$\mathbf{T}^{fin}$	Common matrix of $\mathbf{T}_{m+1,m}^{fin}$
$\mathbf{T}$	Force transmissibility

$t_1$	Duration of a transient vibration
$u(n)$	Control signal
$v(n)$	Additive noise
$\mathbf{V}_L$	Column vector of general velocities including translations and rotations of the foundation
$\mathbf{V}_{MU}$	Column vector of general velocities including translations and rotations of the mount at the interface of the mount and the foundation
$\mathbf{V}_{ML}$	Column vector of general velocities including translations and rotations of the mount at the interface of the mount and the foundation
$\mathbf{V}_U$	Column vector of general velocities including translations and rotations of the machine
$\hat{\mathbf{w}}_{po}(n)$	Finite impulse response (FIR) adaptive estimator of $H_{po}$
$\hat{\mathbf{w}}_s(n)$	FIR adaptive estimator of $H_s$ .
$\mathbf{w}(n)$	Optimal FIR estimator of the primary and secondary paths of the controlled system
$\hat{\mathbf{w}}(n)$	Real-time FIR estimator of the primary and secondary paths of the controlled system
$\mathbf{Y}_{mj}$	Matrix of mobility from forces at $j^{th}$ junction to velocities at $m^{th}$ junction of a finite periodic structure
$\mathbf{W}$	Matrix coupling the sub-structures in a periodic cell

$y(n)$	Output of a controlled system
$\hat{y}(n)$	Estimated output of a controlled system
$\mathbf{Z}_M^{(k)}$	Transfer matrix of the $k^{\text{th}}$ mount from the foundation to the machine
$\mathbf{Z}_M$	Transfer matrix of all mounts from the foundation to the machine
$\mathbf{Z}_{mj}$	Matrix of transfer function from forces at $j^{\text{th}}$ junction to forces at $m^{\text{th}}$ junction of a finite periodic structure
$\chi$	Transient power transmissibility
$\varepsilon_n$	Model error
$\hat{\varepsilon}_n$	Approximated model error
$\gamma$	Steady-state power transmissibility
$\eta$	Loss factor
$\mu$	Adjustable parameter in adaptive algorithms
$\nu$	Poisson's Ratio
$\rho$	Density
$\tau_n$	Natural period of the oscillator
$\omega$	Angular forcing frequency
$\omega_n$	Angular natural frequency
$\xi(n)$	Identification error without additive noise

# Table of Contents

<b>Certificate of Originality .....</b>	<b>I</b>
<b>Dedication .....</b>	<b>II</b>
<b>Abstract.....</b>	<b>III</b>
<b>Publications Arising from the Thesis.....</b>	<b>V</b>
<b>Acknowledgements .....</b>	<b>VI</b>
<b>Nomenclature.....</b>	<b>VII</b>
<b>Table of Contents .....</b>	<b>XI</b>
<b>List of Figures .....</b>	<b>XIV</b>
<b>List of Tables .....</b>	<b>XVIII</b>
<b>Chapter 1.....</b>	<b>1</b>
<b>Introduction .....</b>	<b>1</b>
1.1 Background .....	1
1.2 Performance Indicators of Vibration Isolation .....	3
1.3 Broadband Vibration Control of Non-rigid Systems Using Periodic Structures.....	5
1.4 Active Control of Periodically Time-varying Systems .....	10
1.5 Objectives and Scope of Research .....	13
<b>Chapter 2.....</b>	<b>16</b>
<b>An Indicator for the Assessment of Isolation Performance of Transient Vibration .....</b>	<b>16</b>
2.1 Theoretical Outline.....	17
2.1.1 <i>Performance Index for Steady Vibration Isolation – the Force and         Steady-State Power Transmissibility .....</i>	<i>18</i>
2.1.2 <i>Performance Index for Transient Vibration Isolation – the Shock</i>	

<i>Response Spectrum and Transient Power Transmissibility</i> .....	19
2.2 Numerical Simulation and Analysis .....	23
2.2.1 <i>Case One – A Constant Excitation with Rising Time</i> .....	25
2.2.2 <i>Case Two –A Triangular Pulse</i> .....	30
2.3 Summary .....	34
<b>Chapter 3</b> .....	<b>35</b>
<b>Adaptive-Passive Vibration Isolation between Non-Rigid Machines and Non-Rigid Foundations Using a Dual-Beam Periodic Structure with SMA Transverse Connection</b> .....	<b>35</b>
3.1 The Governing Equation of Transmitted Vibration.....	36
3.1.1 <i>A linear time-invariant (LTI) system</i> .....	37
3.1.2 <i>A system with linear time-varying (LTV) substructures</i> .....	41
3.2 Vibration Control Using SMA Components in a Periodic Structure.....	44
3.2.1 <i>A Database Method for Static Regulation</i> .....	45
3.2.2 <i>Frequency-domain Steepest Gradient Method for Real-time Calculation</i> .....	47
3.3 The Semi-two-dimensional Model.....	55
3.4 Numerical Simulation and Analysis .....	60
3.5 Experimental Study .....	70
3.5.1 <i>Junction mobilities</i> .....	71
3.5.2 <i>The relation between Transition and Transfer Matrices of Finite Periodic Structures and Characteristic Waves</i> .....	73
3.5.3 <i>Experiment</i> .....	79
3.6 Summary .....	87
<b>Chapter 4</b> .....	<b>90</b>
<b>An Active Vibration Control System for Periodically Time-varying Systems</b> .....	<b>90</b>
4.1 Background Information and Objectives .....	91

4.2 System Identification.....	93
4.2.1 Derivation of Online Path Modeling Algorithm .....	93
4.2.2 Analysis of robustness by $H_\infty$ criterion [79] .....	97
4.2.3 Constructing the self-tuning function $f(\cdot)$ .....	100
4.3 Controller Design .....	102
4.4 Numerical Simulation and Analysis .....	104
4.5 Summary .....	108
<b>Chapter 5.....</b>	<b>110</b>
<b>Conclusions and Suggestions for Future Work .....</b>	<b>110</b>
5.1 Conclusions .....	110
5.2 Suggestions for Future Work.....	114
<b>References .....</b>	<b>117</b>



# List of Figures

Figure 2-1 Model of a vibration isolation system.....	17
Figure 2-2 Shock response spectrum [38].....	20
Figure 2-3 Steady-state power transmissibility .....	24
Figure 2-4 Two typical excitations [38]: (a) Constant with a rise in time, (b) Triangular pulse. .....	25
Figure 2-5 Maximum peak power for the 1 <sup>st</sup> case .....	26
Figure 2-6 Transient transmissibility for the 1 <sup>st</sup> case.....	26
Figure 2-7 Maximum peak powers in two frequency bands for the 1 <sup>st</sup> case: (a) Maximum peak power in the low-frequency band; (b) Maximum peak power in the high-frequency band.....	28
Figure 2-8 Transient power transmissibility in two frequency bands for the 1 <sup>st</sup> case: (a) Transient power transmissibility in the low-frequency band; (b) Transient power transmissibility in the high-frequency band.....	29
Figure 2-9 Maximum peak power for the 2 <sup>nd</sup> case.....	31
Figure 2-10 Transient power transmissibility for the 2 <sup>nd</sup> case .....	31
Figure 2-11 Maximum peak powers in two frequency bands for the 2 <sup>nd</sup> case: (a) Maximum	

peak power in the low-frequency band; (b) Maximum peak power in the high-frequency band.....	32
Figure 2-12 Transient power transmissibility in two frequency bands for the 2 <sup>nd</sup> case: (a) Transient power transmissibility in the low-frequency band; (b) Transient power transmissibility in the high-frequency band.....	33
Figure 3-1 A general vibration isolation system with periodic mounts .....	37
Figure 3-2 The semi-two-dimensional system (a) and the compared system (b).....	56
Figure 3-3 Enveloping lines ( <b>—</b> ) and transmission losses when $E_N = 83.1$ Gpa and $\rho_N = 2000$ kg: (a) Vertical force and identical branches; (b) Vertical force and disordered branches; (c) Moment and identical branches; (d) Moment and disordered branches; (e) Horizontal force and identical branches; (f) Horizontal force and disordered branches.....	66
Figure 3-4 Enveloping lines ( <b>—</b> ) and transmission losses when $E_N = 8.31$ Gpa and $\rho_N = 200$ kg: (a) Vertical force and identical branches; (b) Vertical force and disordered branches; (c) Moment and identical branches; (d) Moment and disordered branches; (e) Horizontal force and identical branches; (f) Horizontal force and disordered branches.....	67


Figure 3-5 Enveloping lines (  ) and transmission losses when  $E_N = 8.31$  Gpa and  $\rho_N = 2000$ kg: (a) Vertical force and identical branches; (b) Vertical force and disordered branches; (c) Moment and identical branches; (d) Moment and disordered branches; (e) Horizontal force and identical branches; (f) Horizontal force and disordered branches..... 68




Figure 3-6 Enveloping line in the situation of disordered branches (  ), enveloping line in the situation of identical branches (  ), and the transmission loss in the situation of no branches (  ): (a) Enveloping lines from Fig. 3-3(a) and Fig. 3-3(b); (b) Enveloping lines from Fig. 3-4(a) and Fig. 3-4(b); (c) Enveloping lines from Fig. 3-5(a) and Fig. 3-5(b)..... 69

Figure 3-7 Experimental system..... 80

Figure 3-8 Finite dual-layer periodic structure..... 82

Figure 3-9 Comparison of horizontal mobility of the sixth junction: (---) experiment; (—) theoretical prediction ..... 83

Figure 3-10 Comparison of vertical mobility of the sixth junction: (---) experiment; (—) theoretical prediction ..... 84

Figure 3-11 Comparison of rotational mobility of the sixth junction: (---) experiment; (—) theoretical prediction ..... 84

Figure 3-12 Attenuation constants of symmetrical characteristic wave-types: (—) experiment; (---) theoretical prediction.....	86
Figure 3-13 Attenuation constants of antisymmetrical characteristic wave-types: (—) experiment; (---) theoretical prediction.....	87
Figure 4-1 Block diagram of a typical AVC system: (a) The original system, (b) The equivalent system.....	93
Figure 4-2 The AVC system.....	105
Figure 4-3 Control performance with the self-tuning mechanism: (a) Time domain, (b) Frequency domain.....	107
Figure 4-4 Control performance without the self-tuning mechanism .....	108
Figure 4-5 Control performance after encountering a shock.....	108

# List of Tables

Table 3-1 The structural parameters of the systems in Fig. 3-2.....	61
Table 3-2 The parameters of each periodic element of the experimental structure.....	81

# Chapter 1

## Introduction

### 1.1 Background

People are now very concerned about the problems of machine-induced noise and vibration, especially those problems in modern buildings, as they relate to general well-being and comfort. Due to the concerns, a great number of studies have been conducted to investigate these problems [1-10]. Yun [1-2] has examined the coupled flexural-longitudinal wave propagation in building structures through a semi-two-dimensional multi-layer periodic structure, and then investigated the vibration transmission from two coherent machines to a two-floor (two-layer) building structure. Ou [3-4] has studied the vibroacoustic responses of plate-like structures which serve as the fundamental representation of realistic structures, such as walls, floors and ceilings of buildings. Wang [5-7] has proposed a periodic duct loaded by Helmholtz resonators and developed its application to broadband noise control and ventilation. Mak et al. [8-10] has studied the flow-generated noise produced by in-duct elements, and the flow noise in air ducts is a significant problem in a ventilation systems. Their extensive studies of vibratory and acoustic behavior of building structures and building services structures inspire this author to

investigate other problems for the same purpose of general health and well-being.

This study is devoted to providing solutions to the fundamental problems resulted from the common characteristics of building services equipment, which pose great challenges to current methods of vibration control. Many building services equipment undergo transient excitations, like frequent starting and stopping operation, but existing references focus on the study of steady-state vibration isolation [11-18]. Besides, methods for the broadband vibration control of non-rigid machines and foundations are desirable in the situation of fluctuating frequency of interest and high modal density of the foundation. The frequency of interest may be the frequencies of a disturbance and the resonances of the vibratory system. A welcomed solution may be periodic structures, a class of band-stop filter-type mechanical isolators [19] which place the frequency of interest in certain frequency bands (stop bands) where the characteristic waves decay exponentially and thus mechanical wave propagation is suppressed. However, the traditionally simplified models (including the models using periodic structures as isolators) neglect the coupling between directions of motion at mounting points, which may lead to erroneous prediction of structural dynamics [20-31]. In addition, active vibration control approaches applicable for time-varying systems [32-34] is expected when the assumption of these systems as time-invariant models cannot be satisfied. The

difference between a time-varying system and a time-invariant system is manifested by the analysis of a periodically time-varying system [35]. This difference may be a positive property in some other areas [36-37], but may result in the invalidity of many active vibration control (AVC) algorithms based on that assumption of the time-invariant system. These three problems are not only limited to building services equipment, but widely exist in the research field of machine-induced noise and vibration.

## **1.2 Performance Indicators of Vibration Isolation**

Building services equipment is one of the common vibratory and acoustic sources within structures. Vibration isolation plays an important role in controlling this noise because the structure-borne sound radiation emanating from the floor where the vibratory machine is located is a significant source of it. The performance of vibration isolation in an industrial context has commonly been assessed using the force transmissibility [11-13] in the situation where there is negligible floor mobility. Given this limitation, power transmissibility was then proposed. This index assesses the performance of vibration isolation by taking into account the effect of floor mobility and the interaction of the mounting points between machine and floor [14-18]. However, both the force and power transmissibility approaches only consider the steady-state vibration problem.



In reality, building services equipment often experiences a transient excitation, a rapid enhancement of vibration energy followed by an abrupt release. For example, a potable water pump in a water supply system will start and stop frequently, and a standby generator will start operating suddenly in an emergency. Although the power transmissibility proposed by Mak [14] can evaluate the performance of the steady-state vibration isolation more accurately than force transmissibility, it may not be effective to assess the performance of transient vibration isolation, since the index does not take any transient excitation into consideration. In a transient vibration context, the maximum peak response (that is, the maximum of peaks on the time response curve) is of particular interest. The shock response spectrum is defined as a plot of the maximum peak response of a single-DOF oscillator against its natural period [38-39], which is a measure of the influence of transient excitations on the isolated structure. Nonetheless, like the definition of the force transmissibility, the shock-response spectrum also adopts the assumption of an immovable floor. Moreover, the parameter used in the shock response spectrum to measure the severity of impacts is not as accurate as transmitted power to the floor in terms of predicting the structure-borne sound radiation.

## **1.3 Broadband Vibration Control of Non-rigid Systems Using Periodic Structures**

The investigation of the problem of vibration isolation between nonrigid machines and/or foundations has a long history. Many authors simplify it by assuming the machine-isolator-foundation arrangement is a single-mount system [20-22]. This assumption is only valid where the system is symmetrical and moves with a unidirectional translation, and also where there is decoupling between the mounting points for both the mounted object and the foundation [23]. Erroneous resonances are observed, however, when this assumption is applied to the analysis of the vibration transmission between nonrigid machines and foundations [23]. Owing to the limitations of the single-mount assumption, other authors have investigated the effect of multiple mounts on vibration transmission [24-26]. Despite the inclusion of the transfer mobility between the mounting points, only the translational motion normal to the surface of the foundation is considered in these multi-mount systems. Moments, and their cross coupling with forces, are also omitted in these studies, thus preventing the energy exchange between wave components governed by such cross coupling and resulting in different wave transmission and reflection at the mounting points. Several researchers have also studied the effect of moments, or combined forces and moments, on the total power transmission to a flexible structure and drawn helpful conclusions [27-31]. White and Goyder [27-28] show that the power

resulting from a moment excitation to a beam or plate is more severe in the high-frequency region than that caused by a force excitation. If the location of the excitation source is at or close to a discontinuity, Petersson and Gibbs [29-30] find that moment excitation plays an important role in vibrational energy transmission, even at low frequencies. Additionally, Koh and White [31] demonstrate that by optimizing the moment arms, the power due to the combined force and moment input to the foundations, at low to medium frequencies, might be smaller than that from a force alone. Therefore, it is suggested that it would be valuable to consider the coupling of forces and moments and the multiple directions of motion at every mounting point during the analysis of vibration isolation problems so that the resultant energy exchange will not be neglected.

A periodic structure, or a spatially periodic structure, is composed of a number of identical structural components which are coupled together side-by-side (like in a bridge) or layer-by-layer (like in a building) to form a whole complex. Periodic structures can be divided into three classes [40] 1) the periodic medium, for example, the periodically supported beams [1]; 2) the periodically inhomogeneous medium, like a fluid with its ambient density or sound speed varying periodically [40]; 3) the periodically bounded medium, for instance, the air duct loaded periodically with Helmholtz resonators [5]. This type of structures has been studied for many decades

because of the interesting wave phenomenon – wave propagation is allowed in some frequency bands (called pass bands) while is forbidden in other bands (called stop bands). In stop bands, or band gaps, characteristic waves decay exponentially in the near field of the driving point and thus cannot generate the propagation of mechanical waves. The studies of periodic structures mainly focus on two aspects - the theoretical solution of the characteristic waves and application of the pass-band or stop-band property. The approaches to study characteristic waves are various, including the two most common methods - transfer matrix method [1, 5] and propagation wave method [41-43], Z-transform method, energy method and Fourier transform method [44]. However, compared to the abundant literatures of these systematic approaches for characteristic waves, the studies of the application seem less extensive.

Periodic structures, as alternatives to the rubber-like isolators (springs or rubber rods with stiffness and damping, as used in the research referred to above), are more useful when the system has high modal density or is excited by a source with wideband or fluctuating frequency [45]. This is because the band-gap characteristic of periodic structures guarantees that the attenuation ability of periodic mounts cannot be affected by these factors, provided they are located in the stop bands. Besides, although rubber-like mounts can attenuate vibration in a wide frequency

band (from the natural frequency to high frequency), and although vibration absorbers or other anti-resonance vibration isolators may realize broadband control if active or passive-adaptive control is applied [19], it is much likely that the transmission loss due to these structures is significantly lower than that due to periodic isolators since periodic isolators can lead to the exponential attenuation of characteristic waves. Nonetheless, when the operating and environmental conditions change, the fixed stop bands may no longer cover the change in frequency of interest, for example, a fluctuating exciting frequency or a variation in resonances of systems; the original stop bands may become pass bands of the current frequency of interest, making the isolator a band-pass filter. Hence, researchers are working towards the design of periodic structures with broad stop bands [46-49] or the development of periodic structures with controllable or tunable parameters such that their band-gap characteristic can be adjusted [50-51]. Arish [50] proposes a 1-D hybrid periodic rod composed of several periodic cells with a short rod and piezoelectric insert in each, and install four parallel hybrid periodic rods between two plates to control the vibration transmission from the upper to the lower plate. A new type of periodically layered isolator with embedded fluid elements is developed by Szefi [51] and applied to minimize the vibratory power transmission from meshing gear pairs to fuselage. Many other reports of the utilization of smart periodic structures, periodic structures with smart materials as their tunable components, can now be found in the field of

control of structural wave propagation [52-53]. All of the work [45-53] focuses on the isolation of power transmission solely via unidirectional translation or the attenuation of a longitudinal wave along the waveguide.

A semi-infinite dual-beam periodic structure with all degrees of freedom (DOF) of motion in a plane is proposed by Yun and Mak [1], but its application as a periodic isolator has not yet been explored. This study therefore focuses on developing passive control methods for the application of this semi-two-dimensional structure to broadband vibration isolation and exploring the problem of broadband vibration control using periodic structures. To adjust and widen the stop bands, shape memory alloy (SMA) components are incorporated into the periodic structure. The reason for this is that the Young's modulus of the SMA can be increased to three times its original value on a change of temperature, due to crystalline phase transformation [50-51, 54]. With this property, it is possible to create a stop band covering the frequency band of interest by tuning the Young's moduli of the SMA components. The limitation of SMA for vibration control is the problem of hysteresis [55-56]. The hysteresis may be desirable in other applications, but generally should be mitigated or avoided in the application of vibration control because it may destabilize the control system.

## 1.4 Active Control of Periodically Time-varying Systems

This study focuses on one special category of time-varying system - periodically time-varying (PTV) systems. PTV systems fall into the category of parameter-varying systems whose dynamic parameters change with time or other independent variables [32]. The phenomenon of varying dynamic parameters can be found in various fields [32-34]; for instance, some parameters of unsymmetrical rotating machines vary with time, and the propagation parameters of wave propagation in periodic media vary with distance. This class of structures is governed by differential equations of motion with PTV coefficients, making the systems exhibit remarkable dynamics which is difficult to control. Take linear periodically time-varying (LPTV) systems as an example. According to Claasen and Mecklenbräuker's review [35], the input-output relation for LPTV systems is  $X_{lptv}(f) = \sum_{k=-\infty}^{k=\infty} H_k(f - k/T)F(f - k/T)$ . The input-output relation for LPTV systems shows that the input spectrum  $F(f)$  has an infinite number of shifted versions  $F(f-k/T)$ , where  $T$  is the period of the parametric variation. Consequently, the output spectrum  $X_{lptv}(f)$  is composed of the weighed input spectrum  $F(f)$  and its shifted versions at other frequency values. That is to say, an LPTV system is different from a linear time-invariant (LTI) system in which the response at one frequency only comes from the input spectrum at the same frequency: for example,  $X_{li}(f) = H(f)F(f)$ . As a

result,  $X_{ptv}(f)$  is characterized by a series of separate peaks with an interval of  $1/T$  at the two sides of one frequency because a peak at that frequency can be moved to other frequencies and create those side peaks at  $f-k/T$ . This difference can be utilized for active control, such as feedback control incorporating PTV components [36-37]. However, this study focuses on the active control of PTV systems, and this difference may lead to the invalidity of many active vibration control (AVC) algorithms designed by ignoring the oscillation of time-varying parameters and the resultant side peaks. The situation becomes worse if the systems are nonlinear. Therefore, much research effort has been devoted to the active control of time-varying systems [57-59]. Most of the control schemes are dependent on a mathematical or estimated model and cannot converge the moment the model is obtained.

Online modeling is usually required for AVC because of the difficulty of measuring or recovering systematic parameters and the possible inapplicability of some promising methods (AVC methods without modeling) to a high-order system [60-61]. The time-varying characteristic of some systematic parameters may require a typical AVC system with a fast online modeling process to catch up on systematic changes and an efficiently updated controller to create destructive vibration. Hence, the filtered-x least mean squares (FXLMS) method, characterized by low computational



cost and easy implementation, is potentially a competent candidate for the real-time control of time-varying systems. However, it is very difficult to analyze the coupling effects between the two adaptive processes – online modeling and controller updating. On one hand, the performance of one process may negatively influence the other process, leading to accumulated errors, amplified vibration, and destabilized systems [62]. On the other hand, after one process converges, it may take several samples for the other process to converge. This mismatch in terms of the convergence of the two processes makes it hard to tell whether they converge to their optimal values under the present systems situation.

Given the above disadvantages, in the most recent literature, an active noise control (ANC) system (orthogonal adaptation system) with adaptive system identification and nonadaptive controller design was proposed by Yuan to avoid the coupling effect [63-64]. Although the applicability of this ANC system is limited in time-invariant systems or approximately time-invariant systems, it provided the motivation for this study to propose a control system with adaptive system identification and nonadaptive controller design for PTV systems. Later, Yuan presented a self-learning feedback mechanism, and this mechanism could work as a backup for the orthogonal adaptation system [65]. When the stability threat due to modeling errors is detected, the orthogonal adaptation block is switched off and the feedback block is triggered to

stabilize and optimize the system without using the estimated model. Nonetheless, this trial-and-error method inevitably leads to slow convergence and may induce the intermittent switch between the two blocks when controlling a time-varying system. Therefore, it would be better if a wide range of dynamic uncertainties and external disturbances could be tuned and tolerated inside one control system, leaving other ones which may not commonly happen to the backup system.

## **1.5 Objectives and Scope of Research**

The principle objective of this thesis is to abate the influence of the machine-induced noise and vibration on general health and comfort by providing possible solutions to the problems of transient vibration isolation, broadband vibration control and vibration control of time-varying systems. This main objective has the following sub-objectives.

The first sub-objective of this thesis is to present a new performance indicator for the assessment of transient vibration isolation. Based on the discussion about performance indicators of vibration isolation, it is known that force transmissibility and the steady-state power transmissibility may be incapable of predicting the isolation performance of transient vibration because the applied models do not consider transient excitation. However, the indicator, shock response spectrum,

considers transient excitation and uses the maximum peak response to assess the severity of the effect of the rapid enhancement and abrupt release of energy caused by a transient excitation, which provides a clue to the proposal of the new performance indicator in spite of its assumption of immovable floor.

The second sub-objective of this thesis is to examine the problem of the broadband vibration control of nonrigid systems employing periodic structures with tunable parameters. It investigates this by using a semi-two-dimensional model that applies a dual-beam periodic structure [1] with SMA transverse branches as a parameter-tunable isolator. Given the previous literature review, it is known that conventional study of vibration control problems, including the problem of vibration control by periodic structures, usually reduces systems to equivalent single- or multi-mount models with only a unidirectional translation at a mounting point. This assumption of decoupling leads to the erroneous prediction of vibratory power transmission when designing an isolator for a nonrigid system. Such a periodic structure involves the coupling of vibrations between different mounting points and different directions of motion and is therefore a reasonable simulation of the real-life problem. Measures will be taken to make best use of the variable material property of SMA and avoid the associated limitation of hysteresis.

The third sub-objective of this thesis is to propose an active vibration control system for periodically time-varying systems. Considering the coupling effect between the two adaptive processes of online modeling and controller optimization, and motivated by Yuan's work [63-65], the objective of this study is to apply this decoupling scheme to the active vibration control of PTV systems. The new AVC system for PTV systems proposed in this study will bear the following features. It will consist of one adaptive process for system identification and one nonadaptive process for controller optimization to avoid the coupling effect. Besides, the identification process will be able to suppress the negative influence of dynamic uncertainties and disturbances and exhibit strong robustness to them. Finally, the convergence of one adaptive process and the optimization of the nonadaptive process will be synchronized.

## **Chapter 2**

# **An Indicator for the Assessment of Isolation Performance of Transient Vibration**

In this chapter, the concept of “transient power transmissibility” is proposed as a means of assessing the performance of isolators due to a transient vibration excitation. It is a function of the duration of the transient excitation and the natural period of the oscillator. Like the definition of the shock response spectrum [38-39], it is a measure of the severity of the impact of the rapid enhancement and abrupt release of energy. The transient power transmissibility is based on the ratio of powers within the whole frequency domain. The powers can be decomposed into a series of sub-powers in separate frequency bands, which can be easily realized by wavelet transform and reconstruction [66] so as to reveal the contribution that different modes and frequency distributions of the transient excitation make to the response. A spring-mass-movable floor system is considered in the simulation, and the spring isolator is first selected using the steady-state power transmissibility approach of Mak and Su. A system disturbed by two transient excitations as typically experienced by building services equipment is then analyzed. The results indicate the necessity of using transient power transmissibility in the selection of isolators for a transient

vibration.

## 2.1 Theoretical Outline

A vibration isolation system is described in Fig.2-1. Damping moves a resonant frequency from  $\omega_n$  to  $\omega_d = \omega_n \sqrt{1 - \zeta^2}$ , and attenuates the resonant peaks. It does not fundamentally change the modes of the vibratory system. Therefore, for the assessment of a spring isolator, adding damping only causes unnecessary distractions without affecting the analytical results. Hence, the stiffness is modeled as a real number and the damping effect is not considered in this study. Besides, if there is a need to consider damping, the influence of damping can be included by modeling the stiffness as a complex number.

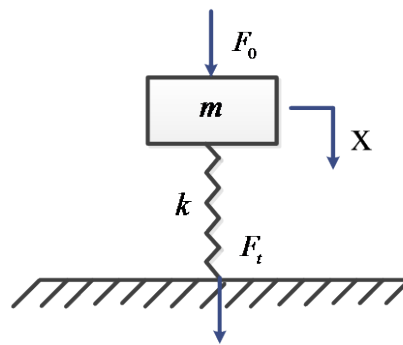


Figure 2-1 Model of a vibration isolation system

## 2.1.1 Performance Index for Steady Vibration Isolation – the Force and Steady-State Power Transmissibility

For the vibration isolation system modeled in Fig. 2-1, the force transmissibility,  $T$ , is usually adopted to evaluate the performance of vibration isolation [11-13]:

$$T = \left| \frac{F_t}{F_0} \right| = \frac{1}{\left| 1 - \left( \frac{\omega}{\omega_n} \right)^2 \right|} \quad (2.1)$$

where  $\omega_n$  is the angular natural frequency;  $\omega$  is the angular forcing frequency;  $F_0$  is the exciting force; and  $F_t$  is the force transmitted from the vibrating machine to the floor structure when the floor is assumed to be immovable, formulated by:

$$F_t = \frac{1}{1 - (\omega / \omega_n)^2} F_0.$$

In order to take into account the effect of floor dynamics and the interactions of mounting points between the floor and the machine, the steady-state power transmissibility [14-18],  $\gamma$ , is proposed as follows:

$$\gamma = \left| \frac{P_s}{P_{ns}} \right| = \left| \frac{1 + j\omega m Y_r}{1 - (\omega / \omega_n)^2 + j\omega m Y_r} \right|^2 \quad (2.2)$$

where

$$P_s = \frac{1}{2} \frac{1}{\left| 1 - (\omega / \omega_n)^2 + j\omega m Y_r \right|^2} |F_0|^2 \operatorname{Re}(Y_r)_s \quad \text{and} \quad P_{ns} = \frac{1}{2} \frac{1}{\left| 1 + j\omega m Y_r \right|^2} |F_0|^2 \operatorname{Re}(Y_r) .$$

$P_s$  and  $P_{ns}$  are the powers transmitted to the floor with and without a spring

isolator;  $Y_r$  denotes the floor mobility.

When  $|j\omega m Y_r| \ll 1$  and  $|j\omega m Y_r| \ll |1 - (\omega / \omega_n)^2|$ , the steady-state power transmissibility can be approximately equal to the force transmissibility:

$$\gamma \approx \frac{1}{|1 - (\omega / \omega_n)^2|^2} = T^2$$

Therefore, the condition that force transmissibility is less than unity when  $\omega / \omega_n > \sqrt{2}$  does not mean that a satisfactory power transmissibility is guaranteed.

The limitation of this method is that it neglects the transmitted displacement of the floor structure and the interaction of mounting points. In the power transmissibility method, however, the transmitted power can directly indicate the structure-borne sound radiation.

## **2.1.2 Performance Index for Transient Vibration Isolation – the Shock Response Spectrum and Transient Power Transmissibility**

Although the steady-state power transmissibility can effectively describe the alleviation or deterioration of the structure-borne sound problem in a given frequency domain, it may not be able to predict the isolation performance of a transient vibration, since the index does not consider any transient excitation. In a



transient vibration scenario, the maximum of peaks on the time response curve (that is, the maximum peak response) is of particular interest since it can measure the severity of the induced vibration during the rapid enhancement and abrupt release of energy in the transient excitation. The shock response spectrum is a plot of the maximum peak response of the single-DOF oscillator as a function of the natural period of the oscillator [38]. Specifically, the shock response spectrum  $\left(\frac{x}{F_0/k}\right)_{max}$  is plotted as a function of  $t_1/\tau_n$  where  $\tau_n$  is the natural period, as shown in Fig. 2-2. Similar to the force transmissibility, the shock-response spectrum is based on the assumption of an immovable floor. Furthermore, as the transmitted power is closer to the structure-borne sound radiation, it cannot be indicated accurately by the parameter used in the shock response spectrum.

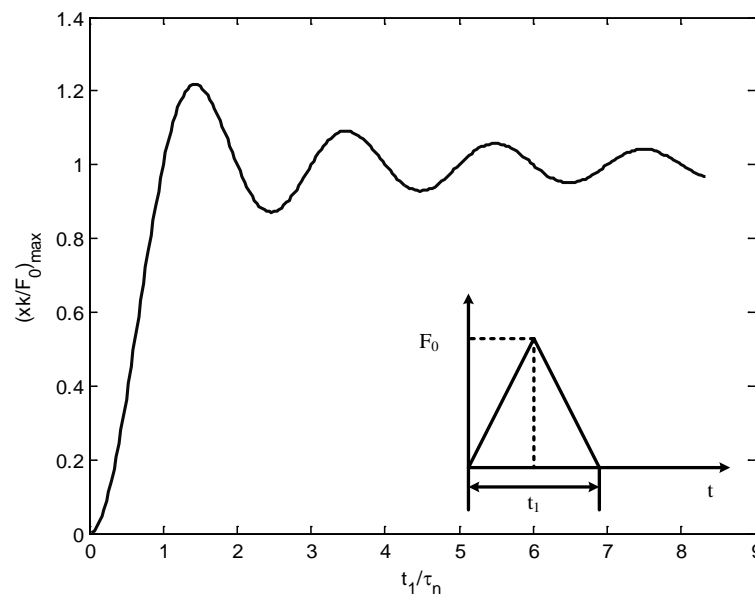


**Figure 2-2 Shock response spectrum [38]**

Therefore, a new performance index, the transient power transmissibility, is defined here as the ratio between the transmitted maximum peak powers with and without the installation of the vibration isolator. That is:

$$\chi = \frac{Mp_s(t_1 / \tau_n)}{Mp_{ns}(t_1 / \tau_n)} \quad (2.3)$$

where

$$\begin{cases} Mp_s(t_1 / \tau_n) = \max(p_s(t, t_1 / \tau_n)) \\ Mp_{ns}(t_1 / \tau_n) = \max(p_{ns}(t, t_1 / \tau_n)) \end{cases},$$

where  $p_s$  and  $p_{ns}$  are the time-domain equivalents of the frequency-domain powers  $P_s$  and  $P_{ns}$  in Eq. (2.2), when the excitation is a transient vibration with a duration of  $t_1$  and the initial values are zeros;  $\tau_n = 2\pi / \omega_n$  is the natural period of the oscillator.

A time-domain power can be easily decomposed into several subpowers in the time domain and rendered equal to the superposition of them by wavelet transform and reconstruction [66]. The  $i^{th}$  subpower corresponds to the  $i^{th}$  frequency band:  $0 \sim \frac{1}{2^N} f_s$  for  $i=1$  and  $\frac{1}{2^{N-i+2}} f_s \sim \frac{1}{2^{N-i+1}} f_s$  for  $i=2, \dots, N$ .  $f_s$  is the sampling frequency and the integer  $N$  is the number of all separate frequency bands, depending on the number of considered modes. After the decomposition, the maximum peak power of each subpower can be obtained, and the transient power transmissibility for  $i^{th}$  frequency band is acquired by Eq. (2.4):

$$\chi_i = \frac{Mp_s(i, t_1/\tau_n)}{Mp_{ns}(i, t_1/\tau_n)}, i = 1, 2 \dots N \quad (2.4)$$

where  $Mp_s(i, t_1/\tau_n)$  and  $Mp_{ns}(i, t_1/\tau_n)$  are the maximum peak power for the  $i^{th}$  frequency band, described by

$$\begin{cases} Mp_s(i, t_1/\tau_n) = \max(p_{si}(t, t_1/\tau_n)) \\ Mp_{ns}(i, t_1/\tau_n) = \max(p_{nsi}(t, t_1/\tau_n)) \end{cases}$$

and  $p_{si}$  and  $p_{nsi}$  are the subpowers generated by the decomposition of the total transmitted powers  $p_s$  and  $p_{ns}$ .

$$\begin{cases} p_s(t, t_1/\tau_n) = \sum_{i=1}^N p_{si}(t, t_1/\tau_n) \\ p_{ns}(t, t_1/\tau_n) = \sum_{i=1}^N p_{nsi}(t, t_1/\tau_n) \end{cases}$$

In each frequency band,  $\chi_i$  is the function of  $t_1/\tau_n$ . If either  $t_1$  or  $\tau_n$  is fixed, the range of the other parameter can be determined by the constraint  $\chi_i < 1$ . The decomposed powers or the transient power transmissibility in a series of frequency bands as expressed in Eq. (2.4) are useful for the analysis of the influence of different modes and the frequency-domain distribution of the transient excitation.

Two typical cases of transient vibration will be discussed in the next section to demonstrate the importance of the transient power transmissibility. When the upper bound of the duration of transient excitation  $t_1$  is known,  $\chi$  can be used for the selection of a spring isolator because the range of  $\tau_n$  or  $\omega_n$  can be determined. The steady-state power transmissibility  $\gamma < 1$  requires  $\omega_n < \omega_{cy}$  while the transient

power transmissibility  $\chi < 1$  requires  $\omega_n < \omega_{c\chi}$ , where  $\omega_{c\gamma}$  and  $\omega_{c\chi}$  are critical values. Hence, the qualified angular natural frequency should be lower than the minimum of the two critical values, that is,  $\omega_n < \min(\omega_{c\gamma}, \omega_{c\chi})$ .

## 2.2 Numerical Simulation and Analysis

The analysis is conducted using a mass-spring system on a flexible square concrete plate. The physical parameters of the plate are: Young's modulus  $E = 2.1 \times 10^{10} \text{ N/m}^2$ , density  $\rho = 2.8 \times 10^3 \text{ kg/m}^3$ , Poisson's Ratio  $\nu = 0.2$ , and loss factor  $\eta = 2 \times 10^{-2}$ . Its dimensions are 3.5m (length)  $\times$  3.5m (width)  $\times$  0.24m (thickness). Only the first two modes of the plate are considered in the calculation of the mobility [67] because the contribution of the other modes to the transmitted power is negligible by comparison. Hence, the total frequency range is divided into two frequency bands for the decomposition of the transmitted power:  $0 \sim \frac{1}{2} f_s$  and  $\frac{1}{2} f_s \sim \frac{1}{2} f_s$ , where the sampling frequency  $f_s = 600\text{Hz}$ .

If the mass of the machine is 2000kg, the power transmissibility is less than unity at  $\omega / \omega_n > \sqrt{2}$  when the natural frequency of the chosen spring is no more than 7Hz. The steady-state power transmissibility with the natural frequency set at 6Hz, as shown in Fig. 2-3, demonstrates satisfactory vibration isolation performance.

However, this may not be guaranteed when transient excitations are considered. Accordingly, two cases will now be discussed to confirm the need for assessment using the proposed transient power transmissibility. Two typical excitations in the cases are shown in Fig. 2-4. In the first case, a signal with a constant magnitude after a short rise time as shown in Fig. 2-4(a) is adopted to simulate the starting or stopping period of the vibratory machine. In the second case, a triangular pulse as shown in Fig. 2-4(b) is chosen to represent the occasional shocks experienced by the vibratory machine, as this is often a good approximation to actual pulse shapes.

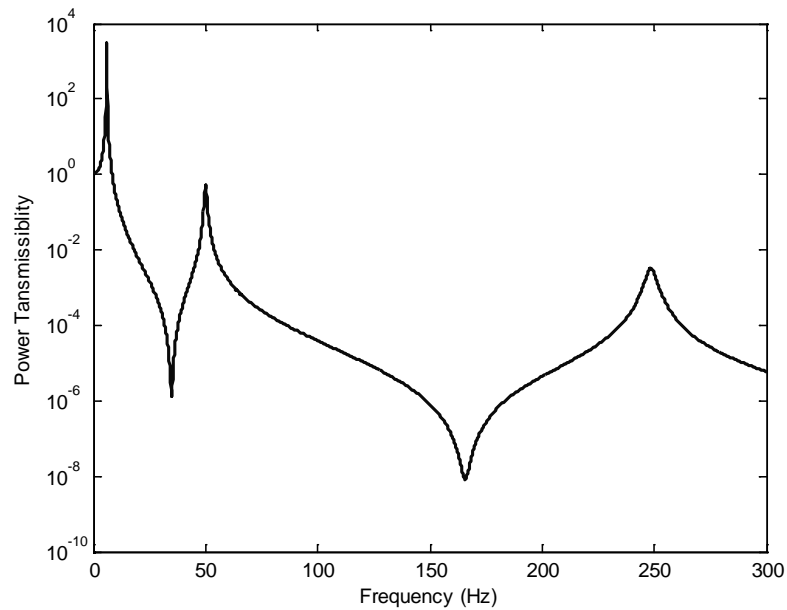


**Figure 2-3 Steady-state power transmissibility**

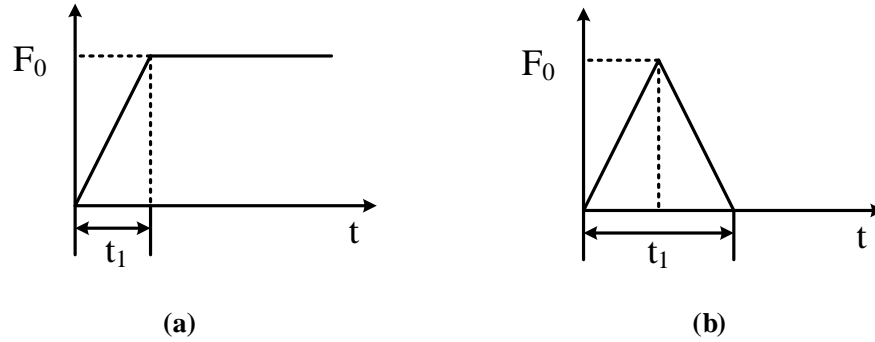


**Figure 2-4 Two typical excitations [38]: (a) Constant with a rise in time, (b) Triangular pulse.**

### 2.2.1 Case One – A Constant Excitation with Rising Time

To investigate the vibration transmission when a vibratory machine experiences a starting or stopping period followed by a steady-state stage, the constant excitation after a short rise time shown in Fig. 2-4(a) is adopted. The maximum peak powers with and without the isolator and the transient power transmissibility in Eq. (2.3) are shown in Figs. 2-5 and 2-6. For vibration isolation to be achieved,  $\chi$  must be less than unity. Thus, according to Fig. 2-6, for the example of an excitation with a constant magnitude after a short rise time, this requires:

$$t_1 < 0.6\tau_n.$$

In other words, when the duration is less than  $0.6\tau_n$ , the design of the spring isolator is acceptable according to the transient power transmissibility. For a known transient input, we can work out the required angular natural frequency,  $\omega_{c\chi}$ . The qualified angular natural frequency will then be lower than the minimum of the two critical values, that is,  $\omega_n < \min(\omega_{c\gamma}, \omega_{c\chi})$ .

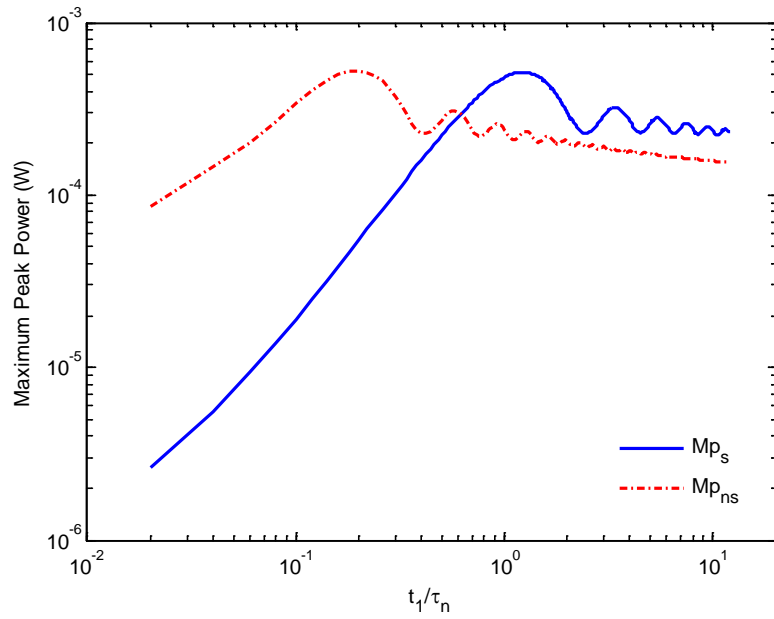


Figure 2-5 Maximum peak power for the 1<sup>st</sup> case

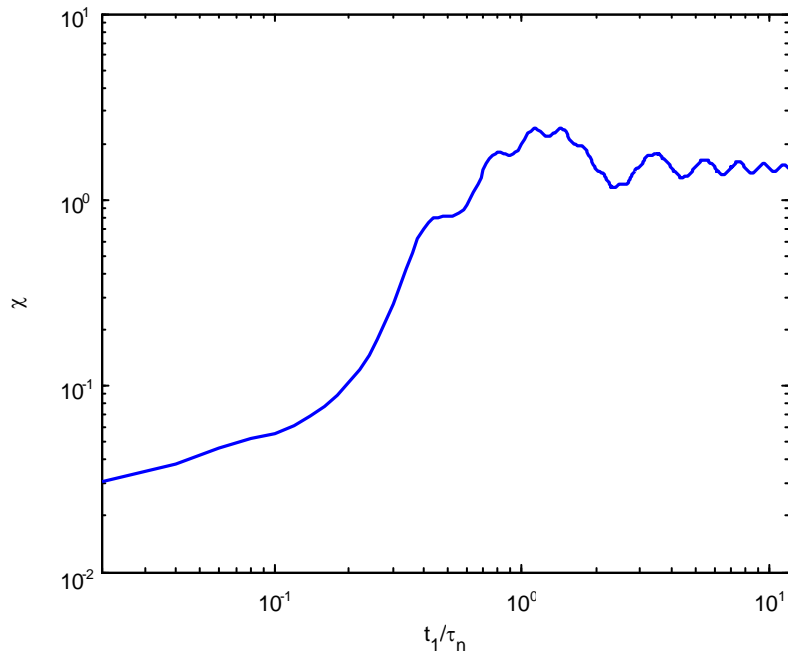
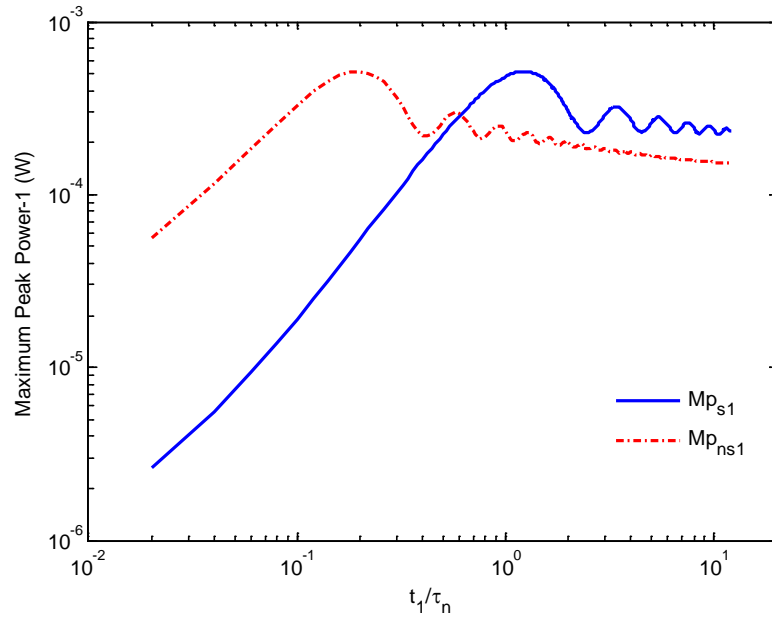


Figure 2-6 Transient transmissibility for the 1<sup>st</sup> case

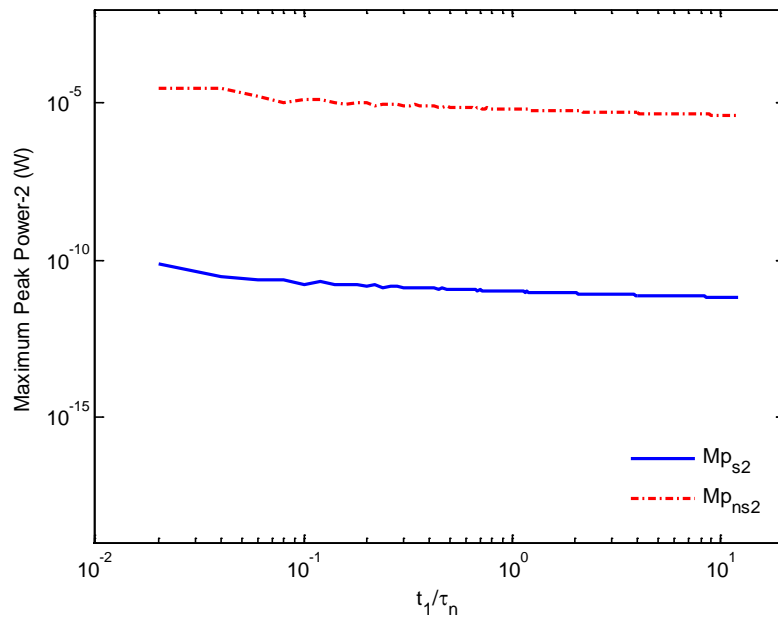
For a further analysis, the transient power transmissibility in two frequency bands is calculated according to Eq. (2.4). The maximum peak powers in each band with and without the isolator are shown in Fig. 2-7. It can be seen that the two responses in the high-frequency band shown in Fig. 2-7(b) are much lower than those in the low-frequency band shown in Fig. 2-7(a), and the two maximum peak powers in the low-frequency band are considerably closer to those in the whole frequency domain shown in Fig. 2-5. The same can be observed in Fig. 2-8, where the transient transmissibility in the low-frequency band is also prominent. This implies that the maximum peak powers come mainly from the vibration transmission in the low-frequency band.

The reason for this might be that both the low-frequency component of the excitation and the low-order modes of the system have dominantly high magnitudes which coincide in the low-frequency band. This in turn leads to the difference between transient and steady dynamics. For this reason, a vibration spring selected for steady-state vibration generally cannot isolate the transmission of transient excitation, since a steady excitation does not have dominant magnitudes below the natural frequency of the designed spring isolator.



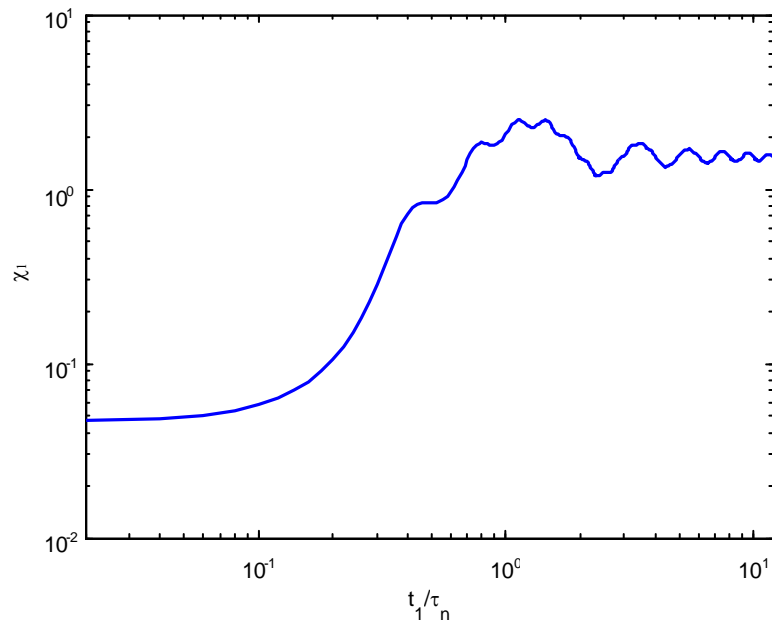


(a)

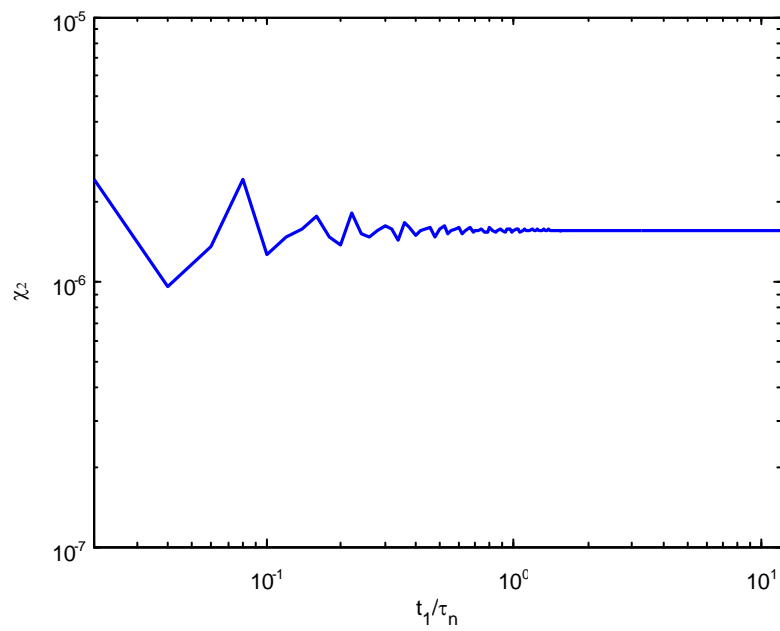


(b)

**Figure 2-7 Maximum peak powers in two frequency bands for the 1<sup>st</sup> case: (a) Maximum peak power in the low-frequency band; (b) Maximum peak power in the high-frequency band.**



(a)



(b)

**Figure 2-8 Transient power transmissibility in two frequency bands for the 1<sup>st</sup> case: (a) Transient power transmissibility in the low-frequency band; (b) Transient power transmissibility in the high-frequency band.**

### 2.2.2 Case Two –A Triangular Pulse

To simulate the situation where a vibratory machine undergoes occasional shocks, the triangular pulse shown in Fig. 2-4(b) is selected because of its good approximation to actual pulse shapes. The maximum peak powers with and without the isolator, and the transient power transmissibility, are shown in Figs. 2-9 and 2-10.

For the triangular pulse excitation, effective isolation is possible when:

$$t_1 < 0.2\tau_n.$$

Therefore, when the pulse time is less than  $0.2\tau_n$ , the design of the spring isolator according to the transient power transmissibility is acceptable.

For a further analysis, transient power transmissibility in two frequency bands is obtained by Eq. (2.4). The maximum peak powers with and without the isolator, and the transient power transmissibility in two frequency bands, are plotted in Figs. 2-11 and 2-12. The conclusions which can be drawn from those figures are similar to those in the first case. The coincidence of the low-frequency component with the high amplitude of the transient excitation and the low-order modes of the system indicates that an isolator selected for the attenuation of steady excitation performs poorly in the isolation of transient vibration transmission.

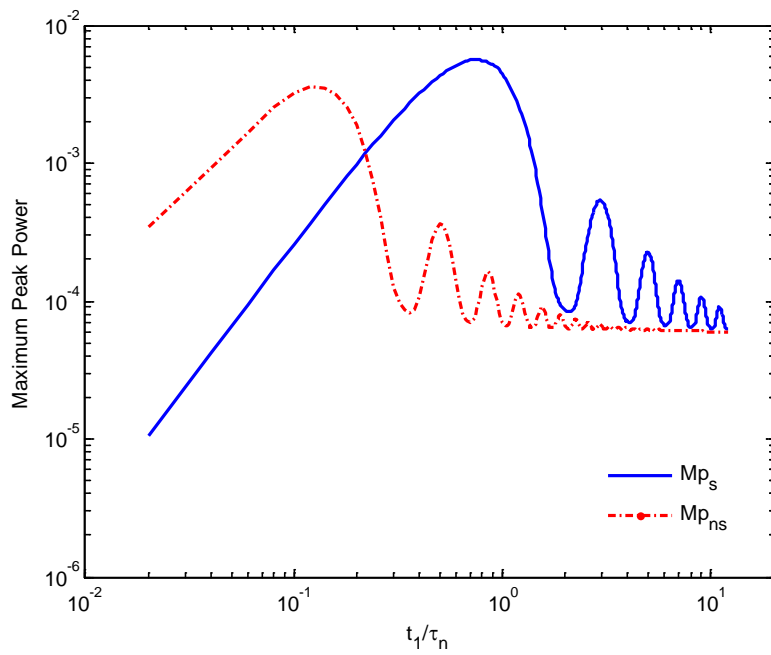


Figure 2-9 Maximum peak power for the 2<sup>nd</sup> case

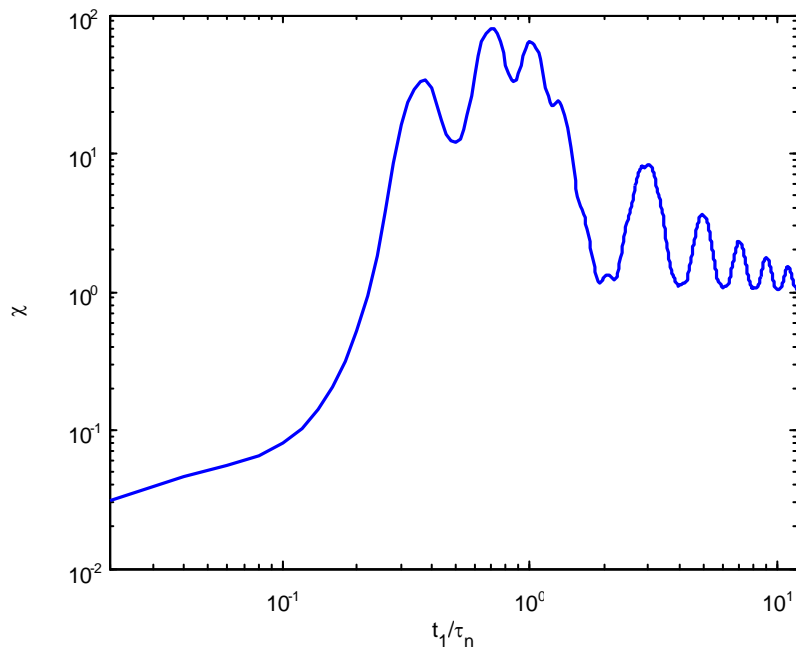
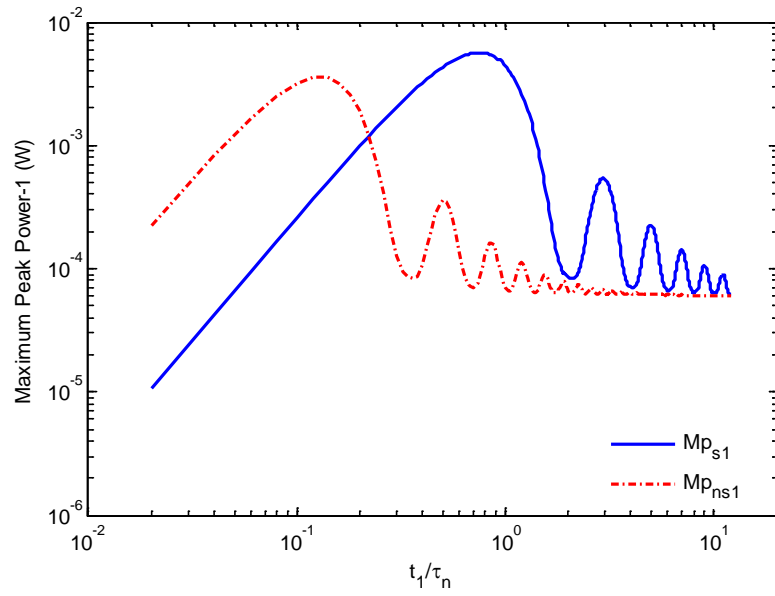
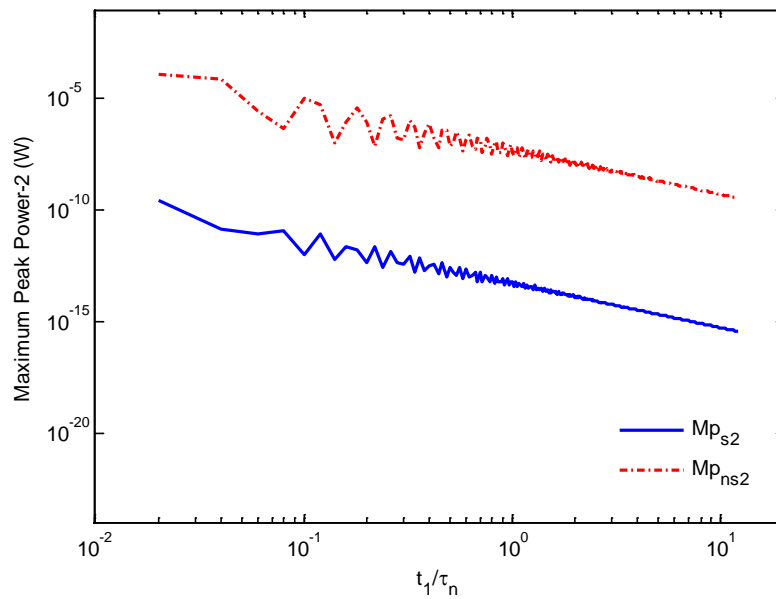


Figure 2-10 Transient power transmissibility for the 2<sup>nd</sup> case

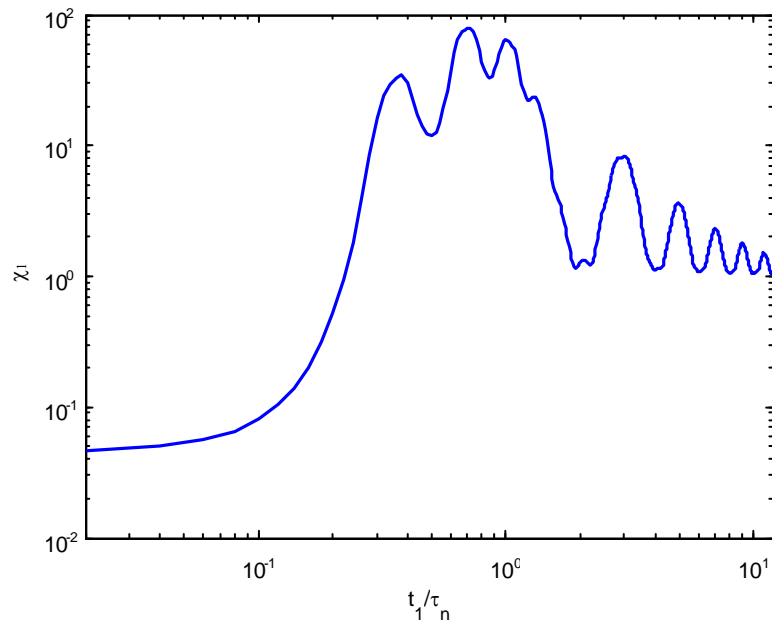


(a)

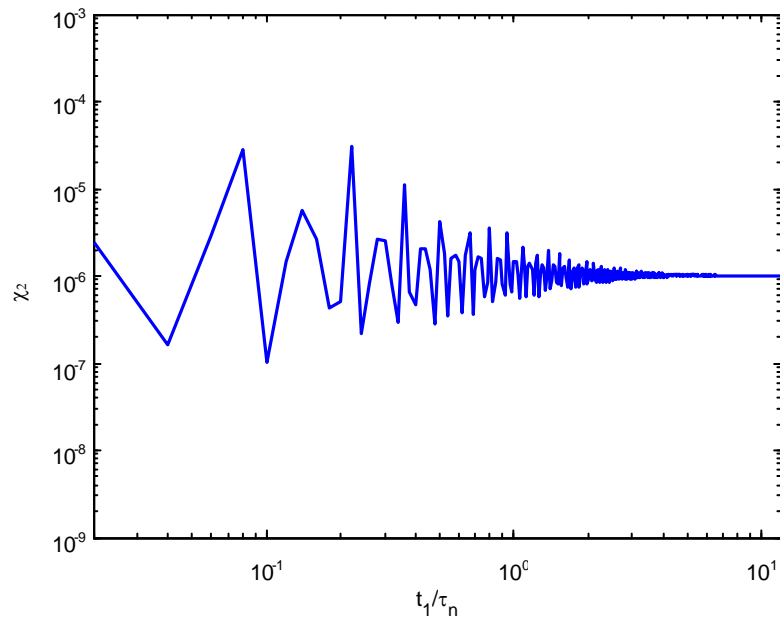


(b)

**Figure 2-11 Maximum peak powers in two frequency bands for the 2<sup>nd</sup> case: (a) Maximum peak power in the low-frequency band; (b) Maximum peak power in the high-frequency band.**



(a)



(b)

**Figure 2-12 Transient power transmissibility in two frequency bands for the 2<sup>nd</sup> case:**  
**(a) Transient power transmissibility in the low-frequency band; (b) Transient power transmissibility in the high-frequency band**

## 2.3 Summary

This chapter sets out an approach to use the transient power transmissibility of the vibration isolator to assess the isolation performance of transient vibration in building services equipment. It consists of the ratio between the transmitted maximum peak powers with and without the installation of vibration isolator. For a further analysis, the transient power transmissibility can be decomposed into a series of frequency bands to investigate the impact of the frequency-domain distribution of transient excitations, and the modal distribution, on the transmitted vibration. Two typical cases of transient excitation are presented to demonstrate the importance of the transient power transmissibility in the selection of the vibration spring for isolating transient vibration. In addition, the failure of the spring for transient vibration isolation is shown to result from the fact that the low-frequency component of the transient excitation generally has larger amplitudes than in the higher-frequency band, and coincides with the low-order modes of the system.

## **Chapter 3**

# **Adaptive-Passive Vibration Isolation between Non-Rigid Machines and Non-Rigid Foundations Using a Dual-Beam Periodic Structure with SMA Transverse Connection**

This chapter focuses on developing passive control methods for the application of a semi-two-dimensional structure to broadband vibration isolation and offering an insight to the problem of broadband vibration control using periodic structures. Given the discussion in the literature review in chapter 1, the application of this dual-beam periodic structure with transverse branches as a periodic isolator has not been proposed since it was presented. Non-SMA beams and SMA branches are proposed to construct this periodic structure in order to make best use of the significantly variable property of SMA and to avoid the associated limitation of hysteresis. The two non-SMA beams support the machine, and the SMA branches adjust and widen the stop bands. Through this configuration, this structure can accentuate the advantage of the significant variation in the SMA's Young's modulus because the moduli of the branches considerably influence the characteristics of the power transmission loss, and can also bypass the disadvantage of possible hysteresis



caused by large vertical deflection. Two approaches are proposed to determining the optimal Young's moduli of the SMA branches to maximizing the transmission loss after the derivation of the transmitted power of a general vibratory system with periodic isolators. One is used to obtain a database from which such moduli can be withdrawn in order to isolate vibrations according to the characteristics of the frequencies of interest, and the other is applicable to the real-time calculation of proper Young's moduli. Although the problem of broadband vibration control is investigated in this chapter through a semi-two-dimensional model, the theoretical development can also be expanded to a three-dimensional system. The numerical results prove that adaptive SMA branches with proper temperatures can isolate vibration transmission in wide-frequency bands. Experimental results indirectly verify the derivation of the governing equation of the transmitted vibration and the derivation is the basis of the development of the two approaches.

### **3.1 The Governing Equation of Transmitted Vibration**

A general vibration isolation system may be depicted as Fig. 1 and consists of a nonrigid machine and foundation connected by several mounts. This system is divided into three substructures for the purpose of deriving the governing equations of responses; the machine (the upper substructure  $\mathbf{H}$  with mobility  $\mathbf{H}_U$ ), the mounts

(the middle substructure  $\mathbf{M}$  with transfer matrix  $\mathbf{Z}_M$ ), and the foundation (the lower substructure  $\mathbf{G}$  with mobility  $\mathbf{G}_L$ ).

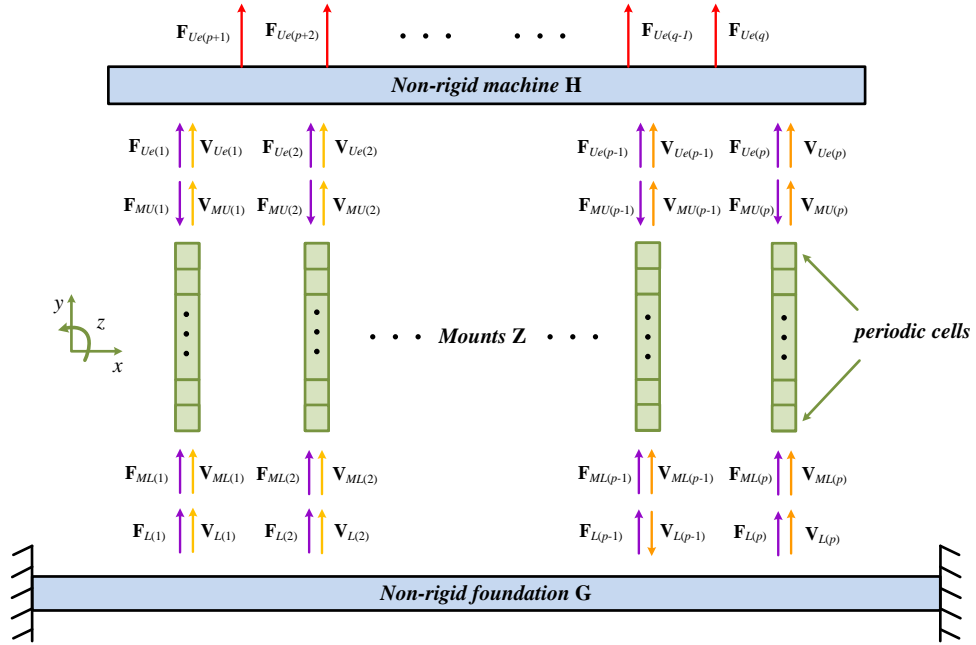


Figure 3-1 A general vibration isolation system with periodic mounts

### 3.1.1 A linear time-invariant (LTI) system

If there are  $q$  contact points with  $s$  DOF at each, and the  $q$  points include  $p$  mounting points and  $(q-p)$  externally excited points, the governing equation of the machine can be formulated as

$$\mathbf{V}_U = \mathbf{H}_U \mathbf{F}_U \quad (3.1)$$

where  $\mathbf{H}_U$  is a  $(s \times q)^{th}$  square matrix of mobilities,  $\mathbf{V}_U = [\mathbf{V}_{U1}^T, \mathbf{V}_{U2}^T, \dots, \mathbf{V}_{Up}^T, \dots, \mathbf{V}_{Uq}^T]^T$  and  $\mathbf{F}_U = [\mathbf{F}_{U1}^T, \mathbf{F}_{U2}^T, \dots, \mathbf{F}_{Up}^T, \dots, \mathbf{F}_{Uq}^T]^T$  are column vectors of general velocities and forces.  $\mathbf{V}_{Uj}$ ,  $j=1 \dots q$ , is a  $s \times 1$  column vector of general velocities including

translations and rotations;  $\mathbf{F}_{Uj}$ ,  $j=1\cdots q$ , is a  $s\times l$  column vector of general forces including forces and moments. Letting  $\mathbf{F}_{Ue}$  and  $\mathbf{F}_{Uc}$  represent external excitations and internal forces at the mounting points, respectively. Eq. (3.1) can be partitioned as

$$\begin{bmatrix} \mathbf{V}_{Uc} \\ \mathbf{V}_{Ue} \end{bmatrix} = \begin{bmatrix} \mathbf{H}_{11} & \mathbf{H}_{12} \\ \mathbf{H}_{21} & \mathbf{H}_{22} \end{bmatrix} \begin{bmatrix} \mathbf{F}_{Uc} \\ \mathbf{F}_{Ue} \end{bmatrix} \quad (3.2)$$

where  $\mathbf{H}_{11}$  is  $(s\times q)^{th}$  square matrix representing the mobilities of the machine at the mounting points. Similarly, the input-output relation of the foundation is

$$\mathbf{V}_L = \mathbf{G}_L \mathbf{F}_L \quad (3.3)$$

where  $\mathbf{G}_L$  is  $(s\times q)^{th}$  square matrix representing mobilities of the foundation;  $\mathbf{V}_L$  and  $\mathbf{F}_L$  are column vectors of general velocities and forces at the mounting points on the foundation. If the periodic structure applied as a mount has  $n$  mounting points and  $r$  periodic cells, the  $p$  mounting points can be divided into  $p/n$  groups. The  $k^{th}$  periodic mount ( $k=1\cdots p/n$ ) is governed by

$$\begin{bmatrix} \mathbf{F}_{Mr}^{(k)} \\ \mathbf{V}_{Mr}^{(k)} \end{bmatrix} = \mathbf{Y}_M^{(k)} \begin{bmatrix} \mathbf{F}_{M1}^{(k)} \\ \mathbf{V}_{M1}^{(k)} \end{bmatrix} = \mathbf{T}^r \begin{bmatrix} \mathbf{F}_{M1}^{(k)} \\ \mathbf{V}_{M1}^{(k)} \end{bmatrix} \quad (3.4a)$$

where  $\mathbf{Y}_M^{(k)} = \mathbf{T}^r$  is the transfer matrix of a periodic structure of which each identical cell has a transfer matrix  $\mathbf{T}$ ;  $\mathbf{F}_{M1}^{(k)} = [\mathbf{F}_{U(kn-n+1)}^T, \cdots, \mathbf{F}_{U(kn)}^T]^T$  and  $\mathbf{V}_{M1}^{(k)} = [\mathbf{V}_{U(kn-n+1)}^T, \cdots, \mathbf{V}_{U(kn)}^T]^T$  are column vectors of general velocities and forces at the contacting points between the machine and the  $k^{th}$  mount.  $\mathbf{F}_{Mr}^{(k)} = [\mathbf{F}_{L(kn-n+1)}^T, \cdots, \mathbf{F}_{L(kn)}^T]^T$  and  $\mathbf{V}_{Mr}^{(k)} = [\mathbf{V}_{L(kn-n+1)}^T, \cdots, \mathbf{V}_{L(kn)}^T]^T$  are column vectors

of general velocities and forces at the contacting points between the foundation and the  $k^{th}$  mount.

When the ideal periodicity of a periodic structure is disordered by design imperfections, material and geometrical variability, and installation and manufacturing errors, its wave transmission ability within the pass bands decreases significantly. In other words, structural vibration is confined to the vicinity of the driving point, owing to the resulting disorder. This phenomenon is a vibratory or acoustic analogue to the so-called Anderson localization in solid-state physics [68-70]. Irregularities or disorders can be intentionally introduced into a strict periodic structure to generate significant attenuation of the wave propagation in pass bands. When irregularities are introduced to a periodic mount, the transfer matrix Eq.(3.4a) becomes

$$\begin{bmatrix} \mathbf{F}_{Mr}^{(k)} \\ \mathbf{V}_{Mr}^{(k)} \end{bmatrix} = \mathbf{Y}_M^{(k)} \begin{bmatrix} \mathbf{F}_{M1}^{(k)} \\ \mathbf{V}_{M1}^{(k)} \end{bmatrix} = \mathbf{T}_r \cdots \mathbf{T}_2 \mathbf{T}_1 \begin{bmatrix} \mathbf{F}_{M1}^{(k)} \\ \mathbf{V}_{M1}^{(k)} \end{bmatrix} \quad (3.4b)$$

where  $\mathbf{T}_l$ ,  $l=1 \cdots r$  is the transfer matrix of each periodic cell of an imperfect periodic structure. The transfer matrix of the  $k^{th}$  periodic mount,  $\mathbf{Y}_M^{(k)}$ , is a  $2 \times s \times n$  square matrix. Let  $\mathbf{Z}_M^{(k)}$  represent the inversion of the transfer matrix, and partition it into four square submatrices, so

$$\mathbf{Z}_M^{(k)} = \begin{bmatrix} \mathbf{Z}_{11}^{(k)} & \mathbf{Z}_{12}^{(k)} \\ \mathbf{Z}_{21}^{(k)} & \mathbf{Z}_{22}^{(k)} \end{bmatrix}$$

Thus, for all periodic mounts 1 to  $p/n$ , we have

$$\begin{bmatrix} \mathbf{F}_{MU} \\ \mathbf{V}_{MU} \end{bmatrix} = \begin{bmatrix} \mathbf{diag}(\mathbf{Z}_{11}^{(k)}) & \mathbf{diag}(\mathbf{Z}_{12}^{(k)}) \\ \mathbf{diag}(\mathbf{Z}_{21}^{(k)}) & \mathbf{diag}(\mathbf{Z}_{22}^{(k)}) \end{bmatrix} \begin{bmatrix} \mathbf{F}_{ML} \\ \mathbf{V}_{ML} \end{bmatrix} \quad (3.5)$$

where  $\mathbf{diag}(\mathbf{Z}^{(k)})$  is a  $(s \times p)^{th}$  order partitioned diagonal matrix having sub-matrices

$$\mathbf{Z}^{(k)}, \quad \mathbf{F}_{MU} = [\mathbf{F}_{M1}^{(1)}, \mathbf{F}_{M1}^{(2)}, \dots, \mathbf{F}_{M1}^{(p/n)}]^T, \quad \mathbf{V}_{MU} = [\mathbf{V}_{M1}^{(1)}, \mathbf{V}_{M1}^{(2)}, \dots, \mathbf{V}_{M1}^{(p/n)}]^T,$$

$$\mathbf{F}_{ML} = [\mathbf{F}_{Mr}^{(1)}, \mathbf{F}_{Mr}^{(2)}, \dots, \mathbf{F}_{Mr}^{(p/n)}]^T, \quad \text{and} \quad \mathbf{V}_{ML} = [\mathbf{V}_{Mr}^{(1)}, \mathbf{V}_{Mr}^{(2)}, \dots, \mathbf{V}_{Mr}^{(p/n)}]^T$$

are column vectors of forces and velocities. Employing the compatibility condition for the

velocities and the equilibrium condition for the forces at the junctions (see Fig. 3.1),

$$\mathbf{V}_{Uc} = \mathbf{V}_{UM}$$

$$\mathbf{F}_{Uc} = -\mathbf{F}_{UM}$$

$$\mathbf{V}_L = \mathbf{V}_{UL}$$

$$\mathbf{F}_L = \mathbf{F}_{UL}$$

and substituting these conditions into Eqs. (3.2), (3.3) and (3.5), the transmitted force

to the foundation is solved.

$$\begin{aligned} \mathbf{F}_L &= [\mathbf{Z}_{M21} + \mathbf{Z}_{M22} \mathbf{G}_L + \mathbf{H}_{11} \mathbf{Z}_{M11} + \mathbf{H}_{11} \mathbf{Z}_{M12} \mathbf{G}_L]^{-1} \mathbf{H}_{12} \mathbf{F}_{Ue} \\ &= \mathbf{R}_1^{-1} \mathbf{H}_{12} \mathbf{F}_{Ue} \\ &\triangleq \mathbf{F}_{L1} \end{aligned} \quad (3.6)$$

Thus, the governing equation of transmitted power is

$$P_{wL1} = \frac{1}{2} \text{Re}(\mathbf{F}_{L1}^H \mathbf{G}_L \mathbf{F}_{L1}) \quad (3.7)$$

where  $H$  denotes conjugate transpose. The transmission loss is given

$$P_{TL} = 10 \log \frac{P_{wU1}}{P_{wL1}} \quad (3.8)$$

$$\text{where } P_{wU1} = \frac{1}{2} \text{Re}(\mathbf{F}_{Ue}^H \mathbf{V}_{Ue}).$$

### 3.1.2 A system with linear time-varying (LTV) substructures

Systems possessing time-varying parameters frequently occur in practice. For example, there are time-varying stiffness existing in a system of an asymmetrical rotating machine and time-varying masses in rotating crankshafts and conveyor systems. The solving process of the response of a system composed of a LTV machine and a LTV foundation and LTI mounts is formulated herein in order to provide an example for the derivation of a LTV system.

A causal linear time-varying system is characterized by an impulse response  $h(t, \tau)$  which describes the response at the observation time  $t$  to an impulse applied at the time of excitation  $\tau$ , according to Claasen and Mecklenbräuker's review [35]. They present the time-domain input–output relation for the class of LTV systems as

$$y(t) = \int_{-\infty}^{\infty} h(t, \tau)x(\tau)d\tau$$

where  $x(t)$  and  $y(t)$  are the time-domain input and output signals of the system. This impulse response  $h(t, \tau)$  corresponds to a bifrequency transfer function  $H(\omega, \Omega)$  which is the Fourier Transform of  $h(t, \tau)$  with respect to  $t$  and  $\tau$ .

$$H(\omega, \Omega) = \int_{-\infty}^{\infty} \int_{-\infty}^{\infty} h(t, \tau)e^{-i(\omega t - \Omega \tau)} dt d\tau$$

Therefore, the frequency-domain input–output relation for the LTV systems is

$$\hat{y}(\omega) = \frac{1}{2\pi} \int_{-\infty}^{\infty} H(\omega, \Omega)\hat{x}(\Omega)d\Omega$$

As the frequency band/bands of interest is the main concern, this infinite integral can

be truncated and approximated by

$$\hat{y}(\omega) = \frac{1}{2\pi} \sum_{m=-N}^{m=N} H(\omega, \Omega_m) x(\Omega_m) \Delta\Omega$$

where  $\Omega_0=0$  represents rigid modes and  $\omega \in [\Omega_{-N}, \Omega_N]$  denotes the frequency region of interest which covers a frequency band or all separate frequency bands of interest. The frequency region therefore consists of the frequency band/bands of interest and irrelevant frequencies. These irrelevant frequencies can be excluded if necessary. For the convenience of denotation, this discrete expression of the above frequency-domain input-output relation can be re-written as

$$\hat{y}(\omega) = \frac{\Delta\Omega}{2\pi} [H(\omega, \Omega_{-N} \sim \Omega_N)] [\hat{x}(\Omega_{-N} \sim \Omega_N)]^T$$

By the same denotation, the time-varying substitution of Eqs. (3.2) - (3.3) and (3.5) become

$$\begin{bmatrix} \mathbf{V}_{Uc}(\omega_\kappa) \\ \mathbf{V}_{Ue}(\omega_\kappa) \end{bmatrix} = \frac{\Delta\Omega}{2\pi} \begin{bmatrix} [\mathbf{H}_{11}(\omega_\kappa, \Omega_{-N} \sim \Omega_N)] & [\mathbf{H}_{12}(\omega_\kappa, \Omega_{-N} \sim \Omega_N)] \\ [\mathbf{H}_{21}(\omega_\kappa, \Omega_{-N} \sim \Omega_N)] & [\mathbf{H}_{22}(\omega_\kappa, \Omega_{-N} \sim \Omega_N)] \end{bmatrix} \begin{bmatrix} [\mathbf{F}_{Uc}(\Omega_{-N} \sim \Omega_N)] \\ [\mathbf{F}_{Ue}(\Omega_{-N} \sim \Omega_N)] \end{bmatrix} \quad (3.9)$$

$$\mathbf{V}_L(\omega_\kappa) = \frac{\Delta\Omega}{2\pi} [\mathbf{G}_L(\omega_\kappa, \Omega_{-N} \sim \Omega_N)] [\mathbf{F}_L(\Omega_{-N} \sim \Omega_N)] \quad (3.10)$$

and

$$\begin{bmatrix} \mathbf{F}_{MU}(\omega_\kappa) \\ \mathbf{V}_{MU}(\omega_\kappa) \end{bmatrix} = \mathbf{Z}_M(\omega_\kappa) \begin{bmatrix} \mathbf{F}_{ML}(\omega_\kappa) \\ \mathbf{V}_{ML}(\omega_\kappa) \end{bmatrix} \quad (3.11)$$

where  $[\mathbf{H}_{ij}(\omega_\kappa, \Omega_{-N} \sim \Omega_N)]$ ,  $i, j=1,2$ , denotes the horizontal concatenation of matrices  $\mathbf{H}_{ij}(\omega_\kappa, \Omega_{-N}) \cdots \mathbf{H}_{ij}(\omega_\kappa, \Omega_N)$ , and column vectors, like  $[\mathbf{F}_{Uc}(\Omega_{-N} \sim \Omega_N)]$ , denotes the vertical concatenation of the values of original column vectors in Eqs. (2)-(3) and (5) at  $[\Omega_{-N} \cdots \Omega_N]$ . Similarly,  $[\mathbf{H}_{ij}(\omega_{-N} \sim \omega_N, \Omega_{-N} \sim \Omega_N)]$  denotes the

vertical concatenation of matrices  $[\mathbf{H}_{ij}(\omega_\kappa, \Omega_{-N} \sim \Omega_N)]$  where  $\kappa = -N \dots N$ . Letting  $[\omega_{-N} \sim \omega_N] = [\Omega_{-N} \sim \Omega_N]$  and combining Eqs. (3.9)-(3.11) and the compatibility and equilibrium conditions, the solution of the transmitted force to the foundation is solved.

$$\begin{aligned} & [\mathbf{F}_L(\Omega_{-N} \sim \Omega_N)] \\ &= \mathbf{R}_2^{-1} [\mathbf{H}_{12}(\omega_{-N} \sim \omega_N, \Omega_{-N} \sim \Omega_N)] [\mathbf{F}_{Ue}(\Omega_{-N} \sim \Omega_N)] \\ &\triangleq [\mathbf{F}_{L2}(\Omega_{-N} \sim \Omega_N)] \end{aligned} \quad (3.12)$$

where

$$\begin{aligned} \mathbf{R}_2 &= \left[ [\mathbf{H}_{11}(\omega_{-N} \sim \omega_N, \Omega_{-N} \sim \Omega_N)] \quad \mathbf{I} \right] \mathbf{\Theta}_2 \begin{bmatrix} \mathbf{I} \\ [\mathbf{G}_L(\omega_{-N} \sim \omega_N, \Omega_{-N} \sim \Omega_N)] \end{bmatrix} \\ \mathbf{\Theta}_2 &= \begin{bmatrix} \mathbf{diag}(\mathbf{Z}_{M11}(\Omega_m)) & \mathbf{diag}(\mathbf{Z}_{M12}(\Omega_m)) \frac{\Delta\Omega}{2\pi} \\ \mathbf{diag}(\mathbf{Z}_{M21}(\Omega_m)) \frac{2\pi}{\Delta\Omega} & \mathbf{diag}(\mathbf{Z}_{M22}(\Omega_m)) \end{bmatrix} \end{aligned}$$

Then, the total transmitted power in the frequency region of interest is obtained (see (Eq. (3.13))). The values at the irrelevant frequencies in this region can be excluded from  $[\mathbf{F}_L(\Omega_{-N} \sim \Omega_N)]$  if they have significant influence on the total power  $P_{wL2}$ .

$$P_{wL2} = \frac{1}{2} \text{Re} \left( [\mathbf{F}_{L2}(\Omega_{-N} \sim \Omega_N)]^H [\mathbf{G}_L(\omega_{-N} \sim \omega_N, \Omega_{-N} \sim \Omega_N)] [\mathbf{F}_{L2}(\Omega_{-N} \sim \Omega_N)] \right) \quad (3.13)$$

The transmission loss of this LTV system is given

$$P_{TL} = 10 \log \frac{P_{wU2}}{P_{wL2}} \quad (3.14)$$

$$\text{where } P_{wU2} = \frac{1}{2} \text{Re} \left( [\mathbf{F}_{Ue}(\Omega_{-N} \sim \Omega_N)]^H [\mathbf{V}_{Ue}(\Omega_{-N} \sim \Omega_N)] \right).$$



## **3.2 Vibration Control Using SMA Components in a Periodic Structure**

SMA's are a class of alloys well known for their shape memory effect - the ability to recover from plastic deformations to the original shape through the application of heat. This effect occurs when the material undergoes martensitic transformation – a phase transformation between a low-temperature-state martensite and a high-temperature-state austenite. During this transformation, the Young's modulus will increase as much as three times, a distinct effect which runs alongside the shape memory phenomena. Accompanying it is the temperature hysteresis that may destabilize the vibration control system. However, this can be avoided if the displacement and stress are small [51, 54]. Therefore, this property of significantly varying modulus induced by martensitic transformation can be applicable to vibration control if the assumption of small displacement and stress is satisfied.

In addition to the martensitic transformation, a rhombohedral phase (R-phase) transformation may be observed with the application of appropriate heat treatment. A little or none temperature hysteresis, but a significant variation of modulus, can be achieved by this R-phase transformation [55-56]. Another limitation of SMA's may be their relatively low yielding strength, for example SMA Nitinol [55]. Such plastic yielding may augment the hysteretic effect. Nonetheless, this shortcoming can be

circumvented by not supporting heavy structures or by adding non-SMA material with high yielding strength in parallel to the SMA structure. These two measures are conducive to satisfying the assumption of small deflection and stress which are indirectly required by this limitation. To sum up, with reasonable assumptions or appropriate heat treatment in place, SMAs can exploit their advantages of significantly varying modulus and bypass their disadvantages of temperature hysteresis and relatively low yielding strength, all for the purpose of vibration control. The assumption of small deflection and stress is adopted in this investigation. The hysteretic behavior indicates a complex elastic modulus, so a little hysteresis enables the material to be modeled by a real elastic modulus. To obtain proper Young's moduli and achieve significant vibration attenuation, two methods are developed to take advantage of SMA materials and apply them to broadband vibration control.

### **3.2.1 A Database Method for Static Regulation**

This approach is based on Eq. (3.8) or (3.14), and can be divided into the following steps for practical purposes.

Firstly, based on the values obtained for the Young's modulus of the SMA at different temperatures, the relation between the Young's modulus  $E$  and temperature

$T, E(T)$ , can be established. The method to establish the relation  $E(T)$  is found in the work of Williams [56]. The Young's modulus of the SMA can be changed to any value in the range of  $[E_1, E_2]$  with the change of temperature, where  $E_1$  and  $E_2$  are the lower and upper bounds of the Young's modulus.

Secondly, the relation  $P_{TL}(E)$  in the range of  $[E_1, E_2]$  can be established by applying a unit impulse excitation (transformed as a unit load in frequency domain) correspondent to each DOF of motion being considered and calculating the transmission loss  $P_{TL}$  at every value in the range. Subsequently, a database can be built to save the relation  $P_{TL}(E)$  or  $P_{TL}(T)$ . It is suggested that the transmission loss  $P_{TL}$  under other excitations is normalized to the  $P_{TL}$  under a unit impulse excitation.

Thirdly, for different  $P_{TL}(T)$  curves, there are different pass and stop bands, and peak frequencies. The most proper  $P_{TL}(T)$  curve, which covers the frequencies of interest, can be selected from the database according to the characteristics of the vibratory source (such as the peak frequencies of the power spectral density (PSD) and the frequency bands where energy is most intense).

Finally, the temperature which corresponds to the most proper  $P_{TL}(T)$  curve can be obtained, which leads to the maximum energy attenuation in the frequency region of

interest.

### 3.2.2 Frequency-domain Steepest Gradient Method for Real-time Calculation

The Young's modulus of SMA may vary with temperature nonlinearly, but it is not necessary that the Young's modulus of the SMA components changes with time nonlinearly. For a linear system, the optimal Young's modulus of the SMA components is a fix value or a linearly time-varying value. Many numerical methods exist to solve an optimal parameter and minimize the transmitted power especially when its derivative is available [71]. One possible method is the steepest gradient algorithm. The frequency-domain steepest gradient algorithm is chosen herein because its principle is to achieve real-time updating by using the data in contain frequency bands or in whole frequency domain [72]. Before applying this algorithm to the systems examined in Section 3.1, Eq. (3.5) of a LTI system and Eq. (3.11) of a system with LTV sub-structures should be replaced by Eq. (3.15) such that the influence of continuously updated transfer matrix of periodic mounts on the response can be taken into account.

$$\begin{bmatrix} \mathbf{F}_{MU}(\omega_\kappa) \\ \mathbf{V}_{MU}(\omega_\kappa) \end{bmatrix} = \begin{bmatrix} \left[ \hat{\mathbf{Z}}_{M11}(\omega_\kappa, \Omega_{-N} \sim \Omega_{-N}) \right] & \left[ \hat{\mathbf{Z}}_{M12}(\omega_\kappa, \Omega_{-N} \sim \Omega_{-N}) \right] \\ \left[ \hat{\mathbf{Z}}_{M21}(\omega_\kappa, \Omega_{-N} \sim \Omega_{-N}) \right] & \left[ \hat{\mathbf{Z}}_{M22}(\omega_\kappa, \Omega_{-N} \sim \Omega_{-N}) \right] \end{bmatrix} \begin{bmatrix} \mathbf{F}_{ML}(\Omega_{-N} \sim \Omega_{-N}) \\ \mathbf{V}_{ML}(\Omega_{-N} \sim \Omega_{-N}) \end{bmatrix} \frac{\Delta\Omega}{2\pi} \quad (3.15)$$

where

$$\mathbf{Z}_M(t_n, \Omega_m) = \mathbf{Z}_M(\Omega_m) \Big|_{E=E(n\Delta t)}$$

$$\hat{\mathbf{Z}}_M(\bar{\omega}_\kappa, \Omega_m) = \sum_{n=N_0}^{n=N_c} \mathbf{Z}_M(t_n, \Omega_m) e^{-i\bar{\kappa}\Delta\bar{\omega}n\Delta t} \Delta t = \sum_{n=N_0}^{n=N_c} e^{-i\bar{\kappa}\Delta\bar{\omega}n\Delta t} \mathbf{Z}_M(\Omega_m) \Big|_{E=E(n\Delta t)} \Delta t$$

where  $\Delta t$  is the sampling time,  $t_{N_c}$  is the current time and  $t_{N_0}$  is the previous time;  $\hat{\mathbf{Z}}_M(\bar{\omega}_\kappa, \Omega_m)$ , the discrete Fourier Transform of  $\mathbf{Z}_M(t_n, \Omega_m)$ , includes or is equal to  $\hat{\mathbf{Z}}_M(\omega_\kappa, \Omega_m)$ , the part of  $\hat{\mathbf{Z}}_M(\bar{\omega}_\kappa, \Omega_m)$  in the frequency region of interest. This is realized by guaranteeing  $\Delta\omega$ , the difference between  $\omega_\kappa$  and  $\omega_{\kappa+1}$ , is the integral multiple of  $\Delta\bar{\omega}$ . Combining Eqs. (3.2)-(3.3) and (3.15) and the compatibility and equilibrium conditions together, the transmitted force of a system with LTV mounts is obtained.

$$[\mathbf{F}_L(\Omega_{-N} \sim \Omega_N)] = \mathbf{R}_3^{-1} \mathbf{diag}(\mathbf{H}_{12}(\Omega_m)) [\mathbf{F}_{Ue}(\Omega_{-N} \sim \Omega_N)]^T \frac{2\pi}{\Delta\Omega} \triangleq [\mathbf{F}_{L3}(\Omega_{-N} \sim \Omega_N)] \quad (3.16)$$

where

$$\mathbf{R}_3 = \begin{bmatrix} \mathbf{diag}(\mathbf{H}_{11}(\Omega_m)) & \mathbf{I} \end{bmatrix} \Theta_3 \begin{bmatrix} \mathbf{I} \\ \mathbf{diag}(\mathbf{G}_L) \end{bmatrix}$$

$$\Theta_3 = \begin{bmatrix} \left[ \begin{array}{c} \hat{\mathbf{Z}}_{M11}(\omega_{-N} \sim \omega_N, \Omega_{-N} \sim \Omega_N) \\ \hat{\mathbf{Z}}_{M21}(\omega_{-N} \sim \omega_N, \Omega_{-N} \sim \Omega_N) \end{array} \right] & \left[ \begin{array}{c} \hat{\mathbf{Z}}_{M12}(\omega_{-N} \sim \omega_N, \Omega_{-N} \sim \Omega_N) \\ \hat{\mathbf{Z}}_{M22}(\omega_{-N} \sim \omega_N, \Omega_{-N} \sim \Omega_N) \end{array} \right] \end{bmatrix}$$

Then, the total transmitted power of this class of systems in the frequency region of interest is solved, as a modification of Eq. (3.7).

$$P_{wL3} = \frac{1}{2} \text{Re} \left( [\mathbf{F}_{L3}(\Omega_{-N} \sim \Omega_N)]^H \mathbf{diag}(\mathbf{G}_L) [\mathbf{F}_{L3}(\Omega_{-N} \sim \Omega_N)] \right) \quad (3.17)$$

In a similar way, the transmitted force (as a modification of Eq. (13)) and the total transmitted power of a system with LTV machine foundation and mounts in the frequency region of interest are solved, by combing Eqs. (3.9)-(3.10) and (3.15) and

the compatibility and equilibrium conditions.

$$\begin{aligned} & [\mathbf{F}_L(\Omega_{-N} \sim \Omega_N)] \\ &= \mathbf{R}_4^{-1} \frac{2\pi}{\Delta\Omega} [\mathbf{H}_{12}(\omega_{-N} \sim \omega_N, \Omega_{-N} \sim \Omega_N)] [\mathbf{F}_{Ue}(\Omega_{-N} \sim \Omega_N)] \end{aligned} \quad (3.18)$$

$$\begin{aligned} & \triangleq [\mathbf{F}_{L4}(\Omega_{-N} \sim \Omega_N)] \\ & P_{wL4} = \frac{1}{2} \text{Re} \left( [\mathbf{F}_L(\Omega_{-N} \sim \Omega_N)]^H [\mathbf{G}_L(\omega_{-N} \sim \omega_N, \Omega_{-N} \sim \Omega_N)] [\mathbf{F}_L(\Omega_{-N} \sim \Omega_N)] \right) \end{aligned} \quad (3.19)$$

where

$$\begin{aligned} \mathbf{R}_4 &= \left[ [\mathbf{H}_{11}(\omega_{-N} \sim \omega_N, \Omega_{-N} \sim \Omega_N)] \quad \mathbf{I} \right] \mathbf{\Theta}_4 \begin{bmatrix} \mathbf{I} \\ [\mathbf{G}_L(\omega_{-N} \sim \omega_N, \Omega_{-N} \sim \Omega_N)] \end{bmatrix} \\ \mathbf{\Theta}_4 &= \begin{bmatrix} [\hat{\mathbf{Z}}_{M11}(\omega_{-N} \sim \omega_N, \Omega_{-N} \sim \Omega_N)] & [\hat{\mathbf{Z}}_{M12}(\omega_{-N} \sim \omega_N, \Omega_{-N} \sim \Omega_N)] \frac{\Delta\Omega}{2\pi} \\ [\hat{\mathbf{Z}}_{M21}(\omega_{-N} \sim \omega_N, \Omega_{-N} \sim \Omega_N)] \frac{2\pi}{\Delta\Omega} & [\hat{\mathbf{Z}}_{M22}(\omega_{-N} \sim \omega_N, \Omega_{-N} \sim \Omega_N)] \end{bmatrix}. \end{aligned}$$

As the purpose of this analysis is to obtain the optimal Young's modulus of periodic components in the mounts, the power is differentiated with respect to  $E$ .

$$\frac{dP_{wL3}}{dE} = \frac{1}{2} \left( \frac{d\mathbf{F}_{L3}^H}{dE} \text{Re}(\mathbf{diag}(\mathbf{G}_L)) \mathbf{F}_{L3} + \mathbf{F}_{L3}^H \text{Re}(\mathbf{diag}(\mathbf{G}_L)) \frac{d\mathbf{F}_{L3}}{dE} \right) \quad (3.20a)$$

$$\frac{dP_{wL4}}{dE} = \frac{1}{2} \left( \frac{d[\mathbf{F}_{L4}(\Omega_{-N} \sim \Omega_N)]^H}{dE} \text{Re}([\mathbf{G}_L(\omega_{-N} \sim \omega_N, \Omega_{-N} \sim \Omega_N)]) [\mathbf{F}_{L4}(\Omega_{-N} \sim \Omega_N)] \right. \\ \left. + [\mathbf{F}_{L4}(\Omega_{-N} \sim \Omega_N)]^H \text{Re}([\mathbf{G}_L(\omega_{-N} \sim \omega_N, \Omega_{-N} \sim \Omega_N)]) \frac{d[\mathbf{F}_{L4}(\Omega_{-N} \sim \Omega_N)]}{dE} \right) \quad (3.20b)$$

For the periodic structure with perfectly identical cells, the derivative of  $\mathbf{F}_{L3}$  is given,

$$\mathbf{Z}^{(k)} = (\mathbf{T}^r)^{-1}$$

$$\frac{d\mathbf{Z}^{(k)}}{dE} = -r \mathbf{T}^{-r-1} \frac{d\mathbf{T}}{dE}$$

$$\frac{d\mathbf{Z}_M}{dE} = \begin{bmatrix} \mathbf{diag}\left(\frac{d\mathbf{Z}_{11}^{(k)}}{dE}\right) & \mathbf{diag}\left(\frac{d\mathbf{Z}_{12}^{(k)}}{dE}\right) \\ \mathbf{diag}\left(\frac{d\mathbf{Z}_{21}^{(k)}}{dE}\right) & \mathbf{diag}\left(\frac{d\mathbf{Z}_{22}^{(k)}}{dE}\right) \end{bmatrix}$$

$$\frac{d\mathbf{\Theta}_3}{dE} = \begin{bmatrix} \frac{d\left[\hat{\mathbf{Z}}_{M11}(\omega_{-N} \sim \omega_N, \Omega_{-N} \sim \Omega_N)\right]}{dE} & \frac{d\left[\hat{\mathbf{Z}}_{M12}(\omega_{-N} \sim \omega_N, \Omega_{-N} \sim \Omega_N)\right]}{dE} \\ \frac{d\left[\hat{\mathbf{Z}}_{M21}(\omega_{-N} \sim \omega_N, \Omega_{-N} \sim \Omega_N)\right]}{dE} & \frac{d\left[\hat{\mathbf{Z}}_{M22}(\omega_{-N} \sim \omega_N, \Omega_{-N} \sim \Omega_N)\right]}{dE} \end{bmatrix}$$

$$\frac{d\mathbf{R}_3}{dE} = \left[ \mathbf{diag}(\mathbf{H}_{11}(\omega_k)) \quad \mathbf{I} \right] \frac{d\mathbf{\Theta}_3}{dE} \begin{bmatrix} \mathbf{I} \\ \mathbf{diag}(\mathbf{G}_L) \end{bmatrix}$$

$$\frac{d\mathbf{F}_{L3}}{dE} = -\mathbf{R}_3^{-1} \frac{d\mathbf{R}_3}{dE} \mathbf{R}_3 \mathbf{diag}(\mathbf{H}_{12}(\omega_k)) [\mathbf{F}_{Ue}(\omega_{-N} \sim \omega_N)]^T \frac{2\pi}{\Delta\omega}$$

Similarly, the derivative of  $\mathbf{F}_{L4}$  is solved.

$$\frac{d\mathbf{\Theta}_4}{dE} = \begin{bmatrix} \frac{d\left[\hat{\mathbf{Z}}_{M11}(\omega_{-N} \sim \omega_N, \Omega_{-N} \sim \Omega_N)\right]}{dE} & \frac{d\left[\hat{\mathbf{Z}}_{M12}(\omega_{-N} \sim \omega_N, \Omega_{-N} \sim \Omega_N)\right]}{dE} \frac{\Delta\Omega}{2\pi} \\ \frac{d\left[\hat{\mathbf{Z}}_{M21}(\omega_{-N} \sim \omega_N, \Omega_{-N} \sim \Omega_N)\right]}{dE} \frac{2\pi}{\Delta\Omega} & \frac{d\left[\hat{\mathbf{Z}}_{M22}(\omega_{-N} \sim \omega_N, \Omega_{-N} \sim \Omega_N)\right]}{dE} \end{bmatrix}$$

$$\frac{d\mathbf{R}_4}{dE} = \left[ [\mathbf{H}_{11}(\omega_{-N} \sim \omega_N, \Omega_{-N} \sim \Omega_N)] \quad \mathbf{I} \right] \frac{d\mathbf{\Theta}_4}{dE} \begin{bmatrix} \mathbf{I} \\ [\mathbf{G}_L(\omega_{-N} \sim \omega_N, \Omega_{-N} \sim \Omega_N)] \end{bmatrix}$$

$$\frac{d\mathbf{F}_{L4}}{dE} = -\mathbf{R}_4^{-1} \frac{d\mathbf{R}_4}{dE} \mathbf{R}_4 \frac{2\pi}{\Delta\Omega} [\mathbf{H}_{12}(\omega_{-N} \sim \omega_N, \Omega_{-N} \sim \Omega_N)] [\mathbf{F}_{Ue}(\Omega_{-N} \sim \Omega_N)]$$

The optimal Young's modulus of a mount with strictly identical cells can be approximately solved by the frequency-domain steepest gradient method [72]:

$$E(t_{n+1}) = E(t_n) + \mu IFFT \left( \left[ \begin{array}{c} \frac{dP_w}{dE} \\ \left( \frac{dP_w}{dE} \right)^* \end{array} \right]^T \right) \quad (3.21)$$

where  $\mu$  is an adjustable parameter in the steepest gradient algorithm and  $P_w = P_{wL3}$

or  $P_w = P_{wL4}$ , and  $IFFT( )$  represents the inverse FFT of which only the causal part (first half of the result) is used in the adaptation. The Young's modulus of all the identical SMA inserts is updated in time domain by frequency-domain data, specifically by the total vibratory power in the frequency region of interest.  $\frac{dP_w}{dE}$  can be solved by Eq. (3.20) when the models of the machine, the foundation and the mounts are available, or can be approximated by numerical differentiation when it is lack of the information of these models. When these models are available, the heat energy can be applied after the algorithm Eq. (3.21) converges (meanwhile the optimal Young's modulus is obtained) rather than after each step of adaptation. This is why it can be called adaptive-passive control. When it is lack of model information and the heat energy has to be applied to the SMA components after each step of adaptation such that the response corresponding to every newly adapted Young's modulus can be measured to approximately calculate the derivative  $\frac{dP_w}{dE}$ , the method can be called active control. The adaptive-passive control method is adopted here.

To take advantage of the localization effect, disorder is intentionally introduced to the periodic inserts, and all inserts in a periodic mount may have different moduli. For the mounts whose periodic inserts are not identical in terms of the Young's modulus, the derivative of power becomes



$$\frac{dP_w}{d\mathbf{E}} = \left[ \frac{\partial P_w}{\partial E_1}, \frac{\partial P_w}{\partial E_2}, \dots, \frac{\partial P_w}{\partial E_r} \right] \quad (3.22)$$

Since  $P_w = P_{wL3}$  or  $P_w = P_{wL4}$ , the partial derivatives are governed by either one of Eq. (3.23).

$$\frac{\partial P_{wL3}}{\partial E_l} = \frac{1}{2} \left( \frac{\partial \mathbf{F}_{L3}^H}{\partial E_l} \text{Re}(\mathbf{diag}(\mathbf{G}_L)) \mathbf{F}_{L3} + \mathbf{F}_{L3}^H \text{Re}(\mathbf{diag}(\mathbf{G}_L)) \frac{\partial \mathbf{F}_{L3}}{\partial E_l} \right) \quad (3.23a)$$

$$\frac{\partial P_{wL4}}{\partial E_l} = \frac{1}{2} \left( \frac{\partial [\mathbf{F}_{L4}(\Omega_{-N} \sim \Omega_N)]^H}{\partial E_l} \text{Re}([\mathbf{G}_L(\omega_{-N} \sim \omega_N, \Omega_{-N} \sim \Omega_N)]) [\mathbf{F}_{L4}(\Omega_{-N} \sim \Omega_N)] + [\mathbf{F}_{L4}(\Omega_{-N} \sim \Omega_N)]^H \text{Re}([\mathbf{G}_L(\omega_{-N} \sim \omega_N, \Omega_{-N} \sim \Omega_N)]) \frac{\partial [\mathbf{F}_{L4}(\Omega_{-N} \sim \Omega_N)]}{\partial E_l} \right) \quad (3.23b)$$

where the partial derivatives of  $\mathbf{F}_{L3}$  and  $\mathbf{F}_{L4}$  are solved by the following steps.

$$l = 1 \dots r$$

$$\mathbf{Z}^{(k)} = (\mathbf{T}_r \dots \mathbf{T}_2 \mathbf{T}_1)^{-1}$$

$$\frac{\partial \mathbf{Z}^{(k)}}{\partial E_l} = (\mathbf{T}_{l-1} \dots \mathbf{T}_1)^{-1} \frac{\partial \mathbf{T}_l^{-1}}{\partial E_l} (\mathbf{T}_r \dots \mathbf{T}_{l+1})^{-1}$$

$$\frac{\partial \mathbf{Z}_M}{\partial E_l} = \begin{bmatrix} \mathbf{diag} \left( \frac{\partial \mathbf{Z}_{11}^{(k)}}{\partial E_l} \right) & \mathbf{diag} \left( \frac{\partial \mathbf{Z}_{12}^{(k)}}{\partial E_l} \right) \\ \mathbf{diag} \left( \frac{\partial \mathbf{Z}_{21}^{(k)}}{\partial E_l} \right) & \mathbf{diag} \left( \frac{\partial \mathbf{Z}_{22}^{(k)}}{\partial E_l} \right) \end{bmatrix}$$

$$\frac{\partial \mathbf{\Theta}_3}{\partial E_l} = \begin{bmatrix} \frac{\partial [\hat{\mathbf{Z}}_{M11}(\omega_{-N} \sim \omega_N, \Omega_{-N} \sim \Omega_N)]}{\partial E_l} & \frac{\partial [\hat{\mathbf{Z}}_{M12}(\omega_{-N} \sim \omega_N, \Omega_{-N} \sim \Omega_N)]}{\partial E_l} \\ \frac{\partial [\hat{\mathbf{Z}}_{M21}(\omega_{-N} \sim \omega_N, \Omega_{-N} \sim \Omega_N)]}{\partial E_l} & \frac{\partial [\hat{\mathbf{Z}}_{M22}(\omega_{-N} \sim \omega_N, \Omega_{-N} \sim \Omega_N)]}{\partial E_l} \end{bmatrix}$$

$$\frac{\partial \mathbf{R}_3}{\partial E_l} = \left[ \mathbf{diag}(\mathbf{H}_{11}(\omega_\kappa)) \quad \mathbf{I} \right] \frac{\partial \mathbf{\Theta}_3}{\partial E_l} \begin{bmatrix} \mathbf{I} \\ \mathbf{diag}(\mathbf{G}_L) \end{bmatrix}$$

$$\begin{aligned} \frac{\partial \mathbf{F}_{L3}}{\partial E_l} &= -\mathbf{R}_3^{-1} \frac{\partial \mathbf{R}_3}{\partial E_l} \mathbf{R}_3^{-1} \mathbf{diag}(\mathbf{H}_{12}(\omega_\kappa)) [\mathbf{F}_{Ue}(\omega_{-N} \sim \omega_N)]^T \frac{2\pi}{\Delta\omega} \\ \frac{d\mathbf{\Theta}_4}{dE} &= \begin{bmatrix} \frac{d[\hat{\mathbf{Z}}_{M11}(\omega_{-N} \sim \omega_N, \Omega_{-N} \sim \Omega_N)]}{dE} & \frac{d[\hat{\mathbf{Z}}_{M12}(\omega_{-N} \sim \omega_N, \Omega_{-N} \sim \Omega_N)]}{dE} \\ \frac{d[\hat{\mathbf{Z}}_{M21}(\omega_{-N} \sim \omega_N, \Omega_{-N} \sim \Omega_N)]}{dE} \frac{2\pi}{\Delta\Omega} & \frac{d[\hat{\mathbf{Z}}_{M22}(\omega_{-N} \sim \omega_N, \Omega_{-N} \sim \Omega_N)]}{dE} \end{bmatrix} \\ \frac{d\mathbf{R}_4}{dE} &= \begin{bmatrix} [\mathbf{H}_{11}(\omega_{-N} \sim \omega_N, \Omega_{-N} \sim \Omega_N)] & \mathbf{I} \\ \mathbf{G}_L(\omega_{-N} \sim \omega_N, \Omega_{-N} \sim \Omega_N) & \end{bmatrix} \frac{d\mathbf{\Theta}_4}{dE} \\ \frac{d\mathbf{F}_{L4}}{dE} &= -\mathbf{R}_4^{-1} \frac{d\mathbf{R}_4}{dE} \mathbf{R}_4^{-1} \frac{2\pi}{\Delta\Omega} [\mathbf{H}_{12}(\omega_{-N} \sim \omega_N, \Omega_{-N} \sim \Omega_N)] [\mathbf{F}_{Ue}(\Omega_{-N} \sim \Omega_N)] \end{aligned}$$

The optimal Young's moduli of a disordered periodic mount can be approximately obtained by the frequency-domain steepest gradient method [72]:

$$E_l(t_{n+1}) = E_l(t_n) + \mu_l \text{IFFT} \left( \left[ \frac{\partial P_w}{\partial E} \left( \frac{\partial P_w}{\partial E} \right)^* \right]^T \right) \quad (3.24)$$

where  $\mu_l$  is an adjustable parameter in the steepest gradient algorithm and  $\text{IFFT}(\ )$  represents the inverse FFT of which only the causal part (first half of the result) is used in the adaptation. The Young's moduli of all the disordered SMA inserts are updated in time domain by frequency-domain data, specifically by the total vibratory power in the frequency region of interest. Similar with  $\frac{dP_w}{dE}$ ,  $\frac{\partial P_w}{\partial E_l}$  can be solved by Eq. (3.23) when the models of all structures of the whole system are available, or can be approximated by numerical differentiation when these models are not available. The two adaptation modes, adaptive-passive mode and active mode, can be used to apply the algorithm Eq. (3.24) to control the system,

in the same way as used by Eq. (3.21). Whether it is adaptive-passive control or active control depends on when the heat energy is applied to the SMA inserts - after the visual adaptation of the Young's modulus converges or after each step of adaptation. The adaptive-passive method is adopted here.

For both the adaptive-passive adaption and the active adaptation of Eqs. (3.21) and (3.24), the variation of the structural parameters of the machine and foundation should be slower than the adaptation rate. For the adaptive-passive adaption, the speed of the crystalline phase transform of the SMA material should be faster than the convergence speed; for the active adaptation, this speed of the crystalline phase transform of the SMA material should be faster than the adaptation speed of the algorithm. The adjustable parameters  $\mu$  and  $\mu_l$  can be varied according to the transmitted power and the range of the Young's modulus, according to the theory of the steepest gradient algorithm. If it is a time-varying system,  $\mu$  and  $\mu_l$  should be time-varying parameters. By adjusting  $\mu$  and  $\mu_l$ , this method and the first method described in Section 3.2.1 can achieve same control effect. However, they are different in some aspects. The first method provides normalized transmission loss, but needs to examine the characteristics of the fluctuating external excitation frequently such that an optimal parameter can be selected based on these characteristics. The second method is exempted from this concern, but requires

adaptation. Additionally, when models become less valid because of the unexpected change occurring to the system, the database of  $P_{TL}(T)$  obtained by the first method needs to be recalculated. However, the algorithm governing the second method can solve this problem because it is applicable to the situation without accurate models if shifting the mode of adaptive-passive adaptation to the mode of active adaptation.

### **3.3 The Semi-two-dimensional Model**

To apply the above theory more extensively and offer an insight into the problems of the vibration isolation of three-dimensional nonrigid systems using periodic structures, a semi-two-dimensional model is provided (see Fig. 3-2(a)). The free-free beam on the top and the clamped-clamped beam on the bottom represent a machine and a foundation, respectively. Beams are the kind of uncomplicated structures which can be mathematically analyzed easily but possess an infinite number of modes. Hence, they are chosen here to form a realistic representation of nonrigid machines and foundations. The middle part lying between the free-free and the clamped-clamped beams is the modified version of Yun and Mak's periodic structure [1]. This is chosen to be an isolating mount because: (1) the periodic structure has more than one mounting point and thus it is adequate to use one such structure to simulate the multi-mount situation; (2) it is complicated to the extent that it involves all the DOF of motion in a plane, namely the translational vibrations along the x and

y axes and the rotation in the x-y plane; but (3) it is also simple to the extent that an analytical solution can be obtained without approximation. Therefore, this structure is a reasonable simulation for testing the vibration isolation problem of nonrigid systems. To realize broadband vibration control, it is proposed to use SMA transverse branches to create variable stop bands. It is further proposed that the two parallel beams vertically supporting the machine are of a non-SMA elastic material with high modulus so that the gravity of the machine cannot undermine the assumption of small deflection and stress. All the beams in this model have rectangular cross-sections for the convenience of derivation and numerical simulation.

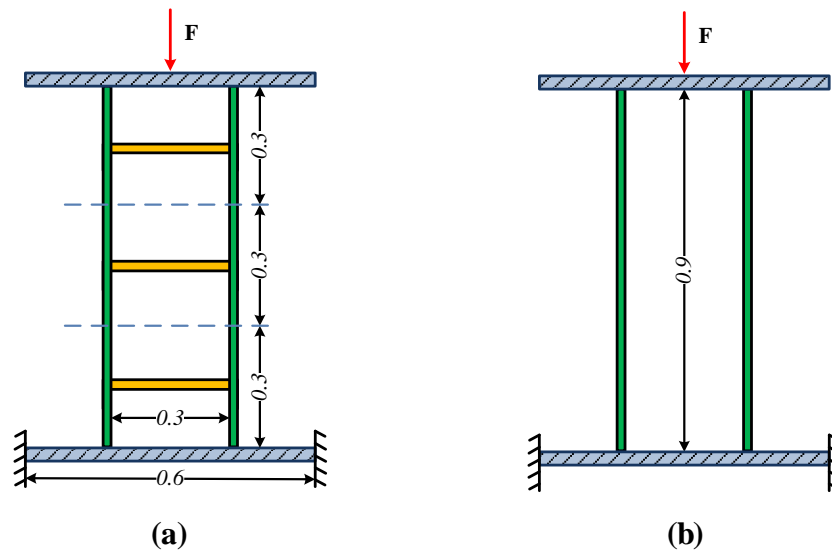


Figure 3-2 The semi-two-dimensional system (a) and the compared system (b)

In this investigation, the translation along the x and y axes and the rotation in the x-y plane are considered as part of the employment of the semi-two-dimensional model. Therefore, the vectors of velocity and force at the  $j^{th}$  contacting point are  $\mathbf{V}_{Uj} = [V_{jy}, V_{j\theta}, V_{jx}]^T$  and  $\mathbf{F}_{Uj} = [F_{jy}, M_{jz}, F_{jx}]^T$  where  $j=1, 2, \dots, q$ , and  $q=3$  if only one periodic structure is used. For the free-free beam, the matrix of mobilities from  $\mathbf{F}_{Ui}$  at an arbitrary position to  $\mathbf{V}_{Uj}$  at another arbitrary position is  $\mathbf{V}_{Uj} = \mathbf{B}_{ji} \mathbf{F}_{Ui}$ , and  $\mathbf{H}_U = (\mathbf{B}_{ji})_{3q \times 3q}$  is the matrix of mobility composed of sub-matrices  $\mathbf{B}_{ji}$ . For the clamped-clamped beam, the matrix of mobilities from  $\mathbf{F}_{Li}$  at an arbitrary position to  $\mathbf{V}_{Lj}$  at another arbitrary position is  $\mathbf{V}_{Lj} = \mathbf{C}_{ji} \mathbf{F}_{Li}$  and  $\mathbf{G}_L = (\mathbf{C}_{ji})_{3p \times 3p} \cdot \mathbf{B}_{ji}$  and  $\mathbf{C}_{ji}$  can be obtained by modal superposition based on the characteristic functions of beams [73]. For the periodic mount containing  $r$  cells, the transfer matrix (from the foundation to the machine) of  $r$  identical cells is  $\mathbf{Z}_M^{(k)} = \mathbf{T}^{-r}$  where  $\mathbf{T} = \mathbf{S}_{FV} \mathbf{P}_{wv}^{1/2} \mathbf{S}_{FV}^{-1} \mathbf{W} \mathbf{S}_{FV} \mathbf{P}_{wv}^{1/2} \mathbf{S}_{FV}^{-1}$  is the transfer matrix (from the machine to the foundation) of one periodic cell. For the periodic structure with different cells, the transfer matrix (from the foundation to the machine) of  $r$  cells is modified as  $\mathbf{Z}_M^{(k)} = (\mathbf{T}_r \cdots \mathbf{T}_2 \mathbf{T}_1)^{-1}$  where  $\mathbf{T}_l = \mathbf{S}_{FV} \mathbf{P}_{wv}^{1/2} \mathbf{S}_{FV}^{-1} \mathbf{W}_l \mathbf{S}_{FV} \mathbf{P}_{wv}^{1/2} \mathbf{S}_{FV}^{-1}$  is the transfer matrix (from the machine to the foundation) of one periodic cell.

$\mathbf{P}_{wv}$ ,  $\mathbf{S}_{FV}$  and  $\mathbf{W}$  are defined by following parameters. Let subscript  $A$  and  $B$  represent the left and right vertical beams of the periodic mount and subscript  $C$

represent the branches.  $\rho_A, \rho_B$  and  $\rho_C$  are the densities of them;  $D_A, D_B$  and  $D_C$  are the bending stiffness of them;  $k_{Af}$  and  $k_{Bf}$  are the flexural wave numbers of them;  $k_{Al}$  and  $k_{Bl}$  are the longitudinal wave numbers of them;  $c_A, c_B$  are  $c_C$  the acoustic speeds of the longitudinal waves of them;  $L_N$  is the length of the vertical beams in each periodic cell and  $L$  is the length of the branches. Then, the matrix governing the propagation of the coupled flexural and longitudinal waves,  $\mathbf{P}_{wv}$ , is expressed as

$$\mathbf{P}_{wv} = \text{diag}(\mathbf{P}_{Af}, \mathbf{P}_{Al}, \mathbf{P}_{Bf}, \mathbf{P}_{Bl}) \quad (3.25)$$

$$\text{where } \mathbf{P}_{Af} = \text{diag}(e^{-jk_{Af}L_N}, e^{-k_{Af}L_N}, e^{jk_{Af}L_N}, e^{k_{Af}L_N}),$$

$$\mathbf{P}_{Al} = \text{diag}(e^{-jk_{Al}L_N}, e^{jk_{Al}L_N}),$$

$$\mathbf{P}_{Bf} = \text{diag}(e^{-jk_{Bf}L_N}, e^{-k_{Bf}L_N}, e^{jk_{Bf}L_N}, e^{k_{Bf}L_N}),$$

$$\text{and } \mathbf{P}_{Bl} = \text{diag}(e^{-jk_{Bl}L_N}, e^{jk_{Bl}L_N}).$$

The matrix describing the relation between the propagating waves and the velocities and forces,  $\mathbf{S}_{FV}$ , is governed by

$$\mathbf{S}_{FV} = \begin{bmatrix} \mathbf{S}_{FA} & \mathbf{O}_{3 \times 6} \\ \mathbf{O}_{3 \times 6} & \mathbf{S}_{FB} \\ \mathbf{S}_{VA} & \mathbf{O}_{3 \times 6} \\ \mathbf{O}_{3 \times 6} & \mathbf{S}_{VB} \end{bmatrix} \quad (3.26)$$

where

$$R_{AM} = \frac{D_A k_{Af}^2}{j\omega}, R_{BM} = \frac{D_B k_{Af}^2}{j\omega}, R_{AF} = \frac{D_A k_{Af}^3}{j\omega}, R_{BF} = \frac{D_B k_{Bf}^3}{j\omega}, R_{Al} = \rho_A c_A, R_{Bl} = \rho_B c_B,$$

$$\mathbf{S}_{FA} = \begin{bmatrix} R_{AM} & -R_{AM} & R_{AM} & -R_{AM} & R_{AI} & -R_{AI} \\ jR_{AF} & -R_{AF} & -jR_{AF} & R_{AF} & & \end{bmatrix},$$

$$\mathbf{S}_{VA} = \begin{bmatrix} & & & & 1 & 1 \\ -jk_{Af} & -k_{Af} & jk_{Af} & k_{Af} & & \\ 1 & 1 & 1 & 1 & & \end{bmatrix},$$

$$\mathbf{S}_{FB} = \begin{bmatrix} R_{BM} & -R_{BM} & R_{BM} & -R_{BM} & R_{BI} & -R_{BI} \\ jR_{BF} & -R_{BF} & -jR_{BF} & R_{BF} & & \end{bmatrix},$$

$$\text{and } \mathbf{S}_{VB} = \begin{bmatrix} & & & & 1 & 1 \\ -jk_{Bf} & -k_{Bf} & jk_{Bf} & k_{Bf} & & \\ 1 & 1 & 1 & 1 & & \end{bmatrix}.$$

The matrices coupling the vertical beams  $A$  and  $B$  and a branch  $C$  in a periodic cell is

$$\mathbf{W} = \begin{bmatrix} \mathbf{I}_6 & -\mathbf{W}_F \mathbf{W}_V^{-1} \\ \mathbf{O}_6 & I_6 \end{bmatrix} \quad (3.27)$$

By defining  $\phi_{Cf} = e^{k_{Cf}L}$ ,  $\phi_{Cl} = e^{k_{Cl}L}$ ,  $\Omega_{CM} = \frac{D_C k_{Cf}^2}{j\omega}$ ,  $\Omega_{CF} = \frac{D_C k_{Cf}^3}{j\omega}$ ,  $R_{Cl} = \rho_C c_C$ ,

sub-matrices  $\mathbf{W}_F$  and  $\mathbf{W}_V$  take the following expressions

$$\mathbf{W}_F = \begin{bmatrix} & & j\Omega_{CF} & j\Omega_{CF} & -j\Omega_{CF} & \Omega_{CF} \\ & & \Omega_{CM} & -\Omega_{CM} & -\Omega_{CM} & -\Omega_{CM} \\ R_{cl} & -R_{cl} & & & & \\ & & -j\phi_{Cf}^{-j}\Omega_{CF} & \phi_{Cf}^{-1}\Omega_{CFc} & j\phi_{Cf}^{-j}\Omega_{CF} & -\phi_{Cf}\Omega_{CF} \\ & & -\phi_{Cf}^{-j}\Omega_{CM} & \phi_{Cf}^{-1}\Omega_{CM} & -\phi_{Cf}^j\Omega_{CM} & \phi_{Cf}\Omega_{CM} \\ -R_{cl}\phi_{Cl}^{-j} & R_{cl}\phi_{Cl}^j & & & & \end{bmatrix},$$



$$\text{and } \mathbf{W}_V = \begin{bmatrix} & & 1 & 1 & 1 & 1 \\ & & -jk_{cf} & -k_{cf} & jk_{cf} & k_{cf} \\ 1 & 1 & & & & \\ & & \phi_{cf}^{-j} & \phi_{cf}^{-1} & \phi_{cf}^j & \phi_{cf} \\ & & -jk_{cf}\phi_{cf}^{-j} & -k_{cf}\phi_{cf}^{-1} & jk_{cf}\phi_{cf}^j & k_{cf}\phi_{cf} \\ \phi_{cl}^{-j} & \phi_{cl}^j & & & & \end{bmatrix}.$$

### 3.4 Numerical Simulation and Analysis

Numerical simulations are conducted on the LTI semi-two-dimensional model (see Fig. 3-2(a)) and the LTI system for comparison (see Fig. 3-2(b)), and the first method in Section 3.2.1 is applied to examine the adaptive-passive control performance of the periodic mount. Fig. 3-2(b) shares same parameters with Fig. 3-2(a) except that it does not have a periodic mount. The non-SMA vertical beams are assumed to have the same physical and geometrical parameters in every simulation, and the subscript  $N$  is used to denote all the parameters which belong to the left (beam  $A$ ) and right (beam  $B$ ) vertical beams in Section 3.3. All the numerical results are normalized to the nondimensional frequency  $\Omega = \omega/\omega_r$  by defining a reference frequency  $\omega_r = \sqrt{E_N I_N / (\rho_N A_N L_N^4)}$ , where  $\omega$  is angular frequency, and  $L_N, A_N, I_N$  and  $E_N$  are the vertical length of each periodic cell, the area, the moment of inertia of the cross-section, and the Young's modulus of the non-SMA vertical beams, respectively.

The three branches shown in Fig. 3-2(a) may be different in terms of their Young's moduli in a simulation. Hereafter, they are referred to as "disordered branches" which is the opposite of identical branches, and their correspondent periodic structure is called the "disordered periodic structure" which is the opposite of a regular periodic structure or a structure with strict periodicity. The physical and geometrical parameters of the machine, the vertical beams, the branches, and the foundation in Fig. 3-2 are listed in Table 3-1. The physical parameters of the SMA material in Table 3-1 are provided by Hodgson [74], and the range of the Young's modulus  $[E_1, E_2]$  is set as [30, 80] Gpa in this section.

**Table 3-1 The structural parameters of the systems in Fig. 3-2**

Structure	Young's modulus (Gpa)	Density (kg/m <sup>3</sup> )	Loss factor	Dimension (m×m×m)
SMA branch				
Martensite	28-41	6450	0	0.03×0.03×0.3
Austenite	83	6450	0	0.03×0.03×0.3
	83.1	2000	0.02	0.03×0.03×0.9
Two non-SMA supporting beams	8.31	200	0.02	0.03×0.03×0.9
	8.31	2000	0.02	0.03×0.03×0.9
Machine (free-free beam)	380	1900	0.02	0.03×0.03×0.6
Foundation (fixed-fixed beam)	380	1900	0.02	0.03×0.03×0.6

The external excitation shown in Fig. 3-2 is expressed as

$$\mathbf{F}_{Ue} = \mathbf{F}_{U3} = [F_{3y}, M_{3z}, F_{3x}]^T, \text{ which represents the forces along the x and y axes and}$$

the moment in the x-y plane. The unit impulse excitations (transformed as unit forces in frequency domains) - the vertical force  $\mathbf{F}_{U_e} = [1, 0, 0]$ , moment  $\mathbf{F}_{U_e} = [0, 1, 0]$ , and horizontal force  $\mathbf{F}_{U_e} = [0, 0, 1]$ - are separately applied to the systems at the third contact point ( $j = 3$ ). The relationship between the power transmission loss and the Young's moduli of the three branches of the semi-two-dimensional model is investigated according to the procedures outlined for the database approach, and the curves of the relationship are depicted in Figs. (3-3)-(3-5). Figs. (3-3)-(3-5) correspond to the three sets of the parameters of the vertically supporting beams listed in Table 3-1 -  $E_N = 83.1$  Gpa and  $\rho_N = 2000$  kg,  $E_N = 8.31$  Gpa and  $\rho_N = 200$ kg, and  $E_N = 8.31$ Gpa and  $\rho_N = 2000$ kg. In each of these figures, the first two ((a), (b)), the middle two ((c), (d)), and the final two ((e), (f)) graphs illustrate the transmission losses under the vertical force, the moment and the horizontal force respectively, and the enveloping lines of these transmission losses. The first, third, and fifth graphs ((a), (c), and (e)) in Figs. (3-3)-(3-5) depict the transmission losses in the situation where the periodic mount has identical branches, while the remainder ((b), (d), and (f)) describe the scenario with disordered branches. Overall, there are 18 graphs in Figs. (3-3)-(3-5), which correspond to the three sets of parameters of the vertical non-SMA beams, the three external loads, and the two situations of branches.

Transmission losses in the situation of identical branches are calculated at the 21 values of Young's modulus equally distributed in the range of [30, 80] Gpa, but only the curves when  $E = [30, 32.5, 42.5, 52.5, 62.5, 72.5]$  Gpa are depicted in the first, third, and fifth graphs in Figs. (3-3)-(3-5). In each graph, the dashed line is the curve of the transmission loss when  $E = 30$  Gpa, and the other five lines (thin and solid) represent the transmission losses at the other five values. These curves are analyzed in the frequency band situated above the value approximately five times the reference frequency Figs. (3-3)-(3-4) and approximately ten times that in Figs. 3-5. This is because the transmission losses in the lower frequency band are decided mainly by the parameters of the vertical beams and the parameters of branches have only a minor influence. By comparing the dashed lines in Fig. 3-3(a), Fig. 3-4(a) and Fig. 3-5(a), it can be seen that after changing the physical parameters of the supporting beams in design stage, the minimum level of transmission losses increases but the peaks of the transmission loss curves remain separate. This indicates that the stop bands exist separately and the pass bands are not canceled, since the former are associated with the peak frequencies. It implies that although the structural parameters of the non-SMA components of the periodic mount can be selected to cover different frequencies of at design stage, the fixed stop-bands may not cover the variations of the frequencies of interest once the isolator is installed. Therefore, the effort in design stage may not guarantee a satisfactory control effect

after the installation of an isolator since the frequency of interest may change with the operating and environmental conditions. Moreover, although the minimum level of transmission losses achieved by changing the parameters of the non-SMA components in the design stage can be increased, this insignificant increase cannot compensate for the drawback caused by the slight extension of the stop bands. This is because in stop bands characteristic waves (that is, fundamental waves propagating along a periodic structure) decay exponentially and this exponential attenuation leads to a significant increase of transmission loss. Hence, in the situation that the stop bands cannot be widened considerably by selecting the parameters of the unadaptable components (like the non-SMA beams) in design stage, adjusting the parameters of components made of the smart material after installation is a reasonable choice. By comparing the six curves in one of the three graphs, it can be seen that with the increase in modulus of the SMA branches after installation, the peak frequencies of the transmission loss curves shift from the dashed line on the left to the thin solid line on the right. This implies that the stop bands are movable and indeed do move to the right with the increase in modulus of the SMA branches. With this shift of the stop bands, the frequencies of interest, including the peak frequencies of the PSD of the vibratory source, may be covered. Furthermore, by increasing the modulus and moving stop bands, the enveloping line (black, thick, and solid) is formed. This curve is formed by the combination of the stop bands of all

transmission loss curves, and meanwhile by the maxima of all the transmission losses at every frequency value. It therefore represents the ability of the SMA branches to attenuate broadband vibration transmissions since it has the widest stop bands and the maximum transmission loss obtainable in the range of [30 80] Gpa. The frequencies of interest can therefore be covered as long as these frequencies are located in the broad stop bands of the enveloping line. A similar control effect can be observed in the other graphs in Figs. (3-3)-(3-5).

Transmission losses in the disordered branches scenario are calculated at the 7 values of Young's modulus that are equally distributed in the range of [30, 80] Gpa, which are depicted in the second, fourth, and sixth graphs ((b), (d), and (f)) in Figs. (3-3)-(3-5). An enveloping curve is formed in each graph, which also indicates the optimal transmission loss obtainable within the range of [30, 80] Gpa. Fig. 3-6 compares the enveloping curves in the first graphs (the identical branches) and second graphs (the disordered branches) in Fig. (3-3)-(3-5) and the transmission loss of the compared system in Fig. 3-2(b). In each graph of Fig. 3-6, the transmission loss of the compared system, denoted by a thin and solid line, is at a much smaller level. Furthermore, the peak frequencies are separate, and the stop bands associated with them are narrow. This contrast shows the advantages of the periodic mount over two rubberlike mounts (two vertical beams).

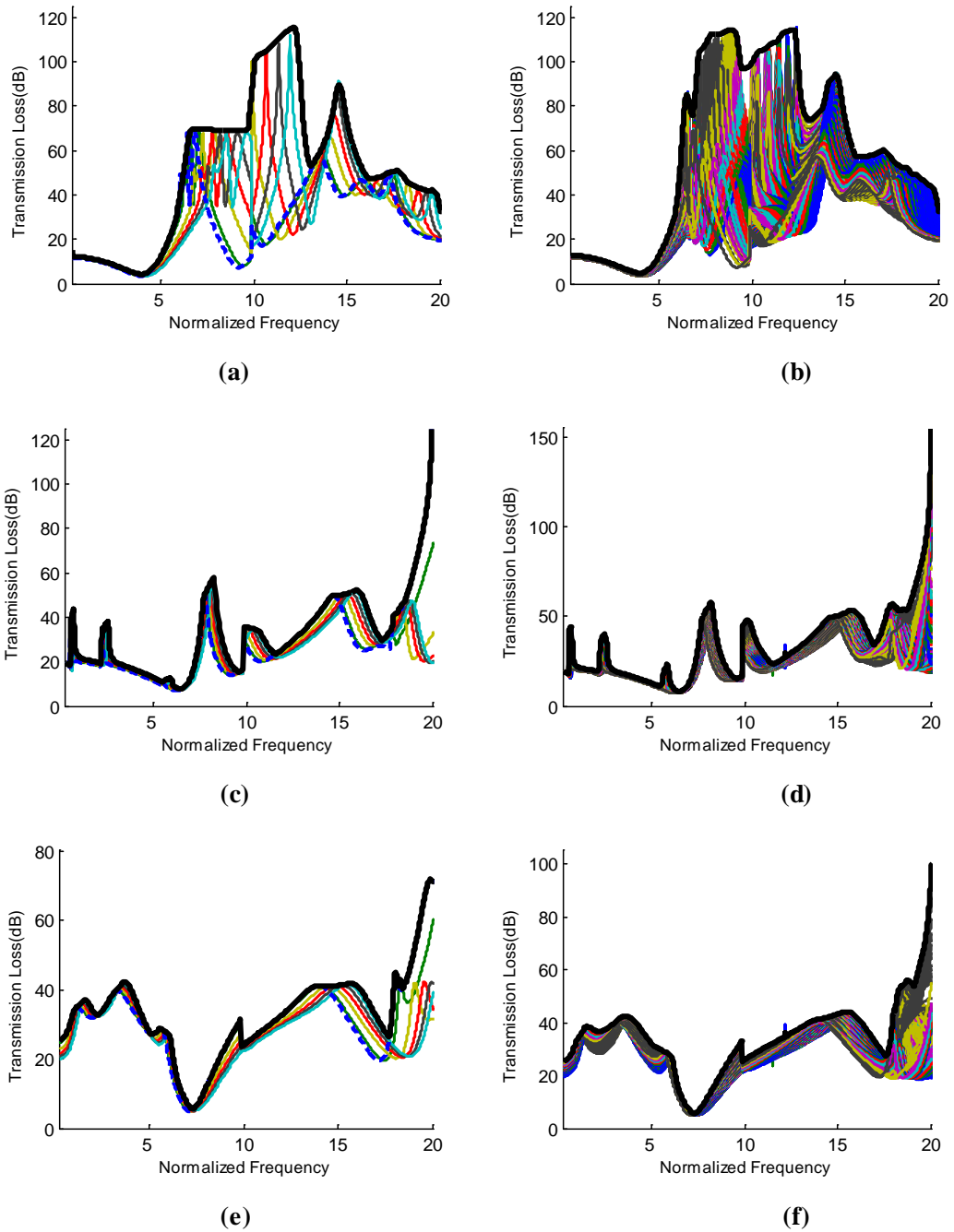


**Figure 3-3 Enveloping lines ( — ) and transmission losses when  $E_N = 83.1$  Gpa and  $\rho_N = 2000$  kg: (a) Vertical force and identical branches; (b) Vertical force and disordered branches; (c) Moment and identical branches; (d) Moment and disordered branches; (e) Horizontal force and identical branches; (f) Horizontal force and disordered branches.**

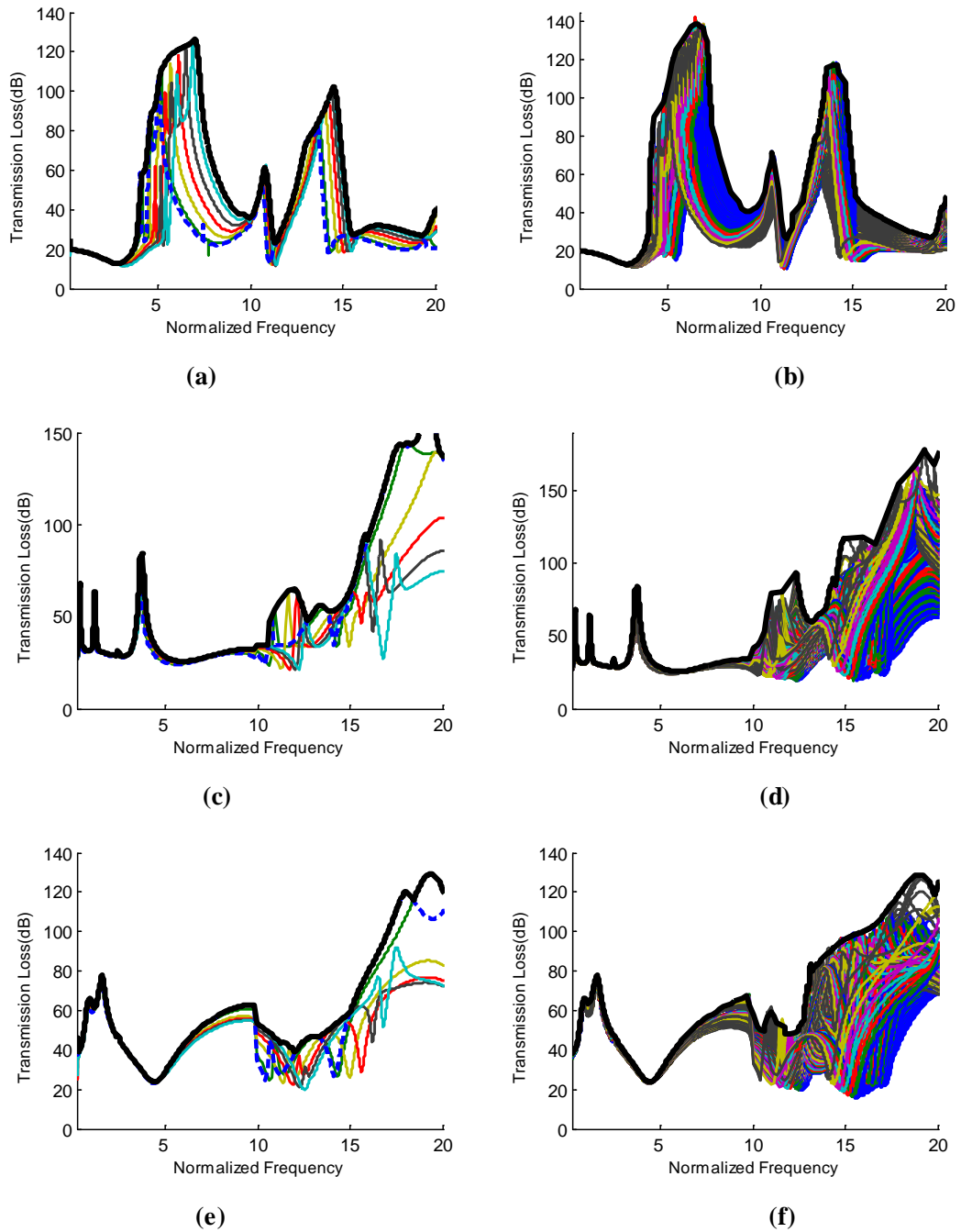
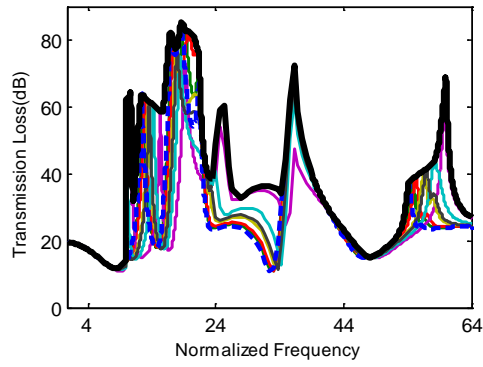
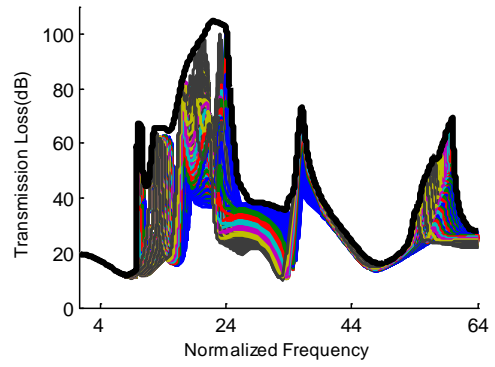


**Figure 3-4 Enveloping lines ( — ) and transmission losses when  $E_N = 8.31$  Gpa and  $\rho_N = 200$  kg: (a) Vertical force and identical branches; (b) Vertical force and disordered branches; (c) Moment and identical branches; (d) Moment and disordered branches; (e) Horizontal force and identical branches; (f) Horizontal force and disordered branches.**

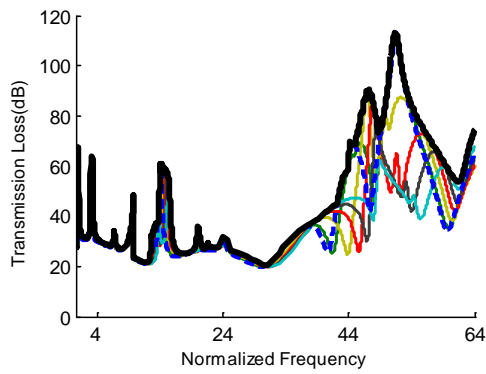




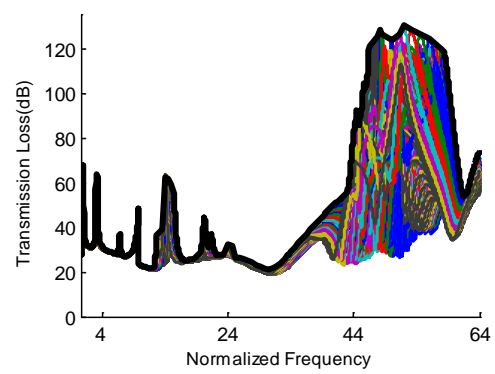
(a)



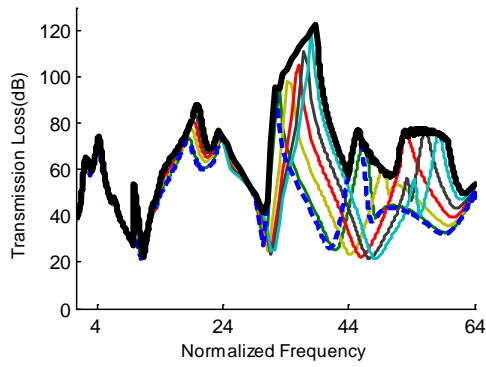
(b)



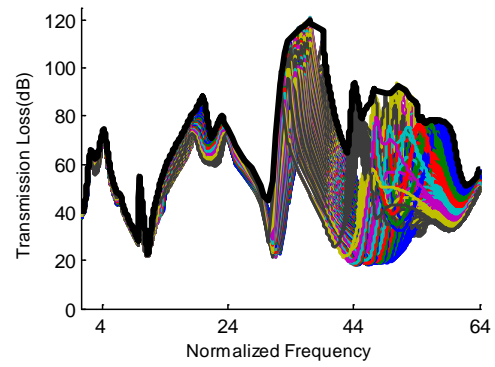
(c)



(d)

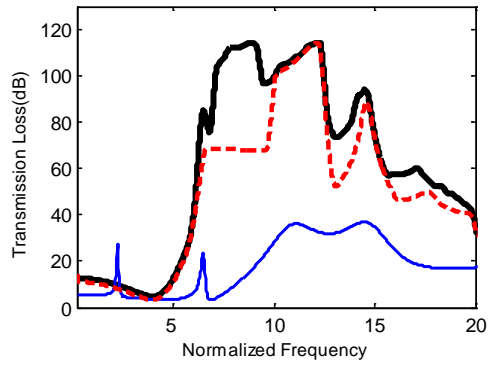


(e)

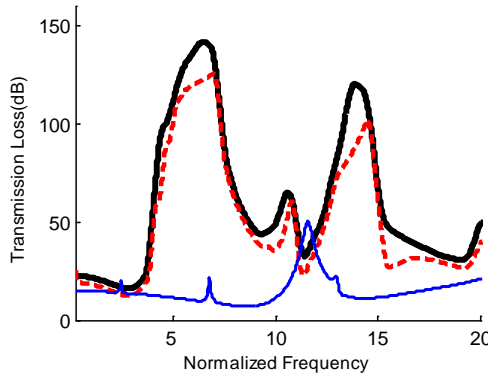


(f)

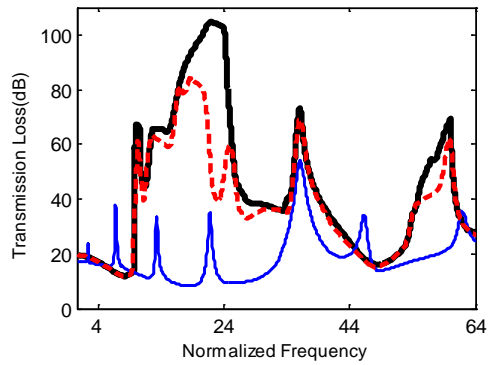
**Figure 3-5 Enveloping lines ( — ) and transmission losses when  $E_N = 8.31$  Gpa and  $\rho_N = 2000$  kg: (a) Vertical force and identical branches; (b) Vertical force and disordered branches; (c) Moment and identical branches; (d) Moment and disordered branches; (e) Horizontal force and identical branches; (f) Horizontal force and disordered branches.**



(a)



(b)



(c)

**Figure 3-6** Enveloping line in the situation of disordered branches ( — ), enveloping line in the situation of identical branches ( - - - ), and the transmission loss in the situation of no branches ( — ): (a) Enveloping lines from Fig. 3-3(a) and Fig. 3-3(b); (b) Enveloping lines from Fig. 3-4(a) and Fig. 3-4(b); (c) Enveloping lines from Fig. 3-5(a) and Fig. 3-5(b).

In addition, it can be seen in every graph of Fig. 3-6 that the vibration control performance achieved by the disordered periodic mount (the black solid line) is better than that achieved by the regular mount (the red dashed line). Only three branches are considered here, so the number of random combinations of branches in terms of Young's modulus is the cube of seven. The superiority of the disordered branches in a periodic mount will be prominent if more periodic cells are added.

### **3.5 Experimental Study**

This experiment is employed to indirectly demonstrate the correctness of the derivation about the periodic mount in Section 3.3 through the comparison of analytical and experimental characteristic waves of a periodic structure. In this section, the relations between the transition and transfer matrices of a finite periodic structure and the characteristic waves (Bloch waves) are analyzed. It is found that they are varied with the change of the location on the periodic structure. However, they can be approximated respectively by two common matrices. One is provided to represent the common relation between all the transition matrices at different positions and characteristic waves; the other is provided to represent the common relation between all the transfer matrices at different positions and characteristic waves. Propagation constants of the characteristic waves can be extracted from a common matrix, and this common matrix can be constructed by responses. This

approach to acquire characteristic waves is a significant departure from the theoretical methods, like transfer matrix method [1, 5] and propagation wave method[41-43].

### 3.5.1 Junction mobilities

For a general one-dimensional or semi-two-dimensional infinite periodic structure, each periodic sub-structure is coupled with two adjacent sub-structures through  $n$  motion coordinates. The transmission relation of  $n$  motions from one periodic element to the next can be described by the transfer matrix [1, 5, 41],

$$\begin{bmatrix} \mathbf{V} \\ \mathbf{F} \end{bmatrix}_{m+1} = \mathbf{T}_{m+1,m} \begin{bmatrix} \mathbf{V} \\ \mathbf{F} \end{bmatrix}_m, m = 1, 2 \dots \infty \quad (3.28)$$

where  $\mathbf{V}$  and  $\mathbf{F}$  represent the  $n$ -dimensional velocity vector and the force vector, and the subscript  $m$  indicates the order number of the coupled location of the  $n$  motions. The transfer matrix  $\mathbf{T}_{m+1,m}$  can be decomposed as

$$\mathbf{T}_{m+1,m} = \begin{bmatrix} \mathbf{v}_+ & \mathbf{v}_- \\ \mathbf{f}_+ & \mathbf{f}_- \end{bmatrix} \begin{bmatrix} \Lambda^{-1} & \\ & \Lambda \end{bmatrix} \begin{bmatrix} \mathbf{v}_+ & \mathbf{v}_- \\ \mathbf{f}_+ & \mathbf{f}_- \end{bmatrix}^{-1} \quad (3.29)$$

Where  $\Lambda$  is a  $n \times n$  diagonal matrix whose elements are  $\lambda_k$  ( $|\lambda_k| \geq 1, k = 1 \dots n$ ).  $1/\lambda_k$  is the adjoint eigenvalue of  $\lambda_k$ . Here,  $\mu_k = \ln(\lambda_k) = \mu_{Rk} + i\mu_{Ik}$  expresses the negative-going wave as one member in a pair of characteristic ‘propagation constants’ while  $-\mu_k = \ln(1/\lambda_k)$  is the other member and represents the positive-going waves, when  $\mu_{Rk}$  and  $\mu_{Ik}$  are defined as positive numbers. The real

part  $\mu_{Rk}$  is the ‘attenuation constant’, describing the exponential attenuating rate, and the imaginary part  $\mu_{Ik}$  is the ‘phase constant’, representing the change in phase of the  $k$ th characteristic waves. In the light of the relation between an eigenvalue  $\lambda$  and the corresponding propagation constant  $\mu$ ,  $\Lambda$  is denoted as  $e_{\Lambda}^{\mu}$ .

$$\mathbf{T}_{m+1,m} = \begin{bmatrix} \mathbf{v}_+ & \mathbf{v}_- \\ \mathbf{f}_+ & \mathbf{f}_- \end{bmatrix} \begin{bmatrix} \mathbf{e}_{\Lambda}^{-\mu} & \\ & \mathbf{e}_{\Lambda}^{\mu} \end{bmatrix} \begin{bmatrix} \mathbf{v}_+ & \mathbf{v}_- \\ \mathbf{f}_+ & \mathbf{f}_- \end{bmatrix}^{-1}$$

Based on the above periodic structure theory and parameters, the mobility of each junction of N-periodicity finite periodic structures has been derived [75] and the general expression of the mobility from  $j^{\text{th}}$  junction to  $m^{\text{th}}$  junction,  $\mathbf{Y}_{mj}$ , is

$$\begin{cases} \mathbf{V}_{mj} = \mathbf{Y}_{mj} \mathbf{F}_j \\ \mathbf{Y}_{mj} = \mathbf{Y}_{Rmj} (I + \mathbf{Y}_{Ljj}^{-1} \mathbf{Y}_{Rjj})^{-1} \end{cases} \quad (3.30)$$

where

$$\mathbf{Y}_{Ljj} = (\mathbf{v}_+ \mathbf{e}_{\Lambda}^{-j\mu} \mathbf{r}_A + \mathbf{v}_- \mathbf{e}_{\Lambda}^{j\mu}) \times (-\mathbf{f}_+ \mathbf{e}_{\Lambda}^{-j\mu} \mathbf{r}_A - \mathbf{f}_- \mathbf{e}_{\Lambda}^{j\mu})^{-1}, \text{ and}$$

$$\mathbf{Y}_{Rmj} = (\mathbf{v}_+ \mathbf{e}_{\Lambda}^{-(m-j)\mu} + \mathbf{v}_- \mathbf{e}_{\Lambda}^{(m-j)\mu} \mathbf{e}_{\Lambda}^{-(N-j)\mu} \mathbf{r}_B \mathbf{e}_{\Lambda}^{-(N-j)\mu}) \times (\mathbf{f}_+ + \mathbf{f}_- \mathbf{e}_{\Lambda}^{-(N-j)\mu} \mathbf{r}_B \mathbf{e}_{\Lambda}^{-(N-j)\mu})^{-1}$$

and  $\mathbf{r}_A$  and  $\mathbf{r}_B$  are respectively the left and right boundary reflection factors related to the left and right boundary impedances.

Using a similar derivation procedure to Friss and Ohlrich, the transfer function matrix  $\mathbf{Z}_{mj}$  from the applied forces at the  $j^{\text{th}}$  junction ( $\mathbf{F}_j$ ) to force responses at the  $m^{\text{th}}$  junction ( $\mathbf{F}_{mj}$ ) can be deduced from the conditions of the continuity of velocity

and equilibrium between the applied and inner forces.

$$\begin{cases} \mathbf{F}_{mj} = \mathbf{Z}_{mj} \mathbf{F}_j \\ \mathbf{Z}_{mj} = \mathbf{Z}_{Rmj} (\mathbf{I} + \mathbf{Y}_{Lij}^{-1} \mathbf{Y}_{Rij})^{-1} \end{cases} \quad (3.31)$$

where

$$\mathbf{Z}_{Rmj} = (\mathbf{f}_+ \mathbf{e}_\Lambda^{-(m-j)\mu} + \mathbf{f}_- \mathbf{e}_\Lambda^{(m-j)\mu} \mathbf{e}_\Lambda^{-(N-j)\mu} \mathbf{r}_B \mathbf{e}_\Lambda^{-(N-j)\mu}) \times (\mathbf{f}_+ + \mathbf{f}_- \mathbf{e}_\Lambda^{-(N-j)\mu} \mathbf{r}_B \mathbf{e}_\Lambda^{-(N-j)\mu})^{-1} .$$

### 3.5.2 The relation between Transition and Transfer Matrices of Finite Periodic Structures and Characteristic Waves

The transfer matrix method is widely used to analyze characteristic waves within infinite periodic structures. For finite structures, a different term, the ‘transition matrix method’, is adopted herein to govern the relation between the transfer matrix of a finite periodic structure and the characteristic waves. The transition matrix for two adjacent periodic cells of a finite periodic structure is defined as the relation of their mobilities,

$$\mathbf{Y}_{m+1,j} = \mathbf{T}_{m+1,m}^{fin} \mathbf{Y}_{mj} \quad (3.32)$$

then, based on the formulas of mobilities governed by Eq. (3.30), the relation between the transition matrix and the characteristic waves takes the following expression [see Eq. (3.33)].

$$\mathbf{T}_{m+1,m}^{fin} = [\mathbf{v}_+, \mathbf{v}_-] \begin{bmatrix} \mathbf{e}_\Lambda^{-\mu} & \\ & \mathbf{e}_\Lambda^{\mu} \end{bmatrix} \times \mathbf{M} \{ [\mathbf{v}_+, \mathbf{v}_-] \mathbf{M} \}^{-1} \quad (3.33)$$

where

$$\mathbf{M} = \begin{bmatrix} \mathbf{e}_\Lambda^{-(m-j)\mu} \\ \mathbf{e}_\Lambda^{(m-j)\mu} \mathbf{e}_\Lambda^{-(N-j)\mu} \mathbf{r}_B \mathbf{e}_\Lambda^{-(N-j)\mu} \end{bmatrix}.$$

Similarly, the relation between the transfer matrix of a finite system and characteristic waves can be described by Eq. (3.34) after some mathematical manipulations to Eqs. (3.30) and (3.31).

$$\begin{bmatrix} \mathbf{Y}_{m+1,j} \\ \mathbf{Z}_{m+1,j} \end{bmatrix} = \mathbf{Tr}_{m+1,m}^{fin} \begin{bmatrix} \mathbf{Y}_{m,j} \\ \mathbf{Z}_{m,j} \end{bmatrix}$$

where

$$\mathbf{Tr}_{m+1,m}^{fin} = \begin{bmatrix} \mathbf{v}_+ & \mathbf{v}_- \\ \mathbf{f}_+ & \mathbf{f}_- \end{bmatrix} \begin{bmatrix} \mathbf{e}_\Lambda^{-\mu} & \\ & \mathbf{e}_\Lambda^\mu \end{bmatrix} \times \mathbf{M} \mathbf{M}^+ \begin{bmatrix} \mathbf{v}_+ & \mathbf{v}_- \\ \mathbf{f}_+ & \mathbf{f}_- \end{bmatrix}^{-1} \quad (3.34)$$

where the superscript '+' represents M-P inverse.

The matrices governed by Eqs. (3.33) and (3.34) have three properties. Based on the following discussions about these properties, a common matrix for each of them will be defined in terms of the responses of finite periodic structures.

Firstly, the two matrices have smaller ranks. Unlike the transfer matrix of infinite periodic structures, the rank of  $\mathbf{T}_{m+1,m}^{fin}$  and  $\mathbf{Tr}_{m+1,m}^{fin}$  is  $n$ , which is equal to the degrees of freedom of motion but exactly half the rank of the transfer matrix of infinite periodic structures. That is because the negative-going characteristic waves are correlated with the positive-going waves. In fact, the former are constructed from the latter by the boundary reflection. If the mobilities do not have a full rank due to

the incomplete excitation of characteristic waves, the rank of  $\mathbf{T}_{m+1,m}^{fin}$  and  $\mathbf{Tr}_{m+1,m}^{fin}$  may be less than  $n$ . In this case, the eigenvalues of the transition matrix corresponding to the unexcited characteristic waves are zero, but Eqs. (3.33) and (3.34) can still represent the relation on the basis of the theory of generalized inverse. The generalized inverse of a diagonal matrix whose elements are  $\lambda_k$  ( $k=1,2,\dots,n$ ) is also a diagonal matrix, and the diagonal elements are  $\lambda_k^+$  ( $k=1,2,\dots,n$ ) [75].  $\lambda_k^+$  is defined as

$$\lambda_k^+ = \begin{cases} 1/\lambda_k, \lambda_k \neq 0, \\ 0, \lambda_k = 0. \end{cases}$$

Therefore, Eqs. (3.33) and (3.34) can change their forms into Eqs. (3.35) and (3.36), in order to explicitly represent both the fully and partly excited situations.

$$\mathbf{T}_{m+1,m}^{fin} = \begin{bmatrix} \mathbf{v}_+ & \mathbf{v}_- \end{bmatrix} \begin{bmatrix} (\mathbf{e}_\Lambda^\mu)^+ & \\ & \mathbf{e}_\Lambda^\mu \end{bmatrix} \mathbf{M} \{ \begin{bmatrix} \mathbf{v}_+ & \mathbf{v}_- \end{bmatrix} \mathbf{M} \}^{-1} \quad (3.35)$$

$$\mathbf{Tr}_{m+1,m}^{fin} = \begin{bmatrix} \mathbf{v}_+ & \mathbf{v}_- \\ \mathbf{f}_+ & \mathbf{f}_- \end{bmatrix} \begin{bmatrix} (\mathbf{e}_\Lambda^\mu)^+ & \\ & \mathbf{e}_\Lambda^\mu \end{bmatrix} \times \mathbf{M} \mathbf{M}^+ \begin{bmatrix} \mathbf{v}_+ & \mathbf{v}_- \\ \mathbf{f}_+ & \mathbf{f}_- \end{bmatrix}^{-1} \quad (3.36)$$

Secondly, they vary with the change of  $m$ . However, the expressions on the right-hand of Eqs. (3.35) and (3.36) are nearly in the form of eigenvalue decomposition, although  $m$  is a variable. More specifically, the matrix at the right side of the diagonal matrix is the least-square approximation of the inverse of the matrix at the left side of the diagonal matrix for Eq. (3.35); for the other formula, the left matrix of the diagonal matrix is the least-square approximation of the inverse of



the right matrix. The process to prove that they are least-square approximations is elaborated as follows.

For Eq.(3.35), the product of the left  $[\mathbf{v}_+, \mathbf{v}_-]$  and the right matrix  $\mathbf{M}\{[\mathbf{v}_+, \mathbf{v}_-]\mathbf{M}\}^{-1}$  of the diagonal matrix in Eq. (3.35) is always a unity matrix (see Eq. (3.37)). Also, according to the definition and properties of the generalized inverse [76-77] the left matrix is always the  $\{1, 2, 4\}$ -inverse of the right matrix and the right matrix is always the  $\{1, 2, 3\}$ -inverse of the left. This kind of reciprocal inverse is very close to the unique M-P inverse in terms of properties, since the M-P inverse is also called the  $\{1, 2, 3, 4\}$ -inverse. Hence, even if the number  $m$  changes, all  $\mathbf{T}_{m+1,m}^{fin}$  approach a common unique matrix  $\mathbf{T}^{fin}$ .

$$[\mathbf{v}_+, \mathbf{v}_-] \times \mathbf{M}\{[\mathbf{v}_+, \mathbf{v}_-]\mathbf{M}\}^{-1} = \mathbf{I} \quad (3.37)$$

For Eq. (3.36), a similar analysis also makes sense. The left matrix of the diagonal matrix is always the  $\{1,3\}$ -inverse of the right matrix, so the following inequality holds,

$$\left\| \mathbf{M}\mathbf{M}^+ \begin{bmatrix} \mathbf{v}_+ & \mathbf{v}_- \\ \mathbf{f}_+ & \mathbf{f}_- \end{bmatrix}^{-1} \begin{bmatrix} \mathbf{v}_+ & \mathbf{v}_- \\ \mathbf{f}_+ & \mathbf{f}_- \end{bmatrix} - \mathbf{I} \right\| \leq \left\{ \left\| \mathbf{M}\mathbf{M}^+ \begin{bmatrix} \mathbf{v}_+ & \mathbf{v}_- \\ \mathbf{f}_+ & \mathbf{f}_- \end{bmatrix}^{-1} \mathbf{x} - \mathbf{I} \right\|, \mathbf{x} \in C^{2n} \right\} \quad (3.38)$$

where  $\|\cdot\|$  denotes the Euclidean norm. That is to say, among all  $\mathbf{x} \in C^{2n}$ , the left matrix of the diagonal matrix is the least-square solution of Eq. (3.39).

$$\mathbf{M}\mathbf{M}^+ \begin{bmatrix} \mathbf{v}_+ & \mathbf{v}_- \\ \mathbf{f}_+ & \mathbf{f}_- \end{bmatrix}^{-1} \mathbf{x} = \mathbf{I} \quad (3.39)$$

This means the product of the right and left matrices has the least-square error with the unity matrix. Therefore, even if the order number of the junction  $m$  is different, all  $\mathbf{Tr}_{m+1,m}^{fin}$  are close to a common unique matrix  $\mathbf{Tr}^{fin}$ .

Thirdly, the errors between individual and common transition matrices can be decreased by exciting fewer characteristic waves. Another thing worth mentioning is that the fewer the excited characteristic waves, the smaller the norm of the difference between the reduced matrix of the product of the left and right matrices and the unity matrix with the same rank, for any one equation in Eqs. (3.35) and (3.36). The reduced matrix is made up of the non-zero rows and columns of the product of the right and left matrices in either Eqs. (3.35) and (3.36) by eliminating the zero rows and columns of the product. Hence, the smaller the number of excited characteristic waves, the closer the right expressions of Eqs. (3.35) and (3.36) approach the ideal form of the eigenvalue decomposition, and the smaller the differences between each of  $\mathbf{T}_{m+1,m}^{fin}$  and  $\mathbf{T}^{fin}$  and  $\mathbf{Tr}_{m+1,m}^{fin}$  and  $\mathbf{Tr}^{fin}$ .

Therefore, based on the above mathematical analysis of the three properties of the two matrices of finite periodic structures, it is reasonable to describe the common transition matrices  $\mathbf{T}^{fin}$  and  $\mathbf{Tr}^{fin}$  by Eqs. (3.40) and (3.41). In other words,

although  $m$  is a variable and the two matrices change with it, it is also feasible to construct the common matrix for either Eqs. (3.35) and (3.36). From the responses of a finite periodic structure. For a periodic structure with  $n$  coupled motion ( $2n$  characteristic wave-types),  $n$  periodic elements and  $n+1$  junctions are adequate for the identification of all characteristic waves by the decomposition of a common matrix, implied by Eqs. (3.40) and (3.41). When the number of excited characteristic waves is smaller than  $n$ , the number of the response vectors in the response matrices can be decreased. As the boundary impedances of different finite periodic structures will change considerably, it is difficult to propose a specific standard method to simplify the matrix  $M$  and then to make the expressions at the right side of Eqs. (3.35) and (3.36) explicitly approach the ideal form of eigenvalue decomposition as closely as possible. However, the guiding principle is that exciting fewer characteristic waves will probably lead to more accuracy. Considering the symmetrical feature of the dual-layer structure, responses excited by only two symmetrical and antisymmetrical loads can be applied to yield the two common matrices in the following section. Moreover, Eqs. (3.40) and (3.41) might produce better identification performance of characteristic waves if a finite structure has heavy damping materials added, as discussed by Heckl [78]. Nevertheless, the method governed by Eqs. (3.40) and (3.41) differs from the traditional approach of solving one periodic element independently because performance is not dominated

by the added damping.

$$\mathbf{T}^{fn} = [\mathbf{V}_{n+j,j}, \mathbf{V}_{n+j-1,j} \cdots \mathbf{V}_{j+1,j}] \times [\mathbf{V}_{n+j-1,j}, \mathbf{V}_{n+j-2,j} \cdots \mathbf{V}_{jj}]^{-1} \quad (3.40)$$

$$\mathbf{Tr}^{fn} = \left\{ \begin{bmatrix} \mathbf{V} \\ \mathbf{F} \end{bmatrix}_{n+j,j}, \begin{bmatrix} \mathbf{V} \\ \mathbf{F} \end{bmatrix}_{n+j-1,j}, \dots, \begin{bmatrix} \mathbf{V} \\ \mathbf{F} \end{bmatrix}_{j+1,j} \right\} \times \left\{ \begin{bmatrix} \mathbf{V} \\ \mathbf{F} \end{bmatrix}_{n+j-1,j}, \begin{bmatrix} \mathbf{V} \\ \mathbf{F} \end{bmatrix}_{n+j-2,j}, \dots, \begin{bmatrix} \mathbf{V} \\ \mathbf{F} \end{bmatrix}_{jj} \right\}^{-1} \quad (3.41)$$

This process of derivation can be analogical with substructure coupling in vibration modal analysis when each periodic element is regarded as one substructure of the finite structure. In addition, for vibration modal analysis, all frequencies of interest should be covered, and some modes may be excited separately for the ease and accuracy of uncoupling of the equation of motion. Likewise, the method governed by Eqs. (3.40) and (3.41) cover all characteristic wave-types, and exciting fewer characteristic waves may lead to easier decoupling and higher accuracy. However, they are different processes. Vibratory modal analysis is the process to determine resonance frequencies, modal coordinates, and mode shapes. But, the decomposition of transition matrices is used to determine propagation constants instead of modal frequencies. Also, coordinate transformation results in characteristic waves (Bloch waves) herein rather than modal coordinates.

### 3.5.3 Experiment

An experiment is conducted to directly verify the analysis of the common relation

between all the transition matrices (or transfer matrices) at different positions and characteristic waves and to indirectly verify the derivation of the transfer matrix of the finite periodic mount in Section 3.3. As shown in Fig. 3-7, a dual-beam structure is suspended by elastic strings to ensure free vibration. Since three degrees of freedom for each junction were considered, the dual-beam structure is designed to have six periodic elements and seven junctions because the transition matrix has a maximum rank of six, based on the analysis in Section 3.5.2. It consists of two parallel beams and seven branches, fastened tightly at the beam-branch connection parts by steel screws to retain total coupling. The connection parts have a length of around 1.7 mm. The other parameters of the dual-beam finite periodic structure are listed in Table 3-2 and some of them are indicatively illustrated in Fig. 3-8, which also shows the three degrees of freedom.



**Figure 3-7 Experimental system**

The dual-layer periodic structure was excited longitudinally by a vibration exciter (Ling Dynamic System Type V403) fed with white noise. A force transducer (PCB ICP F-sensor 208C02) was placed between the vibration exciter and the driven beam to measure the applied force. Data acquisition (DAQ) was realized by the assembly of NI equipment, namely, NI USB-9233 and 9234 embedded in chassis NI cDAQ-9174 on the ground and a host PXI-1042Q with embedded controller PXI-8187 on the table in Fig.3-7. The Kapro-781 P GENESIS™ Level was used to calibrate the horizontality of the suspended structure. When the data were not acquired simultaneously, they were normalized by dividing by the exciting force in the frequency domain.

**Table 3-2 The parameters of each periodic element of the experimental structure**

Main	Density	Young's	Assumed	Loss	Dimension
Material	(kg/m <sup>3</sup> )	modulus (N/m <sup>2</sup> )	factor		(mm)
					Width $d_1$ 38.1
Beam	aluminum	2668	$5.38 \times 10^{10}$	0.01	Length $d_2$ 500
					Thickness $d_3$ 5.9
					Width $l_1$ 38.1
Branch	iron	7560	$1.15 \times 10^{11}$	0.01	Length $l_2$ 320
					Thickness $l_3$ 1.5

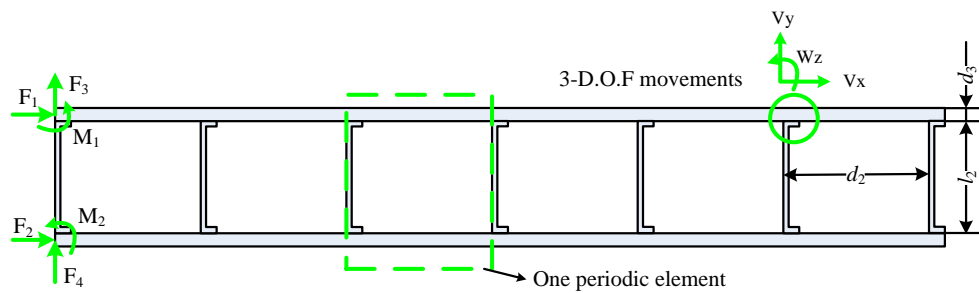


**Figure 3-8 Finite dual-layer periodic structure**

The junction-responses were measured by several accelerometers of the same type (B&K Type 4394), whose layout can be seen in the amplified pictures in Fig. 3-7. The horizontal response of each junction was computed as the average of two signals from the front and back sides of the beam. The vertical response of each junction was represented by the average of the outputs of the eight accelerometers. The four sensors at the top surface of the beam were symmetrical with those at the bottom, and the left four sensors were symmetrical with those on the right along the virtual line between the two screws. Rotational vibration was calculated by the difference between the averaged vibration from the left four and that from the right four accelerometers, divided by the horizontal distance between them. The positions of all accelerometers at the top, bottom, front and back sides of the beam were fixed and adjusted by the white design labels on it (see details in Fig. 3-7).

In order to show the measurement accuracy and provide support for the response superposition in the later part of this section, the responses of the dual-layer finite periodic structure under one longitudinal force were measured. The mobilities from the force longitudinally applied at the left endpoint of the upper beam,  $F_1$  to the velocities of each junction were compared with the theoretical results. The comparison included the horizontal (horizontal velocities divided by the force applied), vertical (vertical velocities divided by the force applied) and rotational (the rotational velocities divided by the force applied) mobilities. A set of comparison results, measured mobilities and theoretically predicted mobilities of the sixth junction is displayed in Figs. 3-9, 3-10, and 3-11, which demonstrate good agreement between experimental and predicted mobilities.

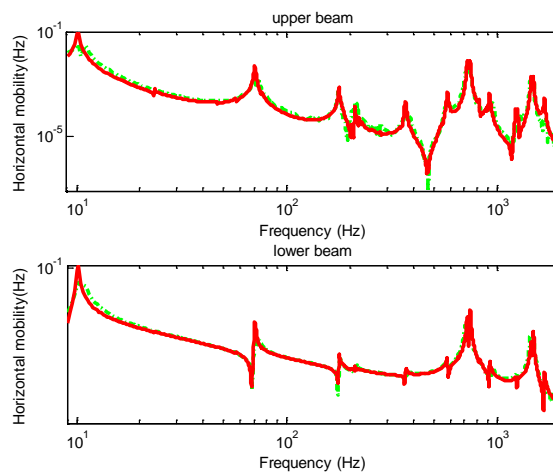


**Figure 3-9 Comparison of horizontal mobility of the sixth junction: (—) experiment; (---) theoretical prediction**



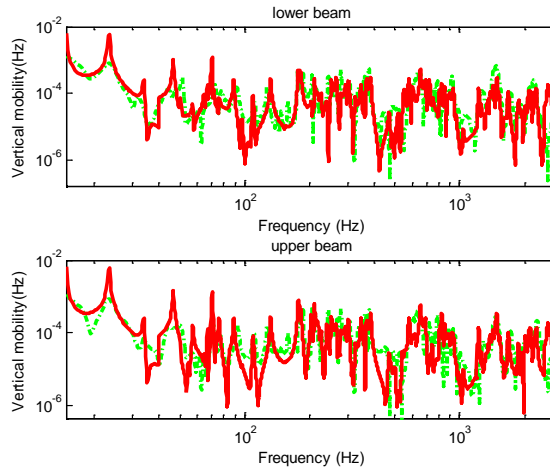


**Figure 3-10 Comparison of vertical mobility of the sixth junction: (---) experiment; (—) theoretical prediction**

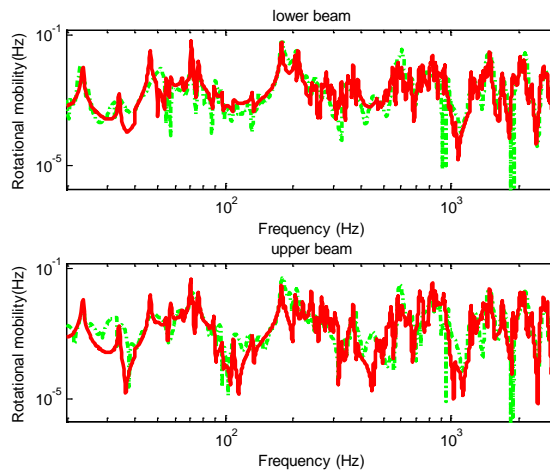


**Figure 3-11 Comparison of rotational mobility of the sixth junction: (---) experiment; (—) theoretical prediction**

For this type of periodic structure, responses under symmetrical force excitation are equivalent to the superposition of those under single forces applied at the left endpoint of the upper and lower beams respectively. When all measurements cannot be finished at the same time, acquired data are normalized by dividing the responses by the exciting force so that the superposition can be realized. In order to excite

fewer characteristic waves and so reach a higher level of accuracy, only two independent forces, namely  $F_1$  and  $F_2$  in Fig. 3-8, were separately applied to the system. The responses under two simultaneously applied symmetrical longitudinal forces were then simulated by the superposition of the normalized responses. In this case, Eq. (3.41) was used to obtain symmetrical characteristic waves. The resultant data for the decomposition of the common transition matrix were smoothed by applying low-order moving filters, since there were some discontinuities of propagation constants due to calculation errors. As near-field characteristic waves attenuate drastically, it is very hard to extract them accurately from experimental responses. Hence, what was obtained for this section was the remaining two pairs of symmetrical characteristic waves. The attenuation constants of the two positive-going symmetrical characteristic wave-types were compared with those of the two negative-going symmetrical characteristic wave-types obtained by the decomposition of the transfer matrix represented in Fig. 3-12. It is obvious from Fig.3-12 that the attenuation constants of the two types of theoretical negative-going characteristic waves are symmetrical with those of the experimental positive-going waves.

Similarly, responses under antisymmetrical force excitation were obtained by the superposition of normalized responses under two separately applied forces  $F_1$  and

$-F_2$ . Eq. (3.41) was utilized to obtain two pairs of antisymmetrical characteristic waves. The resultant data for the decomposition of the common transition matrix were smoothed by low-order moving filters, since there were some discontinuities of propagation constants due to calculation errors. Also, the pair of antisymmetrical near-field characteristic waves was not gained due to their fast attenuation during propagation. The attenuation constants of the two types of positive-going characteristic waves extracted from the common transition matrix of the finite structure were compared with those of the two types of negative-going waves predicted by simulation in Fig.3-13, and also show a very close match.

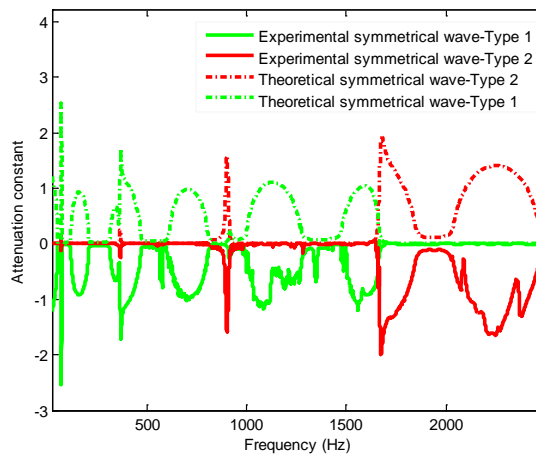


**Figure 3-12 Attenuation constants of symmetrical characteristic wave-types: (—) experiment; (---) theoretical prediction**

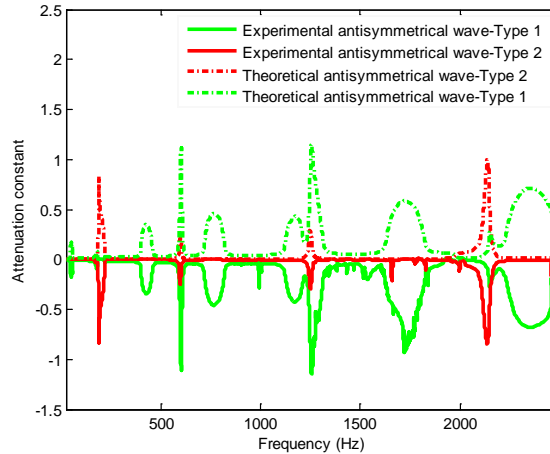


**Figure 3-13 Attenuation constants of antisymmetrical characteristic wave-types: (—) experiment; (---) theoretical prediction**

In addition, when independent applied forces are not fewer than four, Eq. (3.40) can also be utilized to obtain the propagation constants of the four pairs of characteristic waves by exciting the dual-layer periodic structure respectively using symmetrical loads and antisymmetrical loads. This was not done in this experiment.

### 3.6 Summary

This chapter has developed the application of a semi-two-dimensional dual-beam periodic structure to the broadband vibration isolation, and uses a semi-two-dimensional model containing this structure to investigate the general problem of broadband vibration control using periodic structures. SMA branches are proposed as parameter-tunable components in the periodic structure to adapt the

location and broaden the widths of stop bands, and non-SMA supporting beams are also presented to avoid the possible hysteresis induced by a large vertical displacement. Governing equations of the transmitted responses of a nonrigid system isolated by any number of periodic structures is derived. Based on the derived results, two methods are proposed to determine the proper Young's moduli of the SMA branches and maximize the power transmission loss. The experiment indirectly demonstrates the correctness of the derived results of the non-rigid system. Numerical simulations are conducted on this semi-two-dimensional model, and the results demonstrate that the dual-beam periodic structure with SMA branches, when appropriate heat is applied, can bring about the effective control of the broadband vibration of a nonrigid system. This indicates that the methodologies are feasible and effective in determining the proper values of the parameter-adjustable components in a periodic mount. The numerical results also demonstrate that a periodic mount disordered by the random combination of different moduli of branches may achieve better performance than the regular periodic mount. This superiority is predicted to become increasingly prominent as the number of branches increases because more combinations can be created. The method to determine proper Young's moduli and the conclusions of this chapter are also applicable to a three-dimensional nonrigid system, because this model is a realistic representation of the general vibratory system and the theoretical development set out here is not limited to the

semi-two-dimensional system. Nevertheless, a three-dimensional version of the dual-beam periodic mount is needed to be proposed in order to explore its practical application to the broadband vibration control of a realistic system.

## **Chapter 4**

### **An Active Vibration Control System for Periodically Time-varying Systems**

Based on literature review about the problem of active control, it is known that many AVC systems based on the widely applied filtered-x least mean squares (FXLMS) algorithm employ two coupled adaptive processes – online modeling or identification and controller updating – to track the parametric change and realize the real-time updating of the control signal. Errors in one process can affect the other. When one process converges, it takes several samples for the other process to converge. After they both converge, it is difficult to tell whether the controller is optimal or not. Therefore, it is difficult to evaluate the influence of the coupling effect and perform a rigorous derivation. In this study, a new AVC system with adaptive identification and nonadaptive control to avoid the coupling effect is proposed. In this system, the convergence of system identification and the optimization of the controller are synchronized: The controller drives the identification process to converge, and the controller is optimized the moment the identification process converges; the convergence and robustness of the identification process make it likely that an optimal controller will be obtained using the identified model. The robustness of the identification process and the

optimization of the controller are proved by rigorous derivation. Simulation results are presented to verify the stability and effectiveness of the proposed AVC system. The algorithms for both of these processes will be rigorously derived in sections 4.2 and 4.3. Numerical results will be presented in section 4.4 to demonstrate the stability and effectiveness of the new AVC system.

## 4.1 Background Information and Objectives

A typical AVC system can be described by a block diagram (Fig. 4-1), where  $H_{po}$ ,  $H_s$ ,  $H_r$ , and  $H_c$  are the primary path, secondary path, reference path, and the controller respectively and  $\hat{w}_{po}$  and  $\hat{w}_s$  are finite impulse response (FIR) adaptive estimators of  $H_{po}$  and  $H_s$ . With the sensor for the reference signal  $r(n)$  sufficiently collocated with the primary disturbance  $d(n)$ , the reference path  $H_r$  is a minimum-phase system with a stable inverse. Therefore, Fig. 4-1(a) is equivalent to Fig. 4-1(b) since the equivalent primary path  $H_p = H_r^{-1}H_{po}$ . It is commonly assumed by many researchers that primary and secondary paths can be approximated, with acceptable errors, by FIR filters. This study is based on the same assumption, and so the AVC system resulting from it will be applicable to any PTV systems which satisfy this assumption.

Assuming that the output under control  $y(n)$  is governed by the regression model of



Eq. (4.1), the estimated output under control  $\hat{y}(n)$  can be expressed by Eq. (4.2).

$$y(n) = y_p(n) + y_s(n) = \mathbf{w}_p^T(n)\mathbf{r}(n) + \mathbf{w}_s^T(n)\mathbf{u}(n) + v(n) = \mathbf{w}^T(n)\mathbf{X}(n) + v(n) \quad (4.1)$$

$$\hat{y}(n) = \hat{y}_p(n) + \hat{y}_s(n) = \hat{\mathbf{w}}_p^T(n)\mathbf{r}(n) + \hat{\mathbf{w}}_s^T(n)\mathbf{u}(n) = \hat{\mathbf{w}}^T(n)\mathbf{X}(n) \quad (4.2)$$

In Eqs. (4.1) and (4.2),  $\mathbf{w}^T(n) = [\mathbf{w}_p^T(n), \mathbf{w}_s^T(n)]$  is the optimal estimator with  $L_p$  and  $L_s$  as their orders and  $\hat{\mathbf{w}}^T(n) = [\hat{\mathbf{w}}_p^T(n), \hat{\mathbf{w}}_s^T(n)]$  is the real-time estimator;  $\mathbf{X}^T(n) = [\mathbf{r}^T(n), \mathbf{u}^T(n)]$  is the input made up of  $\mathbf{r}^T(n) = [r(n-L_p+1), \dots, r(n)]$  and  $\mathbf{u}^T(n) = [u(n-L_s+1), \dots, u(n)]$ ; and  $v(n)$  is an unknown additive disturbance without any assumptions made about its statistical characterization.

$\xi(n) = (\mathbf{w}(n) - \hat{\mathbf{w}}(n))^T \mathbf{X}(n)$  and  $e(n) = \xi(n) + v(n)$  are called the undisturbed identification error and the disturbed identification error. Therefore, the objective of controller design process is to minimize

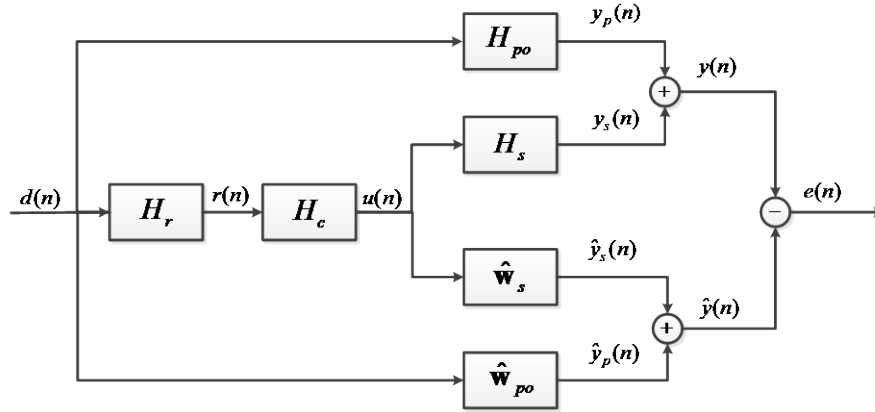
$$J_c = \|\mathbf{w}^T(n)\mathbf{X}(n)\|^2,$$

and the objective of system identification process is to drive  $\hat{\mathbf{w}}(n)$  to converge to  $\mathbf{w}(n)$ , or specifically to minimize the Euclidean norm of model error

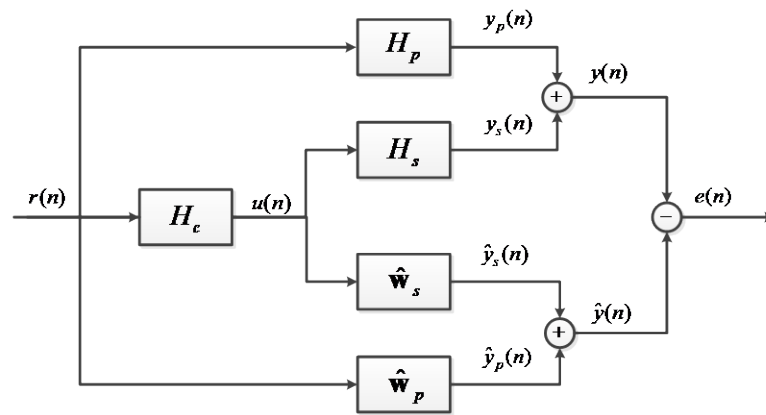
$$\varepsilon(n) = \mathbf{w}(n) - \hat{\mathbf{w}}(n)$$

$$J(n) = \|\mathbf{w}(n) - \hat{\mathbf{w}}(n)\|^2.$$

For simplification of denotation, all of the subscripts in the following text except for  $p$ ,  $s$ , and  $f(\cdot)$  denote the variables in the parentheses: for example,  $\hat{y}_n$  is  $\hat{y}(n)$ .  $f(\cdot)$  is the function for adjusting the abnormal signal and will be used in the identification algorithm in the next section.



(a)



(b)

Figure 4-1 Block diagram of a typical AVC system: (a) The original system, (b) The equivalent system

## 4.2 System Identification

### 4.2.1 Derivation of Online Path Modeling Algorithm

With the expectation that the updated model  $\hat{\mathbf{w}}_{n+1}^T = [\hat{\mathbf{w}}_{p,n+1}^T, \hat{\mathbf{w}}_{s,n+1}^T]$  is close to the present optimal model  $\mathbf{w}_n^T = [\mathbf{w}_{p,n}^T, \mathbf{w}_{s,n}^T]$  with negligible error, an objective function is constructed as a feasible substitute of  $J_n = \|\mathbf{w}_n - \hat{\mathbf{w}}_n\|^2$ ,

$$J_n = \|\hat{\mathbf{w}}_{n+1} - \hat{\mathbf{w}}_n\|^2 + \lambda |y_n - f(\hat{\mathbf{w}}_{n+1}^T \mathbf{X}_n)|^2. \quad (4.3)$$

where  $\tilde{e}_{f,n} = y_n - f(\hat{\mathbf{w}}_{n+1}^T \mathbf{X}_n) = y_n - \tilde{y}_{f,n}$  is the predicted identification error,  $\hat{e}_n = \hat{\mathbf{w}}_{n+1} - \hat{\mathbf{w}}_n$  is the approximated model error, and  $\lambda$  is the weight;  $f(\cdot)$  may be called a self-tuning function which aims at preventing  $\tilde{e}_n = y_n - \hat{\mathbf{w}}_{n+1}^T \mathbf{X}_n = y_n - \tilde{y}_n$  from exceeding a conservatively preset threshold by adjusting  $\hat{\mathbf{w}}_{n+1}^T \mathbf{X}_n$ . For a linear system, this function may be a fix value or a time-varying value. For a nonlinear system, this function changes with time nonlinearly to avoid the divergence of the algorithm, like the way in Ref. [59]. This study focuses on the application to linear PTV systems.

The reason for an unacceptable  $\tilde{e}_n$  is the additive disturbance  $v_n$ . Since there are no restrictions on or assumptions made about  $v_n$ , the sources of  $v_n$  may cover a wide range of dynamic uncertainties and external sources:

- (1) Measurement noise; for example, the noise resulting from imperfect sensors.
- (2) Modeling errors; for example, the error due to the use of an FIR filter to approximate an infinite impulse response filter (IIR) system.
- (3) Other disturbances imposed by unknown sources.

These factors negatively affect identification performance and destabilize a system, and thus it is necessary to take some measures, such as introducing  $f(\cdot)$ , to suppress this negative influence. The impact of the self-tuning function  $f(\cdot)$  on the robustness of the system estimator will be discussed after the algorithm of the

estimator is derived.

To obtain an optimal updated model, the objective function  $J_n$  is differentiated with respect to  $\hat{\mathbf{w}}_{n+1}$ , leading to

$$\hat{\mathbf{w}}_{n+1} = \hat{\mathbf{w}}_n + \lambda \dot{f}_{\tilde{y}_n} \tilde{e}_{f,n} \mathbf{X}_n \quad (4.4)$$

where  $\dot{f}_{\tilde{y}_n} = \left. \frac{df(z)}{dz} \right|_{z=\tilde{y}_n}$ . To solve the unknown multiplier  $\lambda$  and obtain an explicit

expression of Eq. (4.4), three constraint conditions are introduced based on three practical concerns:

(1) The first concern is to avoid the unacceptable predicted identification error  $\tilde{e}_n$ .

This means that  $\tilde{e}_n$  does not need the adjustment and that the identification errors with and without the adjustment by  $f(\cdot)$  are nearly same. In other words, the tuned predicted error  $\tilde{e}_{f,n}$  and the original predicted error  $\tilde{e}_n$  should approach each other as much as possible.

$$\Delta_1^2 = \left[ (\tilde{e}_{f,n})^2 - (\tilde{e}_n)^2 \right]^2 \quad (4.5)$$

Differentiating Eq. (4.5) with respect to  $\hat{\mathbf{w}}_{n+1}$  and setting the result equal to zero,

$$\tilde{e}_n = \dot{f}_{\tilde{y}_n} \tilde{e}_{f,n} \quad (4.6)$$

is obtained, where  $\dot{f}_{\tilde{y}_n} = \left. \frac{\partial f(z)}{\partial z} \right|_{z=\tilde{y}_n}$ .

(2) The second concern is to avoid the unacceptable present identification error  $e_n$ .

This requires that the tuned present error  $e_{f,n}$  and the original present error  $e_n$

should approach each other as much as possible:

$$\Delta_2^2 = \left[ (e_{f,n})^2 - (e_n)^2 \right]^2 \quad (4.7)$$

where  $e_{f,n} = y_n - f(\hat{\mathbf{w}}_n^T \mathbf{X}_n) = y_n - f_{\hat{y}_n}$  is the tuned present error while  $e_n = y_n - \hat{\mathbf{w}}_n^T \mathbf{X}_n = y_n - \hat{y}_n$  is the present error. Differentiating Eq. (4.7) with respect to  $\hat{\mathbf{w}}_n$  and setting the result equal to zero,

$$e_n = \dot{f}_{\hat{y}_n} e_{f,n} \quad (4.8)$$

is obtained, where  $\dot{f}_{\hat{y}_n} = \left. \frac{\partial f(z)}{\partial z} \right|_{z=\hat{y}_n}$ .

(3) The third concern is fast convergence. To reach a higher convergence rate, the objective is to render  $\Delta_3$  negative and minimum by appropriately setting  $\lambda$ .

$$\Delta_3 = \tilde{e}_n^2 - e_n^2 \quad (4.9)$$

Differentiating Eq. (4.9) with respect to  $\lambda$ , substituting Eqs. (4.6) and (4.8), and setting the result equal to zero,

$$\lambda = \frac{\dot{f}_{\hat{y}_n} e_{f,n}}{\dot{f}_{\hat{y}_n} \tilde{e}_{f,n} \mathbf{X}_n^T \mathbf{X}_n} \quad (4.10)$$

is obtained.

Substituting Eq. (4.10) into Eq. (4.4), the explicit expression

$$\hat{\mathbf{w}}_{n+1} = \hat{\mathbf{w}}_n + \frac{\dot{f}_{\hat{y}_n} e_{f,n}}{\mathbf{X}_n^T \mathbf{X}_n} \mathbf{X}_n \quad (4.11)$$

is obtained, which can be slightly modified to

$$\hat{\mathbf{w}}_{n+1} = \hat{\mathbf{w}}_n + \mu \frac{\dot{f}_{\hat{y}_n} e_{f,n}}{\gamma + \mathbf{X}_n^T \mathbf{X}_n} \mathbf{X}_n \quad (4.12)$$

where a small positive parameter  $\gamma$  is introduced to avoid the numerical difficulties caused by a small denominator and a positive real scaling factor  $\mu$  is introduced to control the misadjustment without changing the direction of  $\mathbf{X}_n$ . From Eq. (4.12), we can see that this is a noninvasive process because no probing signal is introduced.

#### 4.2.2 Analysis of robustness by $H_\infty$ criterion [79]

$H_\infty$  norm represents the largest energy gain of a system, and energy gain for an adaptive estimator may be defined as the ratio of the energy due to model error  $|\xi_{f,n}|^2$  or  $|\xi_n|^2$  to the total disturbance energy inputted to the online model  $|v_n|^2$  and  $\|\varepsilon_0\|^2$ . According to Eq. (4.1), the present identification error with and without the self-tuning mechanism can be expressed as

$$\left. \begin{aligned} e_{f,n} &= \xi_{f,n} + v_n \\ e_n &= \xi_n + v_n \end{aligned} \right\} \quad (4.13)$$

where  $\xi_{f,n} = \mathbf{w}_n^T \mathbf{X}_n - f(\hat{\mathbf{w}}_n^T \mathbf{X}_n)$  is the undisturbed estimation error after the self-tuning adjustment.

To compute the  $H_\infty$  norm of the estimator, we proceed as follows. For a periodic time-varying system with  $N$  samples per cycle, the mean-square deviation (MSD) in the  $k^{\text{th}}$  period is defined as

$$D_{kN} = \frac{1}{N} \sum_{n=kN}^{(k+1)N-1} \|\varepsilon_n\|^2 \quad (4.14)$$

So,

$$D_{kN} - D_{(k+1)N} = \frac{1}{N} \sum_{n=kN}^{(k+1)N-1} [\varepsilon_n - \varepsilon_{n+N-1}]^T [\varepsilon_n + \varepsilon_{n+N-1}] \quad (4.15)$$

Substituting Eq. (4.12) into Eq. (4.15) and neglecting  $\gamma$ , an inequality is obtained in an attempt to bound the energy gain:

$$D_{kN} - D_{(k+1)N} \geq \frac{1}{N} \sum_{n=kN}^{(k+1)N-1} \frac{\mu \dot{f}_{\hat{y}_n}}{\mathbf{X}_n^T \mathbf{X}_n} \left[ (2-\mu) \dot{f}_{\hat{y}_n} |\xi_{f,n}|^2 - 2(1-2\dot{f}_{\hat{y}_n} + \mu \dot{f}_{\hat{y}_n}) \xi_{f,n}^T v_n - (2-2\dot{f}_{\hat{y}_n} + \mu \dot{f}_{\hat{y}_n}) |v_n|^2 \right] \quad (4.16)$$

When the condition  $0 < \mu \leq 2 - \frac{1}{\dot{f}_{\hat{y}_n}}$  holds, the inequality of Eq. (4.16) can be recast as

$$D_{kN} - D_{(k+1)N} \geq \frac{1}{N} \sum_{n=kN}^{(k+1)N-1} \frac{\mu \dot{f}_{\hat{y}_n}}{\mathbf{X}_n^T \mathbf{X}_n} \left[ |\xi_{f,n}|^2 - |v_n|^2 \right] \quad (4.17)$$

If the self-tuning mechanism is not triggered, with the consideration of the second constraint in Eq. (4.7), Eq. (4.15) becomes

$$D_{kN} - D_{(k+1)N} \geq \frac{1}{N} \sum_{n=kN}^{(k+1)N-1} \frac{\mu}{\mathbf{X}_n^T \mathbf{X}_n} \left[ (2-\mu) |\xi_n|^2 + 2(1-\mu) v_n - \mu |v_n|^2 \right] \quad (4.18)$$

When the condition  $0 < \mu \leq 1$  is satisfied, the inequality of Eq. (4.18) is followed by

$$D_{kN} - D_{(k+1)N} \geq \frac{1}{N} \sum_{n=kN}^{(k+1)N-1} \frac{\mu}{\mathbf{X}_n^T \mathbf{X}_n} \left[ |\xi_n|^2 - |v_n|^2 \right] \quad (4.19)$$

Suppose the algorithm runs for  $n = (k+1)N$  iterations from  $n = 0$  with the initial condition  $\hat{\mathbf{w}}(0)$ . Letting  $\delta = \max(\mathbf{X}_n^T \mathbf{X}_n)$  and  $\delta_f = \max(\mathbf{X}_n^T \mathbf{X}_n / \dot{f}_{\hat{y}_n})$ , starting from  $\hat{\mathbf{w}}(0)$  and summing the two sides of the inequalities in Eqs. (4.17) and (4.19), the energy gains  $G_f$  and  $G$  are solved.

$$G_f = \frac{\sum_{n=0}^{(K+1)N-1} |\xi_{f,n}|^2}{\frac{N\delta_f}{\mu} D(0) + \sum_{n=0}^{(K+1)N-1} |v_n|^2} \leq 1 \quad (4.20a)$$

$$G = \frac{\sum_{n=0}^{(K+1)N-1} |\xi_n|^2}{\frac{N\delta}{\mu} D(0) + \sum_{n=0}^{(K+1)N-1} |v_n|^2} \leq 1 \quad (4.20b)$$

$G_f$  and  $G$  can be rewritten as Eq. (4.21) by substituting  $\rho = D(0)/\|\varepsilon_0\|^2$  into Eq.

(4.20):

$$G_f = \frac{\sum_{n=0}^{(K+1)N-1} |\xi_{f,n}|^2}{\frac{N\delta_f}{\mu} \rho \|\varepsilon_0\|^2 + \sum_{n=0}^{(K+1)N-1} |v_n|^2} \leq 1 \quad (4.21a)$$

$$G = \frac{\sum_{n=0}^{(K+1)N-1} |\xi_n|^2}{\frac{N\delta}{\mu} \rho \|\varepsilon_0\|^2 + \sum_{n=0}^{(K+1)N-1} |v_n|^2} \leq 1 \quad (4.21b)$$

Eqs. (4.20-4.21) show that the output energy (the numerator) caused by the identification error never exceeds the total input energy (the denominator) caused by the disturbances consisting of the initial model error  $\varepsilon_0$  and the additive disturbance  $v$ .

In the worst case that  $\xi(n)=-v(n)$  and  $\xi_f(n)=-v(n)$ ,  $D(kN) = D(0)$  for all  $k$  because  $e_n = 0$  and  $e_{f,n} = 0$  stop the adaptive algorithm Eq. (4.12) from updating.

$G_f$  and  $G$  can arbitrarily approach unity with the increase in  $N$ . Therefore, the  $H_\infty$  norm of the estimator or the maximum energy gain is unity. Considering the fact



that any filter can never have its maximum energy gain limited below unity, the optimal  $H_\infty$  norm of any filter can never be less than unity. Therefore, the proposed estimator is  $H_\infty$  optimal if  $0 < \mu \leq 1$  and  $\dot{f}_{\hat{y}_n} \geq \frac{1}{2-\mu}$ .

### 4.2.3 Constructing the self-tuning function $f(\cdot)$

The fundamental requirement for the self-tuning function is that it starts to adjust the estimated output  $\hat{y}_n$  when the estimation error exceeds a conservatively preset threshold. So, a preliminary guess may be

$$f(\hat{y}_n) = \alpha \hat{y}_n + (1-\alpha) \begin{cases} \kappa & \hat{y}_n \geq \kappa \\ \hat{y}_n & \hat{y}_n \in (-\kappa, \kappa) \\ -\kappa & \hat{y}_n \leq -\kappa \end{cases} \quad (4.22)$$

where  $\kappa = |y_n| + \sigma$  is the upper bound of the estimated output and  $\alpha$  is an adjustable parameter ( $0 \leq \alpha \leq 1$ ). When  $|\hat{y}_n| - |y_n| \geq \sigma$ , where  $\sigma$  is threshold, it means the model error  $\varepsilon_n = \mathbf{w}_n - \hat{\mathbf{w}}_n$  is unacceptable, and so this self-tuning mechanism is triggered. A signal processing method  $h(\cdot)$ , like averaging  $y_{n-N+1} \cdots y_n$ , may be introduced to alleviate the influence of the additive disturbance  $v$ . Therefore,  $\kappa$  can be modified as  $\kappa = |h(y_n)| + \sigma$ . When no signal processing is imposed,  $h_{y_n} = y_n$ .

As  $\dot{f}_{\hat{y}_n} \geq \frac{1}{2-\mu}$  is required for the estimator to be  $H_\infty$  optimal,  $\alpha = \frac{1}{2-\mu}$  is set.

Eq. (4.22) does not have a continuous derivative, and so the sigmoid function is

chosen to approximate the second term of Eq. (4.22) because of its similar shape to the second term and the continuity of its derivative. Then, the self-tuning function is modified as

$$f(\hat{y}_n) = \frac{1}{2-\mu} \hat{y}_n + \frac{\beta}{g(\kappa)} \frac{1-e^{-\hat{y}_n g(\kappa)}}{1+e^{-\hat{y}_n g(\kappa)}} \quad (4.23)$$

The derivative is

$$\dot{f}_{\hat{y}_n} = \frac{df}{d\hat{y}_n} = \frac{1}{2-\mu} + 2\beta \frac{e^{-\hat{y}_n g(\kappa)}}{(1+e^{-\hat{y}_n g(\kappa)})^2} \quad (4.24)$$

where  $\beta > 0$  and  $g(\kappa) > 0$  are employed to adjust amplitude and threshold. Although they are related to  $(1-\alpha)$ , it is unnecessary to know the analytical solution for the relation of  $(1-\alpha)$ ,  $\beta$ , and  $g(\kappa)$ . This is because the lack of the restriction by the analytical solution creates more flexibility for the configuration of the self-tuning function. After introducing the sigmoid function, the self-tuning function  $f_{\hat{y}_n}$  displays the following properties: when  $\hat{y}_n = 0$ ,  $f_{\hat{y}_n} = \hat{y}_n$ . When  $0 < |\hat{y}_n| < |y_n|$  or  $0 < |\hat{y}_n| < |h_{y_n}|$ ,  $f_{\hat{y}_n} \approx \hat{y}_n$ , with the increase of  $|\hat{y}_n|$ , the increase in  $|f_{\hat{y}_n}|$  becomes slower; the larger  $|\hat{y}_n|$  is, the more slowly  $|f_{\hat{y}_n}|$  increases.  $f_{\hat{y}_n}$  gradually gets close to the shape of the preliminary guess Eq. (4.22) after  $|\hat{y}_n| \geq \kappa$ . This is because the second term of  $\dot{f}_{\hat{y}_n}$  is the derivative of the sigmoid function and it is monotonically decreasing with the increase in  $|\hat{y}_n|$ . This property indicates that  $\dot{f}_{\hat{y}_n}$  becomes very small when  $|\hat{y}_n|$  is unacceptably large, preventing the excessive updating of the path model and a larger model error.

With this self-tuning function, the applicability of this identification algorithm is not only limited to a linear system, but can be extended to some nonlinear systems when the sigmoid function can represent that type of nonlinearity. The reason is listed as follows. In Eq. (4.23), the first term is a line and it means this one part of this function changes linearly, while the second term is sigmoid function which represents a nonlinear adjustment when the estimation error exceeds the threshold.

### 4.3 Controller Design

When the identification error  $e_{f,n}$  converges, the minimization of  $y_n$  requires the minimization of  $\hat{y}_n$  since  $y_n = e_{f,n} + f(\hat{y}_n)$ . Combining  $\hat{y}_n = 0$

and  $\hat{\mathbf{w}}_n = \hat{\mathbf{w}}_{n+1} - \frac{\dot{f}_{\hat{y}_n} e_{f,n}}{\mathbf{X}_n^T \mathbf{X}_n} \mathbf{X}_n$ , we get  $y_n = \hat{\mathbf{w}}_{n+1}^T \mathbf{X}_n$ . This result is desirable and also

expected by the objective function of system identification Eq. (4.3) so that Eq. (4.3)

can approximate  $J_n = \|\mathbf{w}_n - \hat{\mathbf{w}}_n\|^2$  with negligible error. Therefore, any controller

which minimizes  $\hat{y}_n$  guarantees that Eq. (4.3) is a reasonable approximation of

$J_n = \|\mathbf{w}_n - \hat{\mathbf{w}}_n\|^2$ . Additionally, by minimizing  $\hat{y}_n$ , the second term of Eq. (4.3) can be

minimized, which boosts the minimization of Eq. (4.3) and thus drives the proposed

identification algorithm to converge. Hence, any controller which minimizes  $\hat{y}_n$

can drive the adaptive algorithm Eq. (4.12) to converge. In other words, by

minimizing  $\hat{y}_n$ , the controller can drive the adaptive algorithm Eq. (12) to converge,

and when the modeling process converges, the optimal controller can be obtained simultaneously. Therefore, the convergence of the identification process and the optimization of the controller are synchronized.

One possible controller aiming at minimizing  $\hat{y}_n$  is solved by minimizing the practical objective function:

$$J_c(n) = \sum_{k=no}^n |\hat{y}_k|^2 + \lambda_c |u_n|^2,$$

where  $no = n-1, n$  and  $\lambda_c$  is the weight of control signal. Because of the special structure of  $\mathbf{J}$ ,  $no < n-1$  does not yield a control signal different from the  $u_n$  obtained by setting  $no = n-1$ .  $\hat{y}_k$  is formulated by

$$\begin{bmatrix} \hat{y}_o \\ \hat{y}_n \end{bmatrix} = [\mathbf{H}, \mathbf{J}] \begin{bmatrix} \mathbf{u}_o \\ u_n \end{bmatrix} + [\mathbf{M}, \mathbf{N}] \begin{bmatrix} \mathbf{r}_o \\ r_n \end{bmatrix} \quad (4.25)$$

$$\mathbf{H} = \begin{bmatrix} \hat{\mathbf{w}}_{s,no}^T & & & & \\ & \hat{\mathbf{w}}_{s,no+1}^T & & & \\ & & \ddots & & \\ & & & \ddots & \\ & & & & \hat{\mathbf{w}}_{s,n}^T(1:N-1) \end{bmatrix}, \quad \mathbf{J} = \begin{bmatrix} \mathbf{O}_{(n-no) \times 1} \\ \hat{\mathbf{w}}_{s,n}^T(N) \end{bmatrix}$$

$$\mathbf{M} = \begin{bmatrix} \hat{\mathbf{w}}_{p,no}^T & & & & \\ & \hat{\mathbf{w}}_{p,no+1}^T & & & \\ & & \ddots & & \\ & & & \ddots & \\ & & & & \hat{\mathbf{w}}_{p,n}^T(1:M-1) \end{bmatrix}, \quad \mathbf{N} = \begin{bmatrix} \mathbf{O}_{(n-no) \times 1} \\ \hat{\mathbf{w}}_{p,n}^T(M) \end{bmatrix},$$

where the subscript  $o$  indicates old signals.  $u_n$  is the optimal control signal to be determined by the past vibration  $\hat{\mathbf{y}}_o = [y_{no} \cdots y_{n-1}]^T$ , the past control signal  $\mathbf{u}_o = [u_{no-L_s+1} \cdots u_{n-1}]^T$ , and the past and present reference signals

$\mathbf{r}_o = [r_{no-L_p+1} \cdots r_{n-1}]^T$  and  $r_n$ . Differentiating Eq. (4.25) with respect to  $u_n$  and setting the result equal to zero, the optimal control signal  $u_n$  is solved.

$$u_n = -(\lambda_c + \mathbf{J}^T \mathbf{J})^{-1} \mathbf{J}^T (\mathbf{H}\mathbf{u}_p + \mathbf{M}\mathbf{r}_p + \mathbf{N}r_n) \quad (4.26)$$

After the solution of control signal is solved by Eq. (26), the derivation of this AVC system is completed. It is compared with those AVC systems updated by FXLMS method in the following aspects. 1) Those AVC systems are unstable when the phase error during modeling exceeds  $90^\circ$ , while the proposed system possesses  $H_\infty$  robustness and the self-tuning function prevents the estimation error from exceeding a preset threshold; 2) FXLMS is an estimation method, and thus the solution of the controller is not necessarily optimal, but the optimal controller of the presented system can be obtained the moment the modeling process converges; 3) due to the coupling effect, after the modeling process converges, it takes several steps for the controller to converge despite its low computational burden at one step; when the controller converges, it's difficult to know if it is optimal. However, the proposed system successfully apply Yuan's decoupling scheme to the vibration control of PTV systems so that the optimal controller can be obtained the moment the modeling process converges. Therefore, the disadvantages of those AVC systems based on FXLMS method are the advantages of the proposed system.

## 4.4 Numerical Simulation and Analysis

To verify the proposed system, a numerical simulation is conducted on a mass-spring system installed in the center of a simply supported plate (Fig. 4-2). This system is

governed by Eq. (4.27), which consists of a canonical PTV equation with damping and the equation of the motion of the plate at the contact point. The external force is  $F = \cos(2\pi 70t)$  and the control force is  $F_c$ .

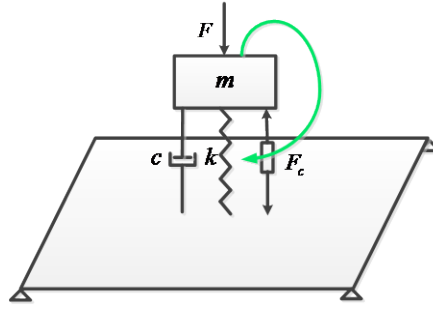


Figure 4-2 The AVC system

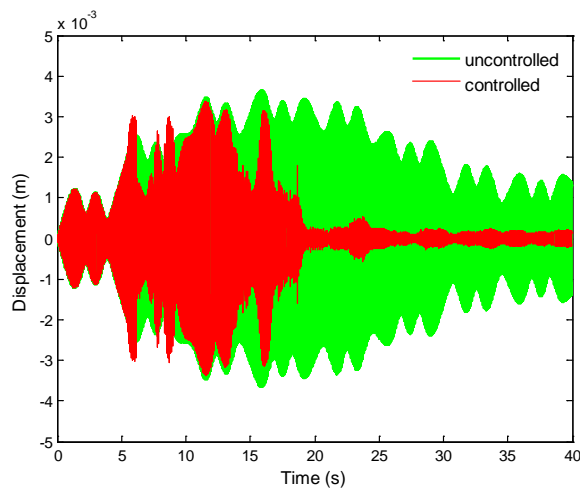
$$\left. \begin{aligned} \ddot{x}_1 + 2\zeta(\dot{x}_1 - \dot{x}_2) + k(1 - 0.02 \sin(2\pi 0.1t))(x_1 - x_2) &= F \\ x_2 &= L^{-1} \left( Y(s) L \left( 2\zeta(\dot{x}_1 - \dot{x}_2) + k(1 - 0.02 \sin(2\pi 0.1t))(x_1 - x_2) \right) \right) \end{aligned} \right\} \quad (4.27)$$

Assuming the period of stiffness oscillation is 10 seconds, separate peaks with an interval of 0.1Hz at the two sides of  $f = 70\text{Hz}$  are excited. The stiffness of the spring varies periodically with an average of  $k = (2\pi 70)^2 \text{ N/m}$ , a mass weighs  $m = 1\text{kg}$ , and the damping ratio is  $\zeta = 0.01$ .  $\zeta$  is related to damping  $c$  by  $\zeta = c/2m\Omega$  and  $\Omega^2 = k/m$ .  $x_1$  is the displacement of the mass, and  $x_2$  the displacement of the center of the plate in time domain. The transfer function at the center of the plate is  $Y(s)$ , and  $L$  in Eq. (4.27) denotes the Laplace transform. The mobility of the simply supported plate, correspondent to  $Y(s)$ , is calculated by its physical parameters [80]: Young's modulus  $E = 2.1 \times 10^{10} \text{ N/m}^2$ , density  $\rho = 2.8 \times 10^3 \text{ kg/m}^3$ , Poisson's Ratio  $\nu = 0.2$ , and loss factor  $\eta = 2 \times 10^{-2}$ . Its

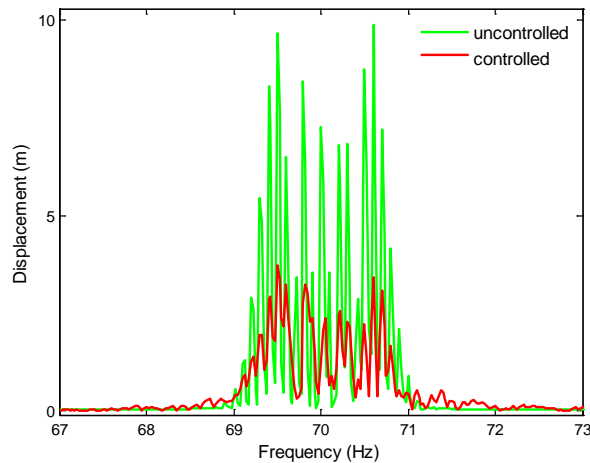
dimensions are 3.5m (length)  $\times$  3.5m (width)  $\times$  0.24m (thickness). Only the first two modes of the plate at about 50Hz and 250 Hz are considered in the calculation of the mobility because of their relatively significant contribution to response of the mass.

The system is solved by the Matlab/Simulink model and program. Two simulations are conducted with the same parameters, but one simulation employs the proposed AVC system while the other does not. The other one utilizes the degraded version of the proposed AVC system in which the self-tuning mechanism is not embedded into the identification process so the identification process is governed by Normalized LMS algorithm. Control results with and without the self-tuning mechanism are respectively shown in Fig. 4-3 and Fig. 4-4. From Fig. 4-3(a), it can be seen that significant attenuation of vibration happens after 10 seconds – the oscillation period of the stiffness. Although Fig. 4-4 also shows alleviated vibration after the control system is introduced, significant oscillation and smaller attenuation are observed. This is because the estimation error (indicator of model errors) for Fig. 4-3 is limited below the preset threshold while that for Fig. 4-4 lacks restriction. Hence, the effectiveness of the proposed algorithm with a self-tuning mechanism is verified by the superiority of the control performance in Fig. 4-3(a). Fig. 4-3(b) shows the separate peaks with an interval of 0.1Hz at the two sides of  $f = 70\text{Hz}$ , and significant attenuation can be observed despite the occurrence of those side peaks

which do not exist in a time-invariant system and may invalidate the AVC system designed for the time-invariant system. Finally, an impulsive noise lasting 0.1 seconds is added to the output at around the 27th second to examine the system's stability to additive disturbances besides the model errors. The convergence after the system encounters this shock is illustrated in Fig. 4-5, which demonstrates the stability of the proposed AVC system to model errors and shock.



(a)



(b)

**Figure 4-3 Control performance with the self-tuning mechanism: (a) Time domain, (b) Frequency domain.**



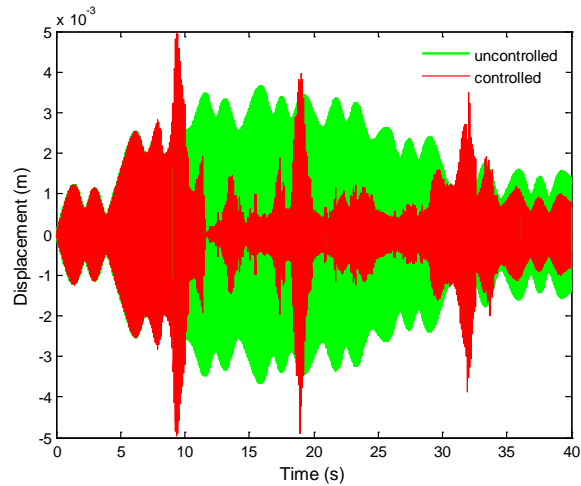


**Figure 4-4 Control performance without the self-tuning mechanism**

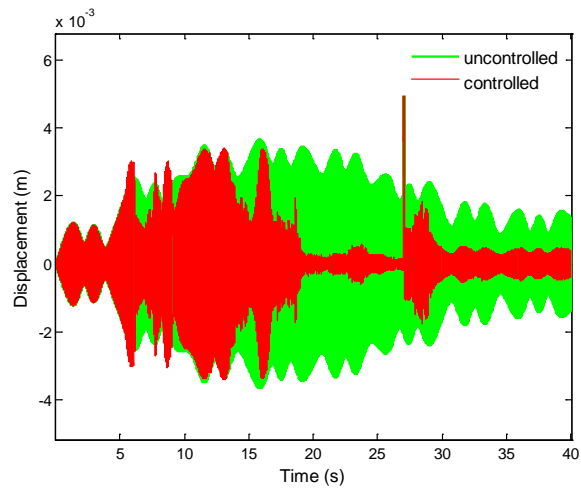


**Figure 4-5 Control performance after encountering a shock**

## 4.5 Summary

An AVC system is proposed to suppress periodically time-varying vibration, and it utilizes a decoupling scheme which is characterized by an adaptive process for system identification and a nonadaptive process for controller optimization to avoid the coupling effect which exists in many AVC systems based on the FXLMS

algorithm. The disadvantages of those systems are the advantages of the presented system because of the application of the decoupling scheme and the robustness of the modeling process. With the decoupling scheme, the two processes can reach synchronous convergence by positively affecting each other. The controller can drive the identification process to converge as long as the controller is optimized by minimizing the output of the estimated model. When the modeling process converges, the controller can be optimized instantly. Therefore, the convergence of system identification and the optimization of the controller are synchronized. Moreover, with the condition that the derivative of the self-tuning function is no less than  $1/(2-\mu)$  where  $\mu$  is the adjustable parameter the  $H_\infty$  robustness of the system is guaranteed. This condition makes it reasonable to assume that an optimal controller can be solved based on the identified model. Both rigorous derivation and numerical simulation conducted on a periodically time-varying system verifies the convergence and stability of the presented AVC system.

# Chapter 5

## Conclusions and Suggestions for Future Work

### 5.1 Conclusions

This thesis has mainly investigated the problems of broadband vibration isolation and periodically time-varying vibration isolation of building services equipment. Effective solutions have been proposed to these problems, and these solutions are applicable to machine-induced vibration and noise control because the theoretical development of these solutions are not limited to building services equipment. The vibration control performance has been verified mainly by numerical simulations and by an experiment conducted in The Hong Kong polytechnic university.

Firstly, a power transmissibility approach has been proposed to assess the isolation performance of transient vibration using spring isolator. It is defined as the ratio of maximum peak power induced by transient excitation and transmitted through an isolator to the foundation to that transmitted to the foundation without an isolator. The existing indicators of isolation performance do not take into consideration the transmitted power caused by transient excitations which are commonly experienced

by some building services equipment. The proposed indicator – transient power transmissibility – can be used to design a spring isolator and also can be applied to re-assess the performance of the traditionally designed isolator in the situation where the isolated system is subjected to transient excitation. The numerical results have demonstrated the necessity of re-assessment by this indicator. This is not the main work of this study, but deserves to be mentioned because of its significance to practical engineering. What's more, this concept of the ratio between the maximum peak powers with and without an isolator is able to be employed to evaluate the performances of any passive isolators.

Furthermore, the problem of broadband vibration control of non-rigid systems using periodic structures has been investigated through a semi-two-dimensional model which employs a dual-beam periodic structure with transverse branches as an isolator. The configuration of SMA branches and non-SMA beams has been proposed to fully exploit the advantage of the variable material property (Young's modulus) of SMA to adjust and widen the stop bands of this periodic isolator and to prevent the associated hysteresis. Two methodologies have been developed to determine the proper Young's moduli of the branches and the correspondent optimal transmission loss, according to the characteristics of the vibratory source. Several cases, involving different parameters of the supporting beams, different types of external loads and different

combination of branches in a mount, were extensively examined in the simulation conducted on this semi-two-dimensional model. Numerical results demonstrated that SMA branches with the application of appropriate heat can effectively realize broadband vibration control of a non-rigid system. This implies the applicability and effectiveness of two methodologies that determine the proper values of the parameter-adjustable components in a periodic mount. Numerical results also demonstrated that the proper combination of branches different in terms of elastic moduli in a periodic mount can be obtained and that combination may achieve better control performance than that achieved by the mount with identical branches. This superiority in control performance is predicted to become increasingly prominent with the increase of branches because more combinations can be created. An experiment has been conducted and indirectly demonstrated the validity of the derivation of the structural response which is the basis of the two methodologies. In addition, the theoretical guidance of that experiment, i.e. the relation between the characteristic waves propagating in an infinite periodic structure and junction responses, provides an alternative way to obtain the characteristic waves. All of above conclusions drawn from the numerical results of the semi-two-dimensional model are applicable to a three-dimensional non-rigid system, because this model is a realistic representation of a general vibratory system and the theoretical development of this study is based on the general vibratory system which is

non-rigid and has three dimensions. Despite that, broadband vibration control of a realistic system cannot be accomplished without the proposal of the three-dimensional version of the semi-two-dimensional periodic mount.

Another main work is the active vibration control (AVC) of a periodically time-varying (PTV) vibratory system. A control system has been proposed with an adaptive process for online modeling and a nonadaptive process for controller optimization to avoid the coupling effect which exists in many active control systems updated by the filtered-x least mean square (FXLMS) algorithm. The controller can drive the modeling process to converge as long as the controller is optimized by minimizing the estimated output. When the modeling process converges, the optimal controller can be solved at the same time. Therefore, the two processes are synchronized. Moreover, the condition for the  $H_\infty$  robustness of the system was presented - the derivative of the self-tuning function is not supposed to be less than  $1/(2-\mu)$  where  $\mu$  is the adjustable parameter in the AVC algorithm. Its implications are twofold. One is that the identified model is the  $H_\infty$  optimal approximation of the real system once the process of identification converges. The other is that this AVC system has strong robustness to dynamic uncertainties and disturbances when the condition is satisfied. This  $H_\infty$  robustness may not be guaranteed if it is a general PTV system instead of a rigorous PTV system, but the

convergence of the system still can be assured by the derivation. Both rigorous derivation and numerical simulation conducted on a periodically time-varying vibratory system demonstrated the convergence and stability of the presented AVC system. In spite of that, it is lack of experimental verification performed on a strict PTV system and a general PTV system.

## **5.2 Suggestions for Future Work**

On the basis of the two main studies, future theoretical and experimental work is recommended as follows:

1. The proposed methods for the broadband vibration control using periodic structures with adjust parameters have not been demonstrated by an experiment conducted on a three-dimensional non-rigid system. Hence, it is expected to design an experimental system in the future to examine the two approaches.
2. The three-dimensional version of the semi-two-dimensional periodic structure employed to realize broadband vibration control is needed to be proposed so that it can be applied in practical engineering.
3. The transient power transmissibility is applicable to a system with periodic mounts, but the work of re-assessing the isolation performance of a periodic mount by this indicator has not been performed. This re-assessment is not

difficult to conduct if the information of the transient excitation is available. In the future, the isolation performance of a periodic structure with tunable parameters may be evaluated by this indicator.

4. The presented AVC algorithm for a PTV system has not been verified by an experiment due to the complication of designing a rigorous PTV system. However, this experimental system is desirable since the active control of a PTV system is a popular research topic. A general PTV may be considered to test robustness of the proposed control system to uncertainties caused by the differences between a general PTV system and a rigorous PTV system. Two possible experimental systems may be considered in future work:

- 1) A motor with the unsymmetrical shaft (for example a shaft with an eccentric mass) supported by isotropic bearings, and

- 2) A motor with the horizontal shaft supported by anisotropic bearings.

The convergence and robustness will be examined, and the control performance will be compared with the FXLMS method.

5. These experimental systems may not possess strict parametric periodicity, but this drawback can be used to test the robustness of proposed control system.
6. The second one of the two approaches to determine proper parameters for the broadband vibration control, a numerical method for the real-time calculation developed in Chapter 3, may be combined with the identification algorithm in the



AVC system in Chapter 4 to realize online adaptation and control, when the machine and the foundation have PTV parameters and they can be approximated by FIR models with acceptable errors.

## References

- [1] Y. Yun and C.M. Mak, A study of coupled flexural-longitudinal wave motion in a periodic dual-beam structure with transverse connection, *Journal of the Acoustical Society of America* 126(1) (2009) 114-121.
- [2] Y. Yun and C.M. Mak, Power transmission from two coherent machines to a dual-layer coupling floor structure, *Journal of Vibration and Control* 17(5) (2011) 711-720.
- [3] D.Y. Ou, C.M. Mak, The effect of elastic supports on the transient vibroacoustic response of a window caused by sonic booms, *Journal of the Acoustical Society of America* 130(2) (2011) 783-790.
- [4] D.Y. Ou, C.M. Mak, Experimental validation of the sound transmission of rectangular baffled plates with general elastic boundary conditions, *Journal of the Acoustical Society of America* 129(6) (2011) EL274-EL279.
- [5] X. Wang, C.M. Mak, Acoustic performance of a duct loaded with identical resonators, *Journal of the Acoustical Society of America* 131(4) (2012), EL316-EL322.
- [6] X. Wang, C.M. Mak, Wave propagation in a duct with a periodic Helmholtz resonators array, *Journal of the Acoustical Society of America* 131(2) (2012)1172-1182.
- [7] X. Wang, *A study of Helmholtz resonators on broadband noise control and their potential application on ventilation*, PhD Thesis, The Hong Kong Polytechnic University, 2012.

- [8] C.M. Mak, A prediction method for aerodynamic sound produced by multiple elements in air ducts, *Journal of Sound and Vibration* 287(2005) 395-403.
- [9] C.M. Mak, W.M. Au, A turbulence-based prediction technique for flow-generated noise produced by in-duct elements in a ventilation system, *Applied Acoustics* 70 (2009) 11-20.
- [10] C.M. Mak, J. Wu, C. Ye and J. Yang, Flow noise from spoilers in ducts, *Journal of the Acoustical Society of America* 125(6) (2009) 3756-3765.
- [11] A. Fry, Vibration isolation, In: *Noise control in building services*, Sound Research Laboratories Ltd., Pergamon Press, Oxford, 1988.
- [12] B.J. Smith, R.J. Peters and S. Owen, Vibration, In: *Acoustics and noise control*, 2<sup>nd</sup> edition, Addison Wesley Longman, Boston, 1996.
- [13] F.S. Tse, I.E. Morse and R.T. Hinkle, *Mechanical vibrations: theory and applications* (2nd ed), Allyn and Bacon, Boston, 1979.
- [14] C.M. Mak, J.X. Su, A power transmissibility method for assessing the performance of vibration isolation of building services equipment, *Applied Acoustics* 63(2002) 1281-1299.
- [15] C.M. Mak, Y. Yun, A study of power transmissibility for the vibration isolation of coherent vibratory machines on the floor of a building, *Applied Acoustics* 71(2010) 368-372.
- [16] C.M. Mak, J.X. Su, A study of the effect of floor mobility on structure-borne sound power transmission, *Building and Environment* 38(3)(2002) 443-455.

- [17] J.C. Tao and C.M. Mak, Effect of viscous damping on power transmissibility for the vibration isolation of building services equipment, *Applied Acoustics* 67(8) (2006)733-742.
- [18] H.L. Sun, H.B. Chen, K. Zhang, P.Q. Zhang, Research on performance indices of vibration isolation system, *Applied Acoustics* 69(2008) 789-795.
- [19] C.Yilmaz, N.Kikuchi, Analysis and design of passive band-stop filter-type vibration isolators for low-frequency applications, *Journal of Sound and Vibration* 291(2006) 1004–1028.
- [20] J.C. Snowdon, Vibration isolation : use and characterization, *The Journal of the Acoustical Society of America* 66 (1979)1245–1274.
- [21] S. Rubin, Design procedure for vibration isolation on nonrigid supporting structures, *SAE Technical Paper* 600037 (1960). doi:10.4271/600037.
- [22] A.O. Sykes, Isolation of vibration when machine and foundation are resilient and when wave effects occur in the mount, *Noise Control* 6(3) (1960) 23-27, 30–38.
- [23] J.I. Soliman, M.G Hallam, Vibration isolation between non-rigid machines and non-rigid foundations, *Journal of Sound and Vibration* 8 (2) (1968) 329–351.
- [24] R.J. Pinnington, R.G White, Power flow through machine isolators to resonant and non-resonant beams, *Journal of Sound and Vibration* 75(2)( 1981) 179–197.
- [25] R.J. Pinnington, Vibrational power transmission to a seating of a vibration isolated motor, *Journal of Sound and Vibration* 118(3) (1987) 515–530.

- [26] J.C. Snowdon, Resilient mounting of machinery on platelike and modified platelike substructures, *The Journal of the Acoustical Society of America* 61(4) (1977) 986-994.
- [27] R.G. White, Chapter 26: Vibration control (II), in: R.G. White and J. G. Walker (Eds.), *Noise and Vibration*, Ellis Horwood, Chichester, 1982.
- [28] H.G.D. Goyder, R.G. White, Vibrational power flow from machines into built-up structures, part III: Power flow through isolation systems, *Journal of Sound and Vibration* 68 (1) (1980) 97-117.
- [29] B.A.T. Petersson, B.M. Gibbs, The influence of source location with respect to vibrational energy transmission, *In 3rd International Congress on Intensity Techniques*, Senlis, France, 1990, pp.449 - 456.
- [30] B.A.T. Petersson, Moment and force excitation at edges and corners of beam and plate like structures, *In International Conference on Recent Advances in structural Dynamics*, ISVR, Southampton, 1991, pp.148 - 157.
- [31] Y.K. Koh, R.G. White, Analysis and control of vibrational power transmission to machinery supporting structures subjected to a multi-excitation system: Parts I-II, *Journal of Sound and Vibration* 196(4) (1997) 469 - 522.
- [32] J.A. Richards, *Analysis of periodically time-varying systems*, Springer-Verlag, New York, 1983.
- [33] A. Lazarus, B. Prabel, D. Combescure, A 3D finite element model for the vibration analysis of asymmetric rotating machines, *Journal of Sound and Vibration* 329 (2010) 3780-3797.

- [34] C. Elachi, Wave in active and passive periodic structures: A review, *Proceedings of the IEEE* 64 (1976) 1666-1698.
- [35] T. A. C. M. Claasen, W. F. G. Mecklenbräuer, On stationary linear time-varying systems, *IEEE Transactions on Circuits and Systems* 29 (1982) 169-184.
- [36] J. L. Nielsen, P. U. Svensson, Performance of some linear time-varying systems in control of acoustic feedback, *Journal of the Acoustical Society of America* 106(1) (1999) 240-254.
- [37] P. U. Svensson, Computer simulations of periodically time-varying filters for acoustic feedback control, *Journal of the Audio Engineering Society* 43 (1995) 667-677.
- [38] W.T. Thomson, M.D. Dahleh, *Theory of vibration with applications*, 5<sup>th</sup> edition, Prentice-Hall, New Jersey, 1998.
- [39] T. Krauthammer, *Modern protective structures*, CRC Press, New York, 2008.
- [40] C.E. Bradley, Acoustic Bloch wave propagation in a periodic wave-guide, *Technical Report of Applied Research Laboratories*, Report No. ARL-TR-91-19 (July), The University of Texas, Austin, 1991.
- [41] L. Friis, M. Ohlrich, Coupling of flexural and longitudinal wave motion in a periodic structure with asymmetrically arranged transverse beams, *Journal of the Acoustical Society of America* 118 (2005) 3010-3020.
- [42] D.J. Mead, Wave propagation and natural modes in periodic systems: I. Mono-coupled systems, *Journal of Sound and Vibration* 40 (1975) 1-18.

- [43] D.J. Mead, Wave propagation and natural modes in periodic systems: II. Multi-coupled systems, with and without damping, *Journal of Sound and Vibration* 40(1975)19-39.
- [44] T.R. Lin, A study of modal characteristics and the control mechanism of finite periodic and irregular ribbed plates, *Journal of the Acoustical Society of America* 123 (2008) 729–737.
- [45] X. Huang, A. Jiang, Z. Zhang and H. Hua, Design and optimization of periodic structure mechanical filter in suppression of foundation resonances, *Journal of Sound and Vibration* 330 (20) (2011) 4689 – 4712.
- [46] W. Jung, Z. Gu and A. Baz, Mechanical filtering characteristics of passive periodic engine mount, *Finite Elements in Analysis and Design* 46( 9) (2010) 685 – 697.
- [47] C. Yilmaz, N. Kikuchi, Analysis and design of passive band-stop filter-type vibration isolators for low-frequency applications, *Journal of Sound and Vibration* 291 (3-5)(2006) 1004 – 1028.
- [48] O. Sigmund and J.S. Jensen, Systematic design of phononic band-gap materials and structures by topology optimization, *Philosophical Transactions of the Royal Society of London, Series A: Mathematical, Physical and Engineering Sciences* 361 (1806) (2003)1001–1019.
- [49] M.I. Hussein, G.M. Hulbert, R.A. Scott, Dispersive elastodynamics of 1D banded materials and structures: design, *Journal of Sound and Vibration* 307 (3–5) (2007) 865 – 893.
- [50] S. Asiri, Tunable mechanical filter for longitudinal vibrations, *Shock and Vibration* 14(5) (2007) 377–391.

- [51] J.T. Szefi, *Helicopter Gearbox Isolation Using Periodically Layered Fluidic Isolators*, PhD thesis, The Pennsylvania State University, Pennsylvania, USA, 2003.
- [52] T. Chen, M. Ruzzene and A. Baz, Control of wave propagation in composite rods using shape memory inserts: theory and experiments, *Journal of Vibration and Control* 6 (2000) 1065–1081.
- [53] B.R. Mace, R.W. Jones, N.R. Harland, Wave transmission through structure inserts, *Journal of the Acoustical Society of America* 109 (2001) 1417–1421.
- [54] M.B. Xu and G. Song, Adaptive control of vibration wave propagation in cylindrical shells using SMA wall joint, *Journal of Sound and Vibration* 278 (2004) 307 – 326.
- [55] K. A. Williams, G. Chiu, R.J. Bernhard, Adaptive-passive absorbers using shape-memory alloys, *Journal of Sound and Vibration* 249 (5) (2002) 835–848.
- [56] K.A. Williams, G. Chiu, R.J. Bernhard, Dynamic modelling of a shape memory alloy adaptive tuned vibration absorber, *Journal of Sound and Vibration* 280 (2005) 211–234.
- [57] F. Deng, D. Rémond, L. Gaudiller, Self-adaptive modal control for time-varying structures, *Journal of Sound and Vibration* 330 (2011) 3301-3315.
- [58] K.J. Yanga, K.S. Hongb, F. Matsuno, Robust adaptive boundary control of an axially moving string under a spatiotemporally varying tension, *Journal of Sound and Vibration* 273 (2004) 1007-1029.



- [59] Z. Zhang, E. Rustighi, Y. Chen and H. Hua, Active control of the longitudinal-lateral vibration of a shaft-plate coupled system, *Journal of Vibration and Acoustics* 134 (2012) 061002.1-061002.11.
- [60] M. Niedzwiecki and M. Meller, A new approach to active noise and vibration control–Part I: The known frequency case, *IEEE Transactions on Signal Processing* 57(9) (2009) 3373-3386.
- [61] M. Niedzwiecki and M. Meller, A new approach to active noise and vibration control–Part II: The unknown frequency case, *IEEE Transactions on Signal Processing* 57(9) (2010) 3387-3398.
- [62] B.J. Kim and D.C. Swanson, Linear independence method for system identification/secondary path modeling for active control, *Journal of the Acoustical Society of America* 118(3) (2005) 1452-1468.
- [63] J. Yuan, Orthogonal adaptation for active noise control, *Journal of the Acoustical Society of America* 120(1) (2006) 204-210.
- [64] J. Yuan, Orthogonal adaptation for multichannel feedforward control, *Journal of the Acoustical Society of America* 120(6) (2006) 3723-3729.
- [65] J. Yuan, Self-learning active noise control, *Journal of the Acoustical Society of America* 124(4) (2008) 2078-2084.
- [66] H.G. Stark, *Wavelets and signal processing: an application-based introduction*, Springer, Berlin, 2005

- [67] L. Cremer, M. Heckl, *Structure-borne sound*, Springer-Verlag, Berlin, 1973
- [68] P.W. Anderson, Absence of diffusion in certain random lattices, *Physical Review* 109 (1958) 1492–1505.
- [69] C.H. Hodges, Confinement of vibration by structural irregularity, *Journal of Sound and Vibration* 82 (1982) 411–424.
- [70] C.H. Hodges, J. Woodhouse, Vibration isolation from irregularity in a nearly periodic structure: Theory and measurements, *The Journal of the Acoustical Society of America* 74 (1983) 894–905.
- [71] W. Cheney, D. Kincaid, *Numerical Mathematics and Computing*, 6<sup>th</sup> edition, Thomson Brooks/Cole, 2008.
- [72] S.J. Elliott, *Signal Processing for Active Control*, Academic, London, 2001.
- [73] D. Young, R.P. Felgar, *Tables of characteristic functions representing normal modes of vibration of a beam*, The university of Texas publication, Austin, 1949.
- [74] D.E. Hodgson, Shape Memory Alloys, *ASM Handbook*, 2 (1990) 897–902.
- [75] L. Friis, M. Ohlrich, Coupled flexural-longitudinal wave motion in a finite periodic structure with asymmetrically arranged transverse beams. *Journal of the Acoustical Society of America* 118 (2005) 3607-3618.
- [76] A.K. Hazra, *Matrix: algebra, calculus and generalized inverse*. Cambridge International Science Publishing, Cambridge, England, 2007.
- [77] G.R. Wang, S.Z. Qiao and Y.M. Wei, *Generalized inverses: theory and computations* Science Press, Beijing, 2004.

- [78] M. Heckl, Wave propagation on beam-plate systems. *Journal of the Acoustical Society of America* 33(1961) 640-651.
- [79] S. Haykin, *Adaptive Filter Theory*, 5<sup>th</sup> edition, Pearson Education, Prentice Hall, New Jersey, 1998.
- [80] J. Wang and C.M. Mak, An indicator for the assessment of isolation performance of transient vibration, *Journal of Vibration and Control* (2012). doi:  
10.1177/1077546312458135.